ELECTROPHYSIOLOGICAL ANALYSIS AND CHARACTERIZATION OF TWO MICROBIAL CHANNELS: THE PAPC USHER OF UPEC AND THE NSP4 VIROPORIN OF ROTAVIRUS

A Dissertation Presented to

the Faculty of the Department of Biology & Biochemistry

University of Houston

In Partial Fulfillment

of the Requirements for the Degree

Doctor of Philosophy

By

Thieng Pham

August 2016

ELECTROPHYSIOLOGICAL ANALYSIS AND CHARACTERIZATION OF TWO MICROBIAL CHANNELS: THE PAPC USHER OF UPEC AND THE NSP4 VIROPORIN OF ROTAVIRUS

Thieng Pham

APPROVED:

Dr. Anne H. Delcour, Chairman

Dr. William R. Widger

Dr. Jokubas Ziburkus

Dr. Peter Christie

Dean, College of Natural Sciences and Mathematics

ELECTROPHYSIOLOGICAL ANALYSIS AND CHARACTERIZATION OF TWO MICROBIAL CHANNELS: THE PAPC USHER OF UPEC AND THE NSP4 VIROPORIN OF ROTAVIRUS

An Abstract of Dissertation

Presented to

the Faculty of the Department of Biology & Biochemistry

University of Houston

In Partial Fulfillment

of the Requirements for the Degree

Doctor of Philosophy

By

Thieng Pham

August 2016

ABSTRACT

Microbes, such as bacteria and viruses, utilize channel proteins that play an important role in the infection process, and thus are considered virulence factors. With the rise in antibiotic resistance and despite the existence of vaccines, there is a need for alternative drug therapies, and these virulence factors can be used as new drug targets. In this work, we examined the molecular properties of a bacterial pore-forming protein (PapC) and a viral ion channel (NSP4) using electrophysiological techniques. The PapC usher is produced by uropathogenic *E. coli*, the causative agent of urinary tract infections, and catalyzes the assembly and surface expression of P pili used to mediate host cell attachment. At rest, the PapC channel is closed by a plug domain that is displaced to allow the passage of the growing pilus. We showed that key residues involved in allosteric and electrostatic networks within the channel govern gating of the usher pore. In particular, a region localized to the periplasmic base of PapC appears to stabilize the usher in a closed configuration. In addition, we showed that the complex of the first pilus subunit associated with its chaperone activates the usher, and partially engages within the channel. Altogether, our work has provided mechanistic insight into usher gating and a basis for alternative drug design.

The second part of our work is centered on the non-structural protein 4 (NSP4) of rotavirus. The expression of NSP4 alone was previously shown to increase cytoplasmic calcium, by releasing calcium stores from the endoplasmic reticulum, and thus NSP4 has been proposed to be a calcium channel. To test this hypothesis, we investigated the electrophysiological properties of the putative, channel-forming viroporin domain (VPD) of NSP4. We demonstrated that NSP4 VPD is indeed a *bona fide* ion channel, capable of

conducting potassium, calcium and barium ions. This property sets it apart from most other viroporins studied to date. The channel is not strictly selective to calcium ions, but appears sensitive to inhibition by classical calcium channel inhibitors, such as cadmium and nickel ions. Altogether, our work established the foundations for future characterization of NSP4 properties using electrophysiology.

TABLE OF CONTENTS

LIST OF FIGURES

CHAPTER 1

Introduction

Parts of this chapter are published in

Pham, T and Delcour, AH (2015) "Electrophysiology of Translocons", in "Electrophysiology of Unconventional Channels and Pores," A. H. Delcour, Ed., Springer Series in Biophysics (B. Martinac, series editor), pp. 123-151.

1.1 Gram-Negative Bacteria

Gram-negative bacteria perform a variety of functions in order survive. In their own surrounding environment, they import a multitude of necessary nutrients and resources. Within the host environment, they release toxic effectors to subjugate host cell machinery. Many of these virulence factors also help to propagate bacterial growth and expansion. However, they must first traverse the bacterial cell envelope in order to perform these functions. This bacterial cell envelope is composed of two lipid bilayers. The membrane at the extracellular surface is commonly known as the outer membrane (OM). An inner membrane (IM) contains the cytoplasmic contents of the cell and is separated from the outer membrane by a periplasmic space containing a thin peptidoglycan cell wall.

1.1.1 Outer Membrane

The inner leaflet of the OM is composed of phospholipids whereas the leaflet at the extracellular interface is composed primarily of lipopolysaccharides (Kamio and Nikaido, 1976). Together these leaflets of different lipid composition form an asymmetric lipid bilayer that serves as the primary barrier between the cell and the outside world. However, this membrane is selectively permeable due to the presence β-barrel proteins embedded within. The OM also contains lipoproteins, which are diverse (Kovacs-Simon et al., 2011). Some lipoproteins have been shown to participate in cellular adhesion. For example, the *Neisseria meningitides* lipoprotein PilP is a primary component required for the biosynthesis of the Type IV pilus (Assalkhou et al., 2007; Balasingham et al., 2007). Other lipoproteins such as those found in the membranes of *Borrelia burgdorferi* are

responsible for the transport of numerous substrates (Dunn et al., 2015). Most of these lipoproteins, however, do not span the entire OM but are often found localized to the inner leaflet in β-sandwich configurations (Miyadai et al., 2004). One of these lipoproteins, Lpp, is essentially responsible for anchoring the OM to the peptidoglycan cell wall underlying the OM inner leaflet (Braun and Wolff, 1975). Proteins that *do* span the entire OM often adopt a β-barrel conformation and primarily function as transporters of small solutes across the membrane (Holland, 2010). OmpF, for example, allows for the passive diffusion of molecules of molecular weights less than 600 Da such as small sugars and amino acids (Delcour, 2003; Nikaido, 2003). PhoE, another outer membrane protein (OMP), is more specific in its transport of anions such as phosphate (Cowan et al., 1992). However, for the transport of larger molecules, gram-negative bacteria employ Ton-B dependent porins. BtuB, a β-barrel comprised of 22 β-strands, (Nikaido, 2003) is used for the import of vitamin B12, for example. Many of these proteins residing in the OM are assembled by a molecular machine known as the β-Barrel Assembly Machinery (BAM) complex. Coincidentally, the BAM complex is composed of a large β-barrel protein and various lipoproteins that also reside in the OM (Nikaido, 2003; Wu et al., 2005). This complex will be discussed in further detail in a section below.

1.1.2 The Cell Wall

As mentioned previously, the OM is anchored to the bacterial cell wall composed of peptidoglycan. This peptidoglycan forms cross-links, which create a rigid structure that determines cell shape (Vollmer et al., 2008a; Vollmer et al., 2008b). More importantly, this cell wall prevents the cell from lysing from its own internal turgor

pressure (Weidel and Pelzer, 1964). As a result, antibiotic treatments that target the peptidoglycan cell wall lead to the rupture of the bacterial cell. Consequently, it is critical that the cell be able to export antibiotics that are detrimental to the structural integrity of its cell wall. These exist in the form of efflux proteins; many of which span the whole cell envelope.

1.1.3 Inner Membrane

As opposed to the OM, the IM is a symmetric bilayer of lipids composed of phospholipids such as: phosphatidyl ethanolamine, phosphatidyl glycerol, phosphatidyl serine, and cardiolipin (Silhavy et al., 2010). One of the more prominent features of the IM is the presence of major machineries involved in protein sorting and trafficking. Sec-dependent proteins require a molecular machine known as the Sec pathway for export into the periplasmic space (Xie and Dalbey, 2008). While the Sec translocase can also insert proteins into the IM, it also functions as the primary exporter of proteins across the IM into the periplasmic space. This pathway is the translocation device responsible for the export of most lipoproteins and β-barrel proteins destined for the OM. It also functions to export a series of proteins destined for secretion. For example, the Sec pathway is responsible for transporting various protein subunits such as those coded by the *pap* operon for assembly into pili at the bacterial-cell surface. In fact, many of the components that are involved in all seven secretion systems found in Gram-negative bacteria are secreted by the Sec pathway (Dalbey and Kuhn, 2012). As such, the proteins in the IM are a critical first step in the export and eventual assembly of secretion systems and effectors essential for virulence. However, these proteins must cross the periplasm.

1.1.4 Periplasm

The cellular compartment between the OM and IM is known as the periplasm. The periplasmic space is highly populated with various proteins creating a much denser and more viscous environment than that of the cytoplasm (Mullineaux et al., 2006). Many of the proteins that reside in the periplasm vary widely in function. For example, there exist several key chaperones that are vital to envelope biogenesis and quality control (Lyu and Zhao, 2015; Merdanovic et al., 2011). Skp and SurA are such chaperones responsible to prevent the aggregation of various OMPs destined for the OM immediately after secretion by the Sec pathway (Walton et al., 2009). DegP is another well-known periplasmic protein that acts as both a chaperone and protease. Misfolded proteins that often result from overproduction are degraded by DegP to prevent damage to the periplasmic space (Lyu and Zhao, 2015). Together, these proteins maintain a healthy periplasmic environment while also functioning to target OMPs to the BAM complex for insertion into the OM.

1.1.5 Translocons

As mentioned previously, many of the virulence factors utilized by Gram-negative bacteria are secreted extracellularly. Some of these are released in the external medium, either by crossing the whole bacterial envelope in a single step or by traversing each of the inner and outer membranes through individual pathways. Others are directly injected into host cells via complex secretion machineries spanning the bacterial envelope and the host plasma membrane. In all cases, the daunting task for a water-soluble protein to pass through membrane barriers is accomplished by macromolecular assemblies

containing a protein-translocation component, or translocon.

Seven types of secretion systems have been identified in Gram-negative bacteria (Holland, 2010), and include at least one translocon. In addition, the transport of protein substrates through the bacterial plasma membrane, together with the membrane insertion machineries that participate in the biogenesis of resident inner or outer membrane proteins, also involve translocons. Translocons vary not only in location, but also in structure and functional mechanisms. OM translocons are β-barrel proteins, similar to most OM proteins. Those assembled in the bacterial inner membrane or the plasma membrane of host cells are α-helical. Most of these machines are gated in some way, i.e. they are not present in a constitutively open state. Such a state would expose the bacterial cell to the influx and efflux of various unwanted molecules that would prove detrimental to survival. Some translocons transport folded polypeptides, while others require unfolded proteins to pass through their narrower diameters.

In all cases, however, translocons contain a hydrophilic pore, and therefore are amenable to electrophysiological techniques, such as planar lipid bilayer and patch clamp. Such techniques have, in the past, established evidence and confirmed that these secreting machines are pore-forming proteins. At present, they are commonly used to analyze the behaviors and kinetics of these channels and associate them with their structures. Thus, electrophysiology plays a key role in determining the structure-function relationship of various translocons. In addition, the transport of protein substrates can also be monitored as a kinetic modification in electrophysiological traces, and therefore electrophysiology may enable a single molecule analysis of translocation. The following sections (1.2-1.3) will summarize the various findings uncovered by the use of

electrophysiological techniques on translocons studied in this manner to date.

1.2 Electrophysiology of Bacterial Translocons

1.2.1 Membrane Biogenesis Proteins

A. The General Secretory Pathway (Sec)

As mentioned briefly above, a large majority of proteins destined for the OM are secreted through the Sec pathway (Driessen and Nouwen, 2008). The Sec pathway utilizes the SecYEG translocon within which the SecY subunit functions as the conduit for translocation. Proteins destined for secretion by the Sec pathway are often translated with an N-terminal signal sequence in their pre-protein configuration. These proteins then associate with SecA (Tang et al., 2011) for targeting to the Sec pathway for signal cleavage and export. In addition, many resident IM proteins complexed with a signal-recognition particle (SRP) and ribosome are delivered directly to the SecYEG translocon by FtsY for co-translational translocation. Regardless, SecA is believed to utilize ATP hydrolysis to cause a step-wise threading of the unfolded polypeptide through the SecY lumen (Chatzi et al., 2014).

The X-ray structure was determined for the homologous complex SecYEβ from the archeon *Methanococcus jannaschii* (Van den Berg et al., 2004) and found to superimpose well on the cryo-EM structure of an active *E. coli* SecYEG complex (Breyton et al., 2002). Sec Y, which contains 10 transmembrane (TM) helices, is organized like a clamshell, with the N-terminal and C-terminal domains, made up of five TM helices each, acting as two halves surrounding a central pore. In the closed state observed in this structure, the pore is obstructed by a plug formed by a distorted helix

connecting the first two TM segments of SecY. A lateral gate at the interface of the membrane lipids and SecY is formed by TM 2 and 7 which come in close proximity, and to which pre-protein signal sequences are known to bind (Van den Berg et al., 2004). It is proposed that the binding of a signal sequence at the lateral gate triggers a conformational change of the clamshell with a concomitant displacement of the plug and widening of the pore (Bonardi et al., 2011). Indeed, the structure of the *Thermotoga maritima* SecYEβ complexed with SecA and presumably in a pre-open state reveals movements of the lateral gates helices and partial removal of the plug (Zimmer et al., 2008). A ring of isoleucine residues constricts the channel to its narrowest diameter of 4 Å, large enough to accommodate a polypeptide chain in its unfolded conformation. However, as long as some opening of the lateral gate is permitted, the pore can accommodate bulky moieties attached to translocation peptides with a diameter extending up to 24 Å (Bonardi et al., 2011). In fact, recent data suggests that the hydrophobic part of the signal sequence forms a helix within the lateral gate and effectively becomes part of the channel wall (Park et al., 2014).

Planar lipid bilayer experiments detect no ion conductance in the presence of purified wildtype (WT) Sec complex, but current deflections are readily observed when complexes with SecY mutants lacking the plug helix are used (Saparov et al., 2007). Single channel conductance of the mutant carrying the largest deletion (from residues 60 to 74) was estimated at ~ 940 pS (presumably in 1 M KCl), with an estimated pore diameter of 7.3 Å (Saparov et al., 2007). These results support a model whereby the plug helix indeed functionally seals the channel shut. They also suggest that the hydrophobic pore ring alone is not sufficient for preventing ion conduction, at least in the absence of

translocating peptides. However, it was suggested that the hydrophobic ring might form a gasket that seals against a translocating peptide, allowing for the maintenance of the proton gradient during protein translocation (Park and Rapoport, 2011).

The first electrophysiological demonstration that signal sequences open the pore was provided by Simon and Blobel two decades ago (Simon and Blobel, 1992). Here, inner membrane vesicles were fused with planar lipid bilayers. The addition of the LamB signal peptide led to an increase in macroscopic currents. With low peptide concentration, the appearance of individual channels could be detected, but only when the signal peptide was applied from the presumed cytoplasmic side of the channel. These initial observations were made on rather crude membrane preparations, but similar results have been obtained more recently with purified SecYEG complexes, where addition of proOmpA signal peptide led to channel openings of conductance (~ 220 pS) similar to those reported by Simon and Blobel (Knyazev et al., 2014). Surprisingly increases in membrane potential to physiological values (~ 130 mV) drove these channels to closures in step-wise fashion. In the presence of a stalled translocation intermediate, the voltage-driven closure of the channel leaves a residual conductance of ~ 6 pS, a value that, according to the authors, would ensure the preservation of the proton-motive force across the bacterial membrane. Thus, perhaps it is not the pore ring that limits ion flow during polypeptide translocation but rather a conformational change in SecYEG itself. The nature of the voltage sensor and the resulting conformational changes remain, however, unresolved.

B. BamA and Outer Membrane Biogenesis

Whereas SecYEG functions in the passage of proteins from the cell cytosol into the periplasmic space, BamA (a.k.a Omp85 or YaeT), in association with other proteins of the BAM (β-barrel Assembly Machinery) complex, functions as the main machinery for the insertion of proteins into the outer membrane (Selkrig et al., 2014). This protein plays such a vital role for the cell that its identification in this process was not accomplished until relatively recently with the use of conditional mutants (Wu et al., 2005). BamA/Omp85 itself is a conserved protein with a widespread distribution among prokaryotes and homologues in mitochondria as well as chloroplasts (Gentle et al., 2005). Members of the Omp85 family are characterized by the presence of 1 to 5 N-terminal POTRA (Polypeptide Translocation Associated) domains, and a C-terminal β-barrel domain inserted in the membrane (Jacob-Dubuisson et al., 2009). These POTRA domains may function as receptors for OMPs that use the BAM complex for insertion into the outer membrane, or to assist in folding of the substrates, or even in the maintenance of the complex as a whole (Selkrig et al., 2014). Recently two structures of BamA have been solved by X-ray crystallography (Noinaj et al., 2013), and suggest possible conformational changes that may occur during the insertion of substrates into the membrane. Based on these results, the authors suggest two possible mechanisms: (**1**) large OMPs might actually fold by β-augmentation using exposed BamA β-strands at a lateral gate to initiate the formation of a barrel which would eventually "bud off" the BamA template, and (**2**) smaller OMPs might reach the BAM complex already in a β-barrel configuration which would interact with the POTRA domains and use the local membrane destabilization provided by BamA to directly insert in the membrane. It is

interesting to note that, although BamA has clear pore-forming properties (see below), neither of these two putative models makes use of the pore function of the protein for the membrane insertion of OMPs.

Electrophysiological recordings were first reported in 2006 in two complementary studies from two distinct groups, using the nomenclature of Omp85 (Robert et al., 2006) and YaeT (Stegmeier and Andersen, 2006). Both reports document that the channels display various conductances, but agree that the dominant conductance is in the order of 400-500 pS in 1 M KCl. The channel appears cation-selective, with a reported P_K/P_{Cl} of 5.7 (Stegmeier and Andersen, 2006), and inactivated by acidic pH (Stegmeier and Andersen, 2006). As was found for Two-Partner Secretion System (TPS) translocons, which also belong to the Omp85 superfamily (see above), the Omp85 proteins from various sources are constructed with a two-domain architecture, with the C-terminal domain forming the pore (Bredemeier et al., 2007; Stegmeier and Andersen, 2006). There are several reports that suggest that the protein might indeed function as a folding platform for nascent β-barrels that are ultimately released laterally in the membrane plane. This proposal was first suggested by Stegmeier and Andersen (2006) based on the observation of multiple conductance levels, in particular when the C-terminal domain was studied in isolation. The appearance of multiple conductance levels hints at a dynamic and perhaps relatively plastic β-barrel structure, which may be linked to its physiological function of laterally opening up toward the membrane environment through a gap in the barrel. Indeed, Estrada Mallinaro et al. (2012) calculated the so-called "barrel-closure energies" reflecting the interactions between the β1-strand and β16-strand of the *Thermophilus thermus* Omp85 homolog (TtOmp85), and found them to be

significantly weaker than the corresponding ones from members of the porin family (Estrada Mallarino et al., 2015). In the same study, the authors report that events of larger conductance appear when TtOmp85 is investigated in presence of peptides originating from a natural substrate OMP. The authors interpret these larger conductance events as representing pores with widened diameters due to β-augmentation by the substrates. In essence, they claim to have caught assembly intermediates made up of compound barrels including the 16 TtOmp85 strands and a few strands of the substrate OMP. Interestingly, these larger events are only seen if peptides corresponding to the C-terminal last or last two β−strands of the substrate OMP are used, but not with N-terminal peptide mimics. These observations agree with prior results showing that larger currents are observed when bilayers containing multiple *E. coli* Omp85 channels are exposed to denatured PhoE or even to a peptide corresponding to the last 10 C-terminal residues of PhoE (Robert et al., 2006). In this paper, the authors interpret the increase in current to opening of the channel. However, because the experiments were performed on bilayers containing multiple channels, it is actually not possible to know if the increased current is truly due increase open probability or increased conductance of a single pore. The latter interpretation would support the model of β-augmentation proposed in more recent studies.

1.2.2 Type I Secretion System – TolC

A. General Introduction

The presence of antibiotics and other harmful chemicals represent a prevailing danger for the continued survival of bacteria. As a defensive mechanism, Gram-negative

bacteria such as *Escherichia coli* and *Pseudomonas aeruginosa* employ drug efflux systems to pump noxious material out of the cell (Du et al., 2015; Nikaido, 2009; Zgurskaya et al., 2015). These macromolecular assemblies contain a component that resides in the outer membrane and extends into the periplasmic space. An example of such a component is TolC (Zgurskaya et al., 2011). Synthesized in the cytoplasm, the nascent protein is targeted to the general secretory pathway for export into the periplasm. Here, because of its peculiar trimeric structure and high α-helical content, it folds in a unique way without the aid of known periplasmic chaperones. It is then believed to insert into the outer membrane via the Beta-barrel Assembly complex (BAM), but more concrete evidence for this is still largely undiscovered (Zgurskaya et al., 2011). TolC can be recruited by a large number of various transporters in the inner membrane for drug efflux or the secretion of large proteins (Zgurskaya et al., 2011). One of the most studied examples is its association with two envelope proteins, the periplasmic AcrA and the inner membrane AcrB, to form a complex pump that generates a conduit spanning from the inner membrane through the periplasmic space to the outer membrane (Nikaido, 2009). As such, it can be used by the bacterium specifically for the efflux of a wide variety of antibiotics.

Initial crystallographic diffraction data identified TolC as an unusual trimeric protein (Koronakis et al., 2000). Each protomer within this oligomer is composed of 4 β-sheets from which 2 pairs of coiled-coil α-helices extend. Together the protomers entwine to create a trimer that exists as a 12-stranded 40 Å-long β-barrel anchored in the outer membrane, with six pairs of coiled-coil α-helices (2 pairs from each protomer) protruding into the periplasm to form a 100 Å long tunnel. Because of this elongated structure, TolC

was coined a “channel-tunnel” (Koronakis et al., 2000). The crystal structure of the TolC trimer also indicated that because the protomers twist around each other, in particular in the coiled-coil region, the entrance to the TolC channel tunnel is constricted and hence closed (Koronakis et al., 2000). The modeled structure of the tripartite complex of TolC, AcrA and AcrB shows that the assembly of the three components in a 3:6:3 stochiometry results in the formation of a complex spanning the whole envelope (Zgurskaya et al., 2011). A recent cyro-EM study provides a pseudo atomic model of the whole isolated drug-efflux pump (with an additional accessory component, AcrZ), suggesting the formation of a continuous internal conduit through the TolC, AcrA, and AcrB oligomers, and thus proposing that the TolC channel must open upon docking with AcrA (Du et al., 2014).

B. Channel Properties

Electrophysiological analysis has been rather critical in elucidating structure-function relationship in order to provide insight into the exact molecular mechanism behind TolC channel opening. Initial studies used purified TolC reconstituted into planar lipid bilayers in order to determine the effects of varying membrane potentials on channel properties (Andersen et al., 2002a). Such experiments with bilayers containing multiple inserted channels identified polarity dependent behavior indicating asymmetry consistent with its structure. This is clearly displayed by different channel noise observed at positive membrane potentials from the behavior seen at negative potentials. Single channel experiments further cemented this observation while providing evidence that purified TolC inserts itself into the lipid bilayer in the same orientation each time. It was also

noted that while no voltage dependent opening or closing of TolC was seen, higher resolution single channel recordings identified the presence of three conductance substates as well as cation selectivity. Cation selectivity was presumed to be due to the highly electronegative aspartate ring at the periplasmic entrance to the TolC tunnel domain. Interestingly, conductance varied depending on positive or negative membrane potentials. In particular, negative membrane potentials relative to the *cis* side resulted in a larger conductance presumably because of increased ion flow from the β-barrel to the periplasm. Experiments utilizing different pHs also provided some insight into the opening mechanism in TolC. Low pH experiments with reconstituted TolC showed a much smaller conductance level. This is believed to be due to the protonation of the periplasmic ring of aspartate residues at lower pHs. Consequently, this would limit ion flow and thus conductance through the channel tunnel. Importantly, these initial studies established a conductance of ~ 80 pS in 1 M KCl, a value that seems too small to represent a pore able to accommodate large protein substrates, and but consistent with a "closed" state of the channel. Based on the X-ray structure, these electrophysiological results suggested that the periplasmic entrance might be the constricting and limiting factor for channel conduction and therefore a critical factor underlying the mechanism for TolC channel gating. In particular, it was hypothesized that the periplasmic entrance to the tunnel domain must somehow untwist in an iris-like fashion in order to allow the export of large proteins or efflux of drugs.

Insight into the molecular mechanism of opening was provided by later studies seeking to test this hypothesis (Andersen et al., 2002b). Close inspection of the X-ray structure and modeling of the open state revealed that the "closed" state of the channel

might be maintained by two intra-monomeric hydrogen bonds, an inter-monomeric salt bridge and an inter-monomeric hydrogen bond, which altogether keep the coiled-coil helices in close proximity. The authors introduced mutations of the residues involved in these interactions to disrupt the links between the coils. Single mutations had relatively marginal effects. However the combination of some mutations resulted in a profound enhancement of the conductance, indicative of an enlarged pore opening. In particular the combined disruption of the inter-monomeric links and one of the inter-monomeric hydrogen bonds produced variants with conductances of 500 to 1000 pS. The channel with the highest conductance also showed a higher propensity at substate gating at negative potentials, indicating a somewhat destabilized structure, with increased flexibility of the α-helices. Altogether, these results support the notion that opening of the channel might occur via the weakening of a ring of links in the coiled-coil domain that keeps the α-helices of this region in close proximity. The open state, though, would need to be maintained in the fully assembled and functional machine, perhaps through interactions of the TolC α-helices with AcrB.

C. The Trojan Horse: Parasitization of TolC by Colicins

Electrophysiological analyses also proved crucial in showing how this translocon can be exploited. Within environments of limited resources, bacterial warfare can be an efficient means by which to eliminate competition in order to ensure continued survival. *Escherichia coli* cells indeed produce and employ an arsenal of antibacterial toxins, known as colicins, to target sensitive strains in the environment (Cascales et al., 2007; Riley and Wertz, 2002a; Riley and Wertz, 2002b). Colicins cytotoxicity ranges from pore

forming to nuclease activity. In order to overcome the permeability barrier of the outer membrane, colicins hijack separate outer membrane proteins to serve as receptors and translocators (Jakes and Cramer, 2012). As an example of this so-called "fishing pole" mechanism of colicin translocation through the OM, BtuB, the normal transporter for the import of vitamin B12 into the periplasm, is used as a receptor by colicin E1 (ColE1), which is then handed over to TolC for translocation through the outer membrane (Zakharov et al., 2004; Zakharov et al., 2012).

In elegant experiments, TolC was indeed confirmed as the passageway for ColE1 in planar lipid bilayers. Purified TolC was added to the *cis* side of a bilayer chamber for insertion into the membrane, and ColE1 to the opposite side. At negative membrane potentials, which would pull ColE1 into the channel towards the *cis* side of the chamber, a marked decrease in channel conductance was observed, suggesting that ColE1 was occluding TolC (Zakharov et al., 2004). Positive membrane potentials, however, were ineffective. Perfusion of the *trans* side of the bilayer chamber restored the full conductance, indicating that the association of ColE1 with TolC was reversible. On the other hand, other colicins failed to occlude TolC. Later studies demonstrated that occlusion of TolC could also occur with an α-helical peptidic segment of the colicin translocation domain (T-domain) (Zakharov et al., 2012). Thus, electrophysiology was essential in demonstrating that the import of ColE1 into the periplasm actually occurs through TolC, although the exact mechanism for this process still remains enigmatic. The extracellular entrance of TolC is large enough to accommodate the α-helical T-domain of ColE1, but navigation through the whole length of the channel tunnel may require unfolding.

1.2.3 Type III Secretion System – Secreted Translocons

A. General Introduction

Various pathogenic Gram-negative bacterial species such as *Pseudomonas* or *Yersinia* are able to manipulate the host cell machinery through numerous effector proteins directly injected into the host cell via a delivery system known as the Type III Secretion System (T3SS) (Burkinshaw and Strynadka, 2014; Cornelis, 2010; Kosarewicz et al., 2012; Mattei et al., 2011).

The "injectisome", composed of over 20 different proteins, represents the secreting component of the T3SS that assembles in the bacterial envelope. It includes the basal body, the proteinaceous needle terminated by a tip complex, and the translocon (Burkinshaw and Strynadka, 2014; Mattei et al., 2011). The basal body is made up of ring-like structures spanning the inner and outer membranes and the periplasm in-between, and an inner rod connecting with the hollow needle. The needle extends outward and was recently confirmed to serve as a conduit for secreted effector proteins (Radics et al., 2014). Because the effective diameter within the needle is only approximately 2 nm (Cordes et al., 2003), secreted effectors are thought to traverse the needle in a mostly unfolded, molten globule, conformation (Dohlich et al., 2014; Faudry et al., 2007). An ATPase is embedded within the inner membrane located at the floor of the basal body facing the cytoplasmic interior, and may serve at enabling the entry of T3SS effectors into the injectisome as they are delivered at the base of the apparatus by dedicated chaperones. The first proteins to be secreted are the components of the translocon that assembles in the eukaryotic host plasma membrane. The translocon contains a hydrophilic protein thought to form an assembly platform at the tip of the

needle to aid in the oligomerization and membrane insertion of two hydrophobic translocator proteins. These two proteins are thought to form a pore within the eukaryotic cell membrane, for the delivery of secreted effectors proteins into the host cell.

B. Electrophysiology of the Yersinia enterocolitica T3SS translocon

Yersinia enterocolitica, which causes gastrointestinal symptoms in humans, along with its more infamous cousin, *Yersinia pestis*, the causative agent of plague, and *Yersinia pseudotuberculosis*, harbors a plasmid encoded T3SS that acts as a major virulence factor (Cornelis, 2002; Cornelis and Wolf-Watz, 1997). Its role is to disarm immune cells, in particular neutrophils and macrophages, by delivering effector proteins into their cytosol. These T3SS effectors disrupt the cytoskeleton and intracellular signaling pathways, thereby promoting survival in the host by blocking phagocytosis and secretion of pro-inflammatory mediators, among other effects. For many years, the Ysc-Yop system of *Yersiniae* was the best-understood T3SS (Cornelis, 2002; Cornelis and Wolf-Watz, 1997). The *Yersiniae* translocon is composed of the hydrophilic platform protein LcrV and the hydrophobic, presumably pore-forming, proteins YopB and YopD, which are thought to form a mixed oligomer (Montagner et al., 2011).

The first electrophysiological experiments that support the formation of a channel by YopB and YopD were performed by fusing with a planar lipid bilayer proteoliposomes, which had been preincubated with bacteria induced to release the Yop proteins in the extracellular medium (Tardy et al., 1999). Using a strain overexpressing YopB, YopD, and LcrV, the authors provided evidence of channel activity upon voltage application across the membrane, and attributed it to the YopBD oligomer. At

physiological salt concentrations, the single channel conductance was approximately 105 pS. Experiments in asymmetric conditions revealed that the channel had essentially no ionic selectivity. Upon impairing the hydrophobic nature of YopD via truncation, the kinetics of the channel in bilayer differed drastically. The channel displayed a predominantly closed configuration with occasional transitions to conductance states of various size and dwell times. This suggested that YopD is critical to assembling a stable channel conformation. On the other hand, YopD alone was unable to form a channel at all, providing evidence for the absolute requirement of YopB in pore formation. These electrophysiological studies support the function of YopB and YopD in forming a channel that may perhaps be responsible for the export of secreted effectors into the host cell cytosol. However, although the presence of YopB and YopD in the liposome membrane was confirmed by SDS-PAGE, validation of these findings would be strengthened by using purified proteins. This was not performed with the Yop system but with the homologous proteins from the T3SS of *Pseudomonas aeruginosa*.

C. The translocon of Pseudomonas aeruginosa

Similarly to *Y. enterocolitica*, *P. aeruginosa* uses a T3SS to break down host immune defenses. In fact, the YopB and YopD homologues of *P. aeruginosa*, PopB and PopD, have been shown to lyse red blood cells as well as disrupt the membrane integrity of macrophages (Goure et al., 2004; Mueller et al., 2008). Dye leakage experiments and other *in vitro* assays demonstrated that PopBD was able to form pores within membranes, even in the absence of the LcrV homologue, PcrV (Faudry et al., 2006). However, electrophysiological experiments helped provide insight into the kinetics of pore

formation *in vitro* (Wager et al., 2013). PopB and PopD were purified in guanidine HCl, which mimicked the unfolded conformation seen *in vivo* during transit through the needle (Faudry et al., 2007). Dilution of an equimolar mixture of PopB and PopD into a planar lipid bilayer chamber allowed the proteins to renature for insertion into the membrane. Upon voltage application, bursts of openings to various conductance states were observed with a delay that was taken to represent time for insertion and/or activation of PopB/PopD oligomers. The use of PopB alone resulted in a longer time of activation necessary to reach the characteristic bursts in conductance associated with the PopB and PopD mixture, suggesting that PopD might facilitate PopB insertion and/or oligomerization. Experiments with PopD only, on the other hand, yielded very little to no channel activity at similar protein concentrations. The kinetic signature of the PopB/PopD mixture was characterized by current fluctuations of various amplitudes. Many are extremely transient and seen as spikes, but are interspersed with square-top events defining genuine channel openings. With time, the channel activity typically ramped up due to the continuous insertions of pores, leading to extremely large transitions and culminating with the rupture of the bilayer. Interestingly, PopB/PopD displayed a very distinct voltage polarity-dependent behavior. With PopB/PopD added to the *cis* side of the membrane, channel activity was robust at positive membrane potentials, but inactivated upon application of negative voltages. The reverse was true when PopB/PopD was added to the *trans* side. This polarity dependence may have important implication *in vivo*, as it would favor the activity of newly released PopB and PopD as they approach a polarized eukaryotic membrane, whose natural membrane potential is relatively more positive on the extracellular side than on the intracellular side.

In order to provide further insight into the process of PopB/PopD pore formation, the properties of the PopB/PopD translocon were investigated in bilayers of different lipid compositions (Wager et al., 2013). The insertion of the translocon into the membrane was found to require higher membrane potentials with thicker bilayers. In addition, the mild cation-selectivity of the pore was further decreased in neutral bilayers. These findings suggested that the nature of the lipids surrounding the pore influences pore properties, and led to the proposal that the PopB/PopD translocon might form a toroidal pore, akin to some antimicrobial peptides. In toroidal pores, the channel wall is lined by both protein residues and lipid headgroups. An example is provided with the bee toxin melittin (Yang et al., 2001), which showed in planar lipid bilayer experiments astonishing similarities with the PopB/PopD translocon, such as bursts of current fluctuations of various sizes and the same polarity dependence of activity.

1.2.4 Secretins

A. General Introduction

The term "secretin" encompasses a broad family of outer membrane proteins that are present across many species of bacteria, and form channels for the translocation of proteinaceous effectors and substrates. In fact, the type II secretion system (T2SS), type III secretion system (T3SS), type IV pili system (T4PS), as well as the phage assembly system all utilize secretins as one of their core components (Korotkov et al., 2011). Many of these systems constitute virulence factors for bacterial pathogens. *In vivo*, targeting and insertion of the channel into the outer membrane often requires the interaction with an accessory lipoprotein known as the pilotin. Secretins are oligomeric in nature, with 12-

15 subunits involved in the quaternary structure, depending on the secretin type. The ensuing ring-like structures, nicely demonstrated in electron microscopy (Bitter et al., 1998; Collins et al., 2003; Crago and Koronakis, 1998; Koster et al., 1997; Nouwen et al., 1999), range from 50 to 100 Å, and therefore are large enough for the transport of folded or partially folded protein substrates. It is assumed that the complex might be gated in some fashion to prevent leakage of periplasmic content or entry of unwanted material. Indeed, in all the secretins investigated to date, plug-like constrictions are observed as localized densities within the channel (Kowal et al., 2013; Tosi et al., 2014). Each monomer is organized in domains with specific functions. The C-terminal domain, which is conserved across members of the family and thus defines the secretin domain, is embedded in the outer membrane, and participates in the formation of the membrane-spanning channel. The very last 50 or so residues of the C-terminal domain interact with the pilotin. The N-terminal domain is periplasmic and, in the multimeric structure, defines a large cavity connected to the outer membrane channel (Tosi et al., 2014). This region interacts with other components of the secretion machinery, and the secreted proteins (Korotkov et al., 2011). Because of their obvious pore-forming architecture, a few secretins have been analyzed by electrophysiology, namely XcpQ of *P. aeruginosa* (Brok et al., 1999), PulD of *Klebsiella oxytoca* (Nouwen et al., 1999), and YscC of *Yersinia enterocolitica* (Burghout et al., 2004).

B. PulD, a T2SS secretin

K. pneumoniae uses the secretin PulD of the T2SS machine for the secretion pullulanase, a cell-surface exposed outer membrane lipoprotein that degrades

pullulan, a form of starch (d'Enfert et al., 1989; d'Enfert et al., 1987). PulD from its close relative *K. oxytoca* was the first secretin investigated by electrophysiology (Nouwen et al., 1999). Purified together with its pilotin PulS, it was incorporated into liposomes. These proteoliposomes were then fused with an artificial membrane in a planar lipid bilayer setup. The experiments revealed that PulD is indeed a channel capable of conducting ions. The channel was predominantly closed at a low membrane potential of +20 mV, but holding the voltage at +80 mV increased the propensity for the channel to open, indicating that it may be voltage sensitive. Negative membrane potentials also yielded different channel kinetics compared to positive ones, as opening transitions were better defined and regular in occurrence. It is interesting that opening transitions were observed, despite the presence of an apparent plug at the center of the channel, as revealed by cryo-EM in the same study. The conductance of these events is however ~ 300 pS, presumably too small to originate from an unplugged channel. It is possible that these transitions represent small fluctuations in the ionic pathway, possibly due to small movements of the plug. Recent dye leakage experiments actually suggest that, in its resting, non-protein translocating state, PulD might exist in a leaky conformation of size comparable to the open state of general diffusion porins (Disconzi et al., 2014). The authors suggest that the discrepancy with earlier studies may stem from different membrane insertion protocols, in particular with respect to detergents.

C. YscC, a T3SS secretin

The secretin YscC from *Y. enterocolitica* functions as the outer membrane component of the T3SS basal body (Koster et al., 1997). Purified YscC was initially

reported to form a homooligomer containing 13 subunits (Burghout et al., 2004), but a more recent study rather suggests a dodecameric quaternary structure, as in PulD (Kowal et al., 2013). Near the bacterial cell surface, the YscC oligomer forms a large opening of 70 Å in diameter to enclose the proteinaceous needle that forms the extracellular part of the T3SS (Kowal et al., 2013). Similarly to PulD, the YscC secretin has a large domain protruding into the periplasm to connect with the inner membrane rings that form the rest of the basal body.

The channel conducting property of the YscC secretin was also established via planar lipid bilayer experiments demonstrating the usefulness of electrophysiological analysis as a means to identify pore-forming proteins (Burghout et al., 2004). Insertions of purified YscC revealed two different levels of conductance at 2.6 nS and 3.0 nS (in 1 M KCl), and occasional 0.5 nS transitions shortly after a 2.6 nS insertion, suggesting that the YscC secretin might be able to undergo a conformational change that allows it to increase from 2.6 nS to its maximal open state at 3.0 nS. Surprisingly, the channel appeared to be more selective for chloride than potassium. Unlike PulD, YscC was found to be in a permanently open state. Despite increasing the membrane potential to voltages upwards of +/- 200 mV, no closing transitions were observed. The conductance remained linear in voltage-ramps unlike PulD, which appeared to be voltage sensitive. YscC's lack of voltage dependence as well as its 100 percent open probability indicates that the T3SS system may be constitutively open *in vivo* to allow a continuous conduit for effectors to reach the hollow needle that will deliver them into the host target cell.

1.2.5 Autotransporters and Two-Partner Secretion Systems

A. General Introduction

Gram-negative bacteria also use dedicated secretion systems for the cell surface display of proteases, adhesins, and other enzymes. Two such protein-export machineries are autotransporters and two partner secretion systems (Leo et al., 2012; van Ulsen et al., 2014). An autotransporter is composed of a (**1**) N-terminal signal peptide, (**2**) a functional passenger domain, and (**3**) a translocator domain. The N-terminal signal peptide targets the protein to the general secretory pathway of the plasma membrane, then it is cleaved once it emerges in the periplasmic space. Chaperones and the β-barrel assembly machinery (BAM) complex are involved in the insertion of the C-terminal translocator domain into the outer membrane. There, this domain behaves as a conduit for the translocation of its passenger domain into the extracellular environment. In a similar pathway, the two-partner secretion system, the passenger and translocator functions are found on two individual proteins, the passenger exoprotein commonly referred to as TpsA, and the transporter protein, TpsB, that serves as the translocon for its partner. Both TpsA and TpsB each have an N-terminal signal peptide sequence that targets them to the general secretory pathway for export into the periplasm. Upon cleavage of the TpsA N-terminal signal peptide, a targeting sequence, called the TPS domain, is revealed to allow the TpsA to recognize its cognate TpsB in the outer membrane. The similarities between these two systems lend support to the idea that they may have evolved and diverged from a common ancestral secretory pathway. Because TpsBs and the translocator domains of autotransporters are thought to provide a passageway for protein substrates, they have

been the focus of electrophysiological investigations designed to demonstrate their pore-forming capabilities.

B. The Autotransporters NalP and Hbp

Neisseria meningitidis, the causative agent of meningitis, utilizes the autotransporter NalP to secrete a protease, which processes other autotransporters and important virulence factors at the cell surface (van Ulsen et al., 2014). High-resolution crystal structure data of the translocator domain of NalP (Oomen et al., 2004) indicates that it is a 12-stranded β-barrel embedded within the outer membrane and protruding slightly into the extracellular space. The interior core of the channel is very hydrophilic but is plugged by a highly charged N-terminal α-helix extending outward from the base of the barrel, which is thought to provide stability to the barrel (Roussel-Jazede et al., 2011). This α-helix represents the remnant of the cleaved passenger domain after its translocation through the translocator domain and proteolysis by other neighboring cell surface exposed NalPs (van Ulsen et al., 2014). Because the translocator domain of NalP is predicted to be a channel for the translocation of its passenger domain, its pore activity was measured *in vitro* via electrophysiological techniques. Purified NalP translocator domain containing the alpha helical plug was reconstituted into planar lipid bilayers (Oomen et al., 2004; Roussel-Jazede et al., 2011). Membrane potential clamped to +100 mV revealed large openings of conductance ~ 1.3 nS, with additional small conductance steps of ~ 150 pS (in 1 M KCl). The authors hypothesized that the large conductance, corresponding to an estimated internal lumen diameter of 8.4 Å, represents the channel without the inserted alpha-helix, while the small conductance would correspond to an

obstructed channel with small water-filled conduits at the interface of the helix and the barrel wall. The displacement of the α-helix was attributed to the possible effect of salt and detergent disrupting the interactions between the α-helix and barrel wall, but this proposal was never confirmed. Unfortunately, purified NalP translocator domain lacking the α-helix (NalP TD Δα) did not show stable openings, similar to those postulated to represent NalP with a displaced α-helix. On the contrary, the recordings from the NalP TD Δα showed frequent variable fluctuations, indicating an unstable channel (Roussel-Jazede et al., 2011).

The hemoglobin protease Hbp is an autotransporter from a virulent strain of *Escherichia coli*. Here the passenger domain cleaves human hemoglobin to release heme, which can be used by the bacteria to scavenge iron. Hbp belongs to the family of SPATE (serine protease autotransporters of *Enterobacteriaceae*) autotransporters, which undergo a spontaneous autoproteolytic reaction within the β-domain itself to release the passenger domain (van Ulsen et al., 2014). The structure of an engineered non-cleavable Hbp mutant shows that the structure of the Hbp translocator domain is very similar that of NalP (Tajima et al., 2010). The channel properties of Hbp translocator domain were compared to those of NalP (Roussel-Jazede et al., 2011). Here the Hbp translocator domain was purified from inclusion bodies and was found to have undergone spontaneous cleavage at the site of release of the passenger domain. For this reason, the α-helix appears to be stably lodged within the channel lumen, and only small openings of ~ 0.2 nS were observed. This was in contrast with another Hbp construct, with just one additional N-terminal amino acid ahead of the cleavage side, which showed only the large conductance steps, as in NalP. It is interesting that, whether the cleavage releasing

the passenger domain is intramolecular, as in the case of Hbp, or intermolecular, as for NalP (van Ulsen et al., 2014), the remaining α-helix is likely to efficiently block the channel lumen after translocation, thus preventing leakage of periplasmic components.

C. FHA and FhaC: a Two-Partner Secretion System

The bacterium responsible for whooping cough is *Bordetella pertussis*. In the initial stages of infection, *B. pertussis* adheres to the ciliated and non-ciliated epithelial cells of the upper respiratory tract (Locht et al., 1993). The infection then proceeds to the lungs, which may constitute a bacterial reservoir. A major virulence factor of this bacterium is the filamentous haemagglutinin adhesin FHA, which is secreted by a two-partner secretion system and represents the TpsA exotoxin in this pathway (van Ulsen et al., 2014). FHA is actually derived from a precursor FhaB (Coutte et al., 2001), which reaches the cell surface by translocating in an unfolded confirmation through its cognate TpsB, FhaC (Baud et al., 2014). Upon exit from FhaC, FHA then folds and is proteolytically cleaved to be released into the extracellular milieu (Coutte et al., 2001), although a significant amount of the protein also remains associated with the bacterium. The presence of a carbohydrate binding site on FHA allows it to bind to sulphated polysaccahrides on the ciliated epithelium and macrophages, while binding to non-ciliated cells involves a heparin binding site (Locht et al., 1993; Mattoo et al., 2001). FHA also appears to play a major role in the formation of *B. pertussis* biofilms in the respiratory tract (Serra et al., 2011).

The high-resolution crystal structure of FhaC represented a major advance in the understanding of the two-partner secretions system (Clantin et al., 2007), and confirmed

the predicted domain organization of the protein, which is now known to be a hallmark of the Omp85-TpsB superfamily (Jacob-Dubuisson et al., 2009). The translocation domain is a single 16-stranded β-barrel found at the C-terminus. Two salient features of the β-domain are the fact that it is plugged by the N-terminal α-helix H1, and further obstructed by the presence of a large extracellular loop L6, which folds as a hairpin back inside the β-barrel. Modeling of the FhaC structure with the H1 α-helix removed reveals that the pore delineated by the β-barrel itself has an 8 Å diameter. Two N-terminal POTRA (polypeptide transport associated) domains, canonical features of the members of this family, form a so-called "periplasmic module", and have been shown to recognize the FHA TPS domain (targeting sequence) in an unfolded conformation (Jacob-Dubuisson et al., 2009).

FhaC is one of the first secretion translocons to be investigated by electrophysiology (Jacob-Dubuisson et al., 1999). In planar lipid bilayers, the conductance generated by FhaC in 1M KCl was approximately 1.2 nS. This conductance is similar to that of NalP, and as for this protein, is assumed to represent a configuration where the internal alpha helix is dislodged from the pore (Clantin et al., 2007). FhaC behaves as a predominantly closed channel with frequent well-resolved openings at both negative and positive membrane potentials. At negative voltages, the kinetics revealed the existence of a sub-conductance state. A number of mutated constructs of FhaC have been examined to establish structure-function relationships and gain insight into the mechanism of FhaC. In particular, it was clearly established that the C-terminal 350 amino acids of the protein are responsible for channel activity, although these mutants lacking the first 200 N-terminal residues displayed a noisy kinetic signature, suggesting

some destabilization of the protein (Meli et al., 2006). This domain organization was later validated by the crystal structure (Clantin et al., 2007). The deletion of the inwardly folded loop L6 has drastic functional consequences: (**1**) it abolished secretion of FHA, (**2**) impacted the channel conductance, and (**3**) increased antibiotic sensitivity. This later phenotype, together with the intra-barrel location of the loop, suggests a role for L6 in constricting the channel, and thus its possible displacement upon substrate translocation.

Recently, further insight into the mechanism of channel opening was obtained in an innovative study that combines EPR spectroscopy and electrophysiology to probe the conformational dynamics of the protein (Guerin et al., 2014). The authors reported that FhaC can adopt different conformations, even in the absence of substrates, and in particular that the H1 α-helix can spontaneously slide out of the pore, into the periplasmic side, where it can interact with the POTRA2 domain. Additional experiments suggested that the conformation with H1 displaced into the periplasm is prevalent during substrate secretion. Interestingly, in the course of this study, the authors purified a FhaC variant which contained a sub-population of proteins with an intermolecular disulfide bond linking the extracellular tip of the H1 α-helix to the extracellular loop L7. This variant yielded two types of channel recordings, presumably originating from the two protein populations found in the sample: some had the typical FhaC activity and other displayed very little activity, but could be converted to the regular pattern upon application of a reducing agent during the recording. For this reason, this latter activity was attributed to the population of channels with the intramolecular disulfide bond. These results suggest that hampering the displacement of the H1 α-helix towards the cytoplasm essentially maintains the channel in a constricted conformation and that the sliding of the H1 α-helix

in and out of the pore might correlate with the dynamics of channel activity.

D. Other two-partner secretion systems

Electrophysiological experiments have also confirmed the pore-forming activity of other TpsB proteins, such as HMW1B (Duret et al., 2008), EtpB (Meli et al., 2009), and ShlB (Konninger et al., 1999). In planar lipid bilayer experiments on HMW1B, a TpsB from *Haemophilus influenzae* used for the secretion of an adhesin two levels of current are clearly observed (Duret et al., 2008). The largest one represents a conductance of ~ 1400 pS, a value similar to that of FhaC (1200 pS) (Jacob-Dubuisson et al., 1999) (both in 1 M KCl). The smaller conductance is about 1/4th of the larger one. EtpB also behaves as a pore with clearly defined multiple conductance states (Meli et al., 2009). Interestingly, the smallest one is also 1/4th of the largest one, but an additional, intermediate substate, was also revealed in this case. It is unclear what these substates represent. The HMW1B protein does exist as a tetramer, and it is possible that the different sub-conductance states represent the monomeric and oligomeric form. But, FhaC crystallizes as a monomer, and is believed to function as such. With large, protein-translocating pores, it is often frequent to find sub-conductance states, probably due to some inherent flexibility of the pore constriction itself and the ability of the protein to sample a large number of conformational states.

1.2.6 Chaperone-Usher Pathway

A. General Introduction

While many bacterial species utilize translocons in order to release toxic effectors

into target host cells or the extracellular milieu, translocation machines can also be used for the assembly of pili at the cell surface. For example, uropathogenic *E. coli* utilizes the chaperone-usher pathway for the biogenesis of Type 1 and P pili (Geibel and Waksman, 2014; Kline et al., 2010; Thanassi et al., 2012; Waksman and Hultgren, 2009). Type 1 pili, assembled by the *fim* system, are used in bladder colonization, while P pili, of the *pap* system, are involved in infection of the kidney, leading to pyelonephritis. These pili extend from the cell surface to provide adherence to the host cell epithelium lining the walls of the kidney or urinary tract. This adhesion represents an initial critical step in colonization, and animal studies have shown that pili are essential virulence factors in the disease process (Crepin et al., 2012). Type 1 pili also trigger the internalization of bacteria by the bladder epithelial cells (Martinez et al., 2000), and are required for the formation of intracellular biofilm-like communities in these cells (Wright et al., 2007).

B. Pilus Biogenesis and Structural Features of the Usher

The *fim* and *pap* systems share extensive structural and functional homologies, and the molecular steps taking part in the biogenesis of the type 1 and P pili have been extensively reviewed (Busch and Waksman, 2012; Geibel and Waksman, 2014; Kline et al., 2010; Thanassi et al., 2012; Waksman and Hultgren, 2009). The pili themselves are composite appendages made up of several different types of subunits assembled in a precise stoichiometry and order (Figure 1.1). The terminal subunit plays the role of adhesin and binds to glycolipids or glycoproteins in the host cell membrane. In the Pap system, the secretion machinery comprises a periplasmic chaperone, PapD, and an outer membrane component, the usher PapC. The biogenesis of the pilus begins in the

cytoplasm where all the individual subunits of the pilus and the translocation machinery are synthesized. Each of these subunits contains an N-terminally located signal peptide sequence that targets them for secretion through the Sec translocon into the periplasmic space. Once in the periplasm, the individual pilus subunits associate with the chaperone PapD. This association serves three purposes: (**1**) the PapD chaperone helps to prevent the spontaneous aggregation of pili subunits or assembly of the pilus in the periplasm, (**2**) binding to the chaperone induces the correct folding of the pili subunits into an immunoglobulin-like fold of antiparallel β-sheets, and (**3**) PapD targets the subunits to the base of the PapC usher for translocation and assembly into a functional pilus. Biogenesis of this pilus proceeds in a very sequential step-wise pattern. Due to differential binding affinities, each subunit destined for the pilus rod associates with the PapC usher in a chronological fashion (Li et al., 2010). For example, the adhesive tip subunit, PapG, binds the usher with the highest affinity and is thus always incorporated first. However, it is likely that there are low quantities of the PapG adhesin so as to prevent the incorporation of multiple tip subunits. In addition, another mechanism also prevents the incorporation of additional PapG adhesins as well as functions to polymerize the growing pilus rod. This mechanism is known as donor-strand exchange. As mentioned above, each of the subunits resembles an immunoglobulin-like protein configuration of antiparallel β-sheets. However, *pap* subunits are missing one of these β-sheets, which result in the formation of a binding pocket. Interestingly, the chaperone of the pathway, PapD, has an N-terminal β-sheet extension that binds this groove when PapD associates with a subunit for targeting to the PapC usher. In order for polymerization of the pilus rod to occur, all subunits, with the exception of the adhesin

PapG contains this N-terminal extension. However, their ability to bind the pocket with higher affinity allows them to displace the N-terminal extension of the chaperone and insert themselves as the next step in assembly. Because the PapG adhesin does not contain this extension, it can only be incorporated once into each growing pilus. In contrast, the chaperone has a higher binding affinity for the PapH pocket than any other subunit's N-terminal extension. Consequently, PapH functions as the terminating subunit that anchors the completed pilus rod to the bacterial cell surface (Figure 1.1). Collectively, this repeated sequence of step-wise events for pilus biogenesis is called donor-strand complementation.

Our understanding of the biogenesis process has benefited from major advances in the determination of the three-dimensional structures of the ushers of the *fim* and *pap* systems, FimD and PapC, respectively (Ford et al., 2010; Phan et al., 2011; Remaut et al., 2008). The usher is composed of a twin β-barrel embedded within the outer membrane, and globular N- and C-terminal domains facing the periplasm. Each monomeric β-barrel comprises twenty-four β strands, and a globular plug domain that gates the channel shut. The plug domain extends from two linker regions located at the base of the barrel wall and connecting with β-strands 6 and 7. Additional structural features of importance are a β5-6 hairpin, which constrains the plug domain in place, and an α-helix residing externally to the β5-6 hairpin and stabilizing it. A remarkable snapshot of the translocation process has been provided by the X-ray crystal structure of the complex of the usher, the chaperone and the first pilus subunit of the *fim* system (Phan et al., 2011). The data reveals that the plug domain is displaced from the channel lumen towards the periplasmic side, where it makes extensive contact with the usher N-terminal domain

(Figure 1.1). However, the exact molecular mechanism behind this complex event has yet to be elucidated.

C. Electrophysiological Characteristics of the PapC Usher

Planar lipid bilayer and patch clamp techniques have been used for the analysis of the PapC usher. PapC exhibits a characteristic kinetic signature at relatively low membrane potentials (< 100 mV), which indicates that the usher is a mostly closed, but still extremely dynamic channel. The wild-type (WT) channel exhibits frequent transient openings of small, but varying conductance (50-600 pS in 1 M KCl). These current fluctuations likely originate from ion movements through water-filled conduits that exist at the barrel-plug interface (Mapingire et al., 2009). Interruptions of the current might be due to thermal motion of the plug within the channel lumen or spontaneous conformational changes of the barrel or the periplasmic domains leading to transient occlusions of these small pathways. Initial studies of domain mutants also demonstrated that removal of the plug domain generates a pore with an extremely large conductance (~ 3 nS in 1 M KCl), which, surprisingly, still displays a highly dynamic behavior (Mapingire et al., 2009). The channel tends to spend more time in the open state, but closures remain very frequent. Even in the wild-type channel, occasional spontaneous large transitions of a conductance of approximately 3 nS (in 1M KCl) do occur and are believed to be short plug displacement events (Mapingire et al., 2009). The primary scope of this dissertation revolves around elucidating the molecular mechanism for plug displacement and will be discussed in Chapters 3 and 4.

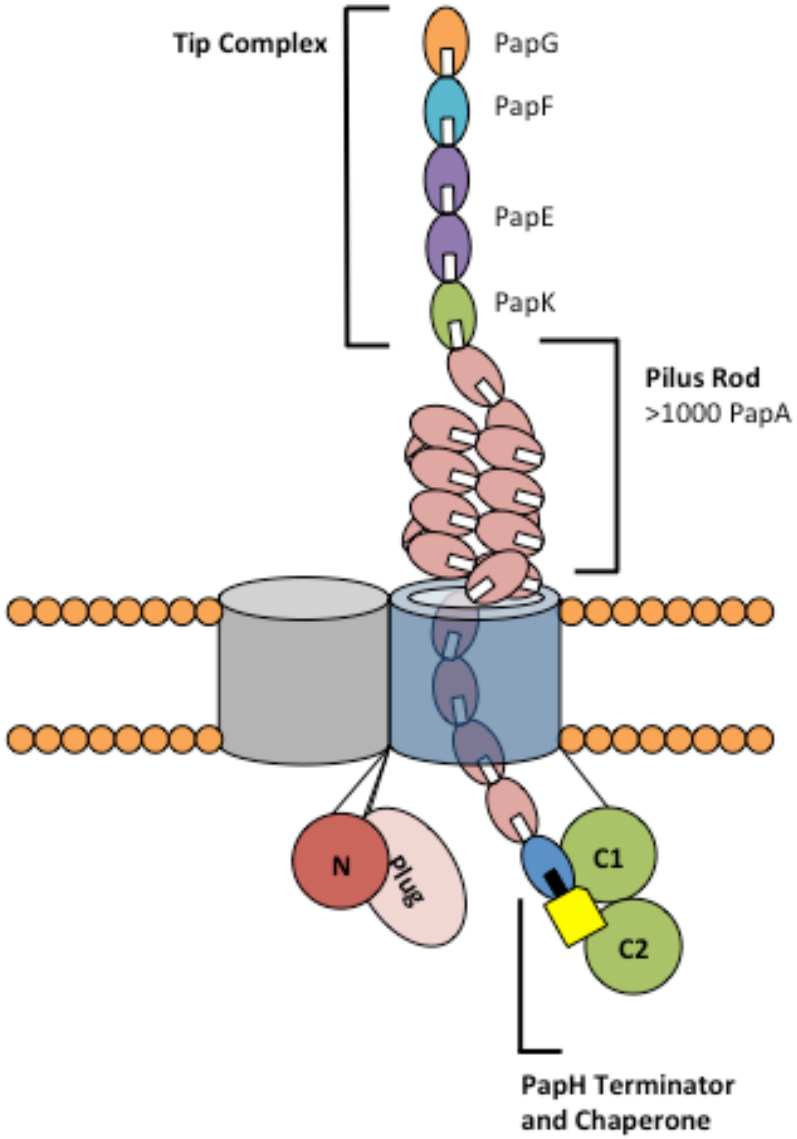

Figure 1.1 Pilus biogenesis via the PapC usher. *Schematic of P pilus biogenesis through a single monomer of the PapC dimer. Inactive barrel is depicted in gray to the left. The plug domain displaces towards the periplasmic side in proximity with the N-terminal globular domain to allow for the translocation of the first subunit, PapG, the adhesive tip protein. The adhesin is subsequently followed by incorporation of PapF, PapE (5-10 subunits), and PapK to comprise the tip complex. This is then followed by the pilus rod which is composed of >1000 PapA subunits. This rod is then completed and anchored to the bacterial cell surface by PapH (blue) and chaperone PapD (yellow).*

1.3 Viral Ion Channels

1.3.1 Viroporins

Similarly to bacteria, viruses also have a wide arsenal of tools to hijack host machinery for replication and expansion. Among these tools is the production of proteins containing 1-2 transmembrane domains (TMD) that have been shown to oligomerize and form ion channels in host cell membranes. It was initially postulated several decades ago that some viral genomes encoded for pore-forming proteins (Carrasco, 1978). However, it was only recently that the identities of these proteins have been discovered. Influenza A virus, for example, encodes for protein M2 that was observed to oligomerize and subsequently cause increases in intracellular pH (Ciampor et al., 1992; Pinto et al., 1992). While this only hinted at the possibility of M2 being a pore-forming protein, voltage-clamp experiments in *Xenopus* oocytes showed that the M2 protein was *indeed* capable of conducting ions (Pinto et al., 1992) and therefore a channel. Furthermore, the anti-viral drug amantadine completely blocked current flux through the M2 channel when the oocyte bath solution was supplemented with the drug (Kozakov et al., 2010; Pinto et al., 1992). Influenza A deficient in M2 protein is highly attenuated and even being considered as a live vaccine (Watanabe et al., 2009). Identification of the M2 ion channel in Influenza A has since then paved the way for the analysis of other viral genomes for pore-forming proteins now commonly referred to as viroporins. In fact, several viroporins have been identified in many viruses including but not limited to: HIV (Gonzalez, 2015; Gonzalez and Carrasco, 2003), Hepatitis C (Madan and Bartenschlager, 2015; Moradpour and Penin, 2013), and Poliovirus (Doedens and Kirkegaard, 1995; Gonzalez and Carrasco, 2003; Martinez-Gil et al., 2011a; Martinez-Gil et al., 2011b).

In contrast to typical ion channels, viroporins are much smaller in size (60-250 amino acids). While there has been little viral channel sequence homology between different viruses, each viroporin identified thus far has been shown to have several distinct structural characteristics (Sze and Tan, 2015). (**1**) Viroporins have been shown to contain at least 1 TMD that is often an amphipathic α-helix (OuYang and Chou, 2014). (**2**) These TMDs often contains an interface that comprises the lumen of the pore they form when oligomerized in the host cell membrane. (**3**) The pores formed can vary widely in the types of ions for which they are selective. For example, the M2 viroporin conducts protons whereas HIV-1's Vpu is cation selective. (**4**) The insertion of these viroporins is typically aided by a cluster of basic residues that promotes association and interaction with negatively charged lipids in membranes. One of the more recent postulated viroporins, non-structural protein 4 (NSP4), shares these characteristics and is encoded by one of the *Reoviridae* family of viruses, Rotavirus (RV).

1.3.2 Rotavirus

RV is the leading cause of acute gastroenteritis in children, and infection often leads to severe dehydration and sometimes death (Parashar et al., 2006). The RV virion contains a triple-layered non-envelope particle that encases the viral RNA genome. Differentiated enterocytes of the small intestine take up RV by means of receptor-mediate endocytosis. Cellular entry then triggers RV to shed its outer layer to leave a transcriptionally active double-layered virion particle that exits the endosome and secretes viral mRNAs into the cytoplasmic space (Trask et al., 2012). Translation of this mRNA into viral proteins produces the components needed to form new double-layered

particles where the replicated viral genome is packaged. Although, there are 6 non-structural proteins encoded by RV, the infectious process is mediated by a viroporin known as Non-Structural Protein 4 (NSP4).

1.3.3 NSP4 and Calcium

In some cases, viruses code for proteins that seek to manipulate ionic gradients within the host cell environment to their advantage. A large majority of these viroporins studied using electrophysiological techniques were found to be either proton-conducting porins such as Influenza A virus' M2 (Pinto et al., 1992; Watanabe et al., 2009) or monovalent cation selective channels such as HIV Vpu (Schubert et al., 1996). Most of the viroporins studied via electrophysiology to date have failed to show selectivity for divalent cations over monovalent cations (Hyser, 2015). There are a select few, however, including the RV viroporin NSP4 which is discussed later in Chapter 5, that are able to conduct divalent cations such as calcium (Hyser et al., 2010; Hyser and Estes, 2015; van Kuppeveld et al., 1997). In particular, these viruses employ their viroporins in order to perturb host cell calcium homeostasis.

In the case of RV, NSP4 is a 28 kDa glycoprotein that is synthesized in the ER membrane. Expression of NSP4 alone is sufficient to raise cytosolic concentrations of calcium significantly (Hyser et al., 2010). This increase in calcium concentration is required by RV for the replication and assembly of more infectious virions. Thus as depicted in Figure 1.2, NSP4 in the ER is believed to form a pore that results in the leakage of calcium stores out into the cytoplasm. This increases the cytosolic calcium concentration. Leakage of ER calcium stores typically triggers the activation of sensor

stromal interaction molecule 1 (STIM1). STIM1 serves to function as a sensor for depleted calcium within the ER (Hogan and Rao, 2015). Once STIM1 senses the shift in calcium concentration in the ER, it relocates to the host cell membrane in order to activate store-operated calcium entry into the cell through Orai1, a known calcium-selective ion channel (Hogan and Rao, 2015). Hyser (2013) postulated that activation of STIM1 and Orai1 would trigger two events in RV pathogenesis: (**1**) it would further increase cytosolic calcium concentrations inducing viral replication, and (**2**) it would also trigger chloride efflux out of the host cell resulting in water efflux and consequently perfuse diarrhea (Figure 1.2). While there had been some preliminary data hinting to the role of NSP4 as a pore-forming viroporin (Hyser et al., 2010), in our studies documented in Chapter 5, we seek to identify NSP4 as a channel capable of conducting ions as well as characterize it as a calcium channel.

1.4 Scope of the Dissertation

It is currently known that the usher of the *fim* chaperone-usher system of *E. coli*, through which the fimbriae assembles and translocates, is gated closed by a plug domain. Crystallographic data captured a snapshot of the biogenesis process mid-translocation. It revealed that the plug domain of the usher is displaced towards the periplasmic side such that the assembling subunits can translocate across the barrel lumen (Phan et al., 2011). Because of the homology with *fim*, we believe that the plug domain of PapC, the usher used for the biogenesis of the P pilus, must also displace towards the periplasm in order to facilitate pilus assembly. However, the exact molecular mechanism underlying plug displacement in the PapC usher is unknown. Although electrophysiological techniques

are typically used to study ion channels, it has also been used to characterize these larger secretion machines, comprising pore-forming proteins, as described above. With the growing trend of antibiotic resistance, the identification of this key event in uropathogenic *E. coli* (UPEC) virulence could provide us with a novel target for drug design and therapy. For example, strains of *Yersinia pestis* deficient in the chaperone-usher pathway were attenuated for virulence relative to the WT strain (Hatkoff et al., 2012). In our studies, we have sought to establish a foothold in this area by investigating structure-function relationships in PapC, in particular by analyzing two distinctly separate yet collaborative networks of residues within the PapC usher that may be responsible for plug domain gating. In one approach, we have explored the existence of a very distinct signal propagation pathway that ultimately triggers a large global conformational change resulting in displacement of the plug for pilus biogenesis. Similarly, we have also explored a network of residues that could potentially function to gate the plug domain through direct electrostatic residue-residue interactions. Together, both networks of residues are believed to participate in the events leading to plug displacement after initial chaperone-subunit binding to the usher, and electrophysiological techniques helped us elucidate this mechanism through usher mutant analysis.

The same electrophysiological techniques also helped us identify and characterize a member of a relatively new class of channels encoded by viruses, called viroporins. Currently, electrophysiological analyses of viroporins have shown that there are no viral ion channels with selectivity for divalent cations over monovalent cations (Zhou et al., 2009). Calcium homeostasis, however, is postulated to be a prime target for disruption by viroporins in order to facilitate and promote viral replication as a part of the infectious

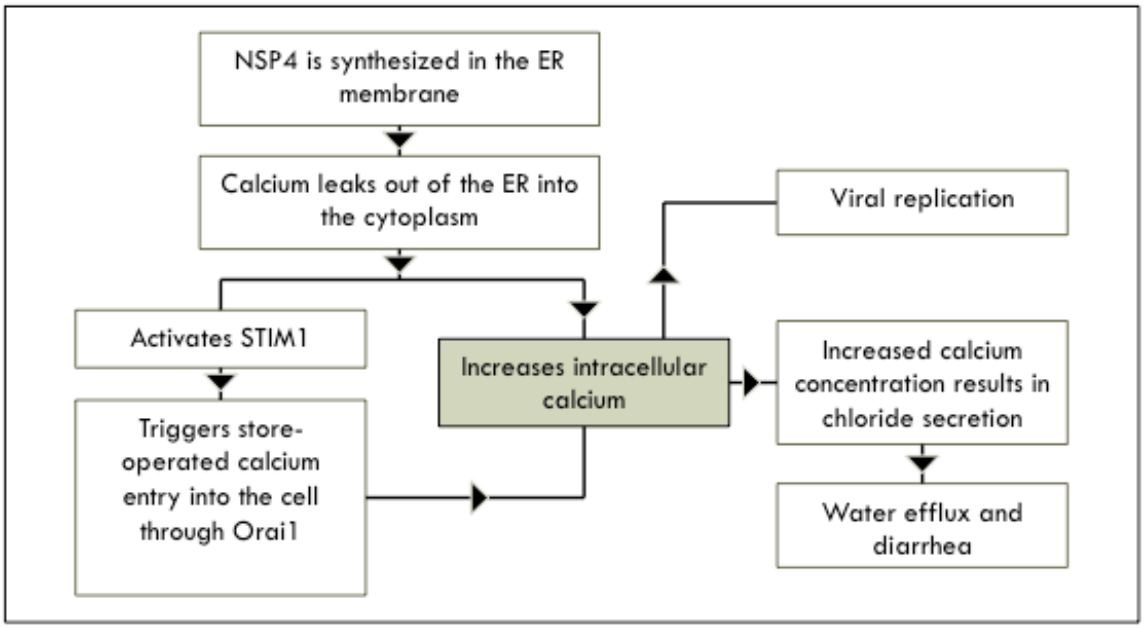

Figure 1.2 Flowchart of calcium manipulation as predicted to be triggered by NSP4. *The flowchart illustrates the model of the cellular events initiated by the rotavirus viroporin NSP4 that take part in the infectious process.*

process (Zhou et al., 2009). A large majority of studies on viroporins only demonstrate calcium conductance through indirect and non-electrophysiological means such as fluorescent calcium imaging. However, in our studies, we utilized planar lipid bilayer and patch-clamp techniques to establish RV NSP4 viroporin as a *bona fide* channel. We also utilized electrophysiology to demonstrate that NSP4 can conduct divalent ions such as calcium and barium. Although research into this field is still in its infancy, we have also come to document a series of procedures required to optimize the study of the viroporin NSP4.

In this dissertation, we will focus on the electrophysiological analysis and characterization of two microbial channels: the PapC usher of UPEC and the NSP4 viroporin of rotavirus.

CHAPTER 2

Materials and Methods

2.1 Strains

E. coli strain DH5α (Grant et al., 1990) was used for the construction of PapC mutants. Strain AAEC185 (Blomfield et al., 1991) was used for HA assays, and the porin-deficient strain BL21(DE3)Omp8 (Prilipov et al., 1998) was used for PapC usher purification. The plasmid pDG2 codes for a wildtype (WT) PapC usher with a C-terminal, thrombin-cleavable hexahistidine-tag as described previously (Li et al., 2004), and new mutants were engineered and derived from this plasmid. For expression, bacteria was grown in LB broth containing 100 μg/ml ampicillin at 37^{o} Celsius with aeration. In order to induce protein expression, 0.1% of L-arabinose was added at a cell density A_{600} of 0.6 for 2 hours.

2.2 Protein Preparations

2.2.1 PapC Allosteric Network Mutants

PapC plasmid construction, expression, and purification for the WT usher and all allosteric network mutants were performed initially by Gilles Phan and later by Sebastian Geibel, in the laboratory of Gabriel Waksman. Mutant and WT proteins were expressed from the pDG2 plasmid (Li et al., 2004). The pDG2 plasmid encodes for WT PapC containing a thrombin cleavage site and hexahistidine-tag located on the C-terminus (Li et al., 2004). Mutations were introduced in the *papC* gene using the QuikChange Site-Directed Mutagenesis Kit (Stratagene). DNA sequence analysis was utilized to confirm the correct mutation. Furthermore, expression of each mutant PapC was compared against the WT via outer membrane (OM) isolation and SDS-PAGE analysis. Stability of each protein in the OM was then tested using a heat-modifiable mobility assay as

described previously (Henderson et al., 2011). In order to test for the ability to form functional pili, PapC WT and mutants were subjected to a hemagglutination assay (Henderson et al., 2011). The results reported the maximum-fold dilution of PapC-expressing bacteria to still agglutinate red blood cells. A high titer indicates the presence of pili at the cell surface. Bacteria expressing WT and mutant PapC were also assayed for antibiotic sensitivity to identify ushers with particularly "leaky" or open phenotypes compared to the WT (Farabella et al., 2014). "Leaky" usher phenotypes were identified by increased antibiotic sensitivity revealed by larger zones of bacterial clearing. Likewise, the presence of closed ushers was indicated by smaller zones of clearing compared to the WT.

The WT and mutant PapC proteins were purified from the bacterial outer membrane as previously described (Mapingire et al., 2009). The purified protein product was stored in a 20 mM Tris-HCl pH 8.0 buffer containing 120 mM NaCl, 5 mM Lauryldimethylamine oxide (LDAO) detergent, and 25% glycerol. This resulting protein sample (2-5 mg/ml) was delivered to our laboratory encased in ice packs overnight for electrophysiological analysis and characterization primarily in planar lipid bilayer. Received samples were aliquoted and stored at 4° Celsius. Prior to experiments in planar lipid bilayer, protein samples were diluted in a 1% detergent-buffer solution described in Section 2.3.3.

2.2.2 PapC Electrostatic Network Mutants

PapC plasmid construction, expression, and purification for the WT usher and all electrostatic network mutants were performed initially by Nadine Henderson and then

later by Glenn Werneburg, in the laboratory of David Thanassi. The plasmid utilized was pDG2, which encodes for WT PapC containing a thrombin cleavage site and hexahistidine-tag located on the C-terminus (Li et al., 2004). All alanine substitution mutants were derived from this plasmid using QuikChange Site-Directed Mutagenesis from Stratagene and expressed in the bacterial outer membrane as described (Mapingire et al., 2009). All mutants were checked for correct construction via DNA sequencing analysis. The WT and mutant PapC proteins were purified from the bacterial outer membrane as previously described (Mapingire et al., 2009), except that the protein was not subjected to gel filtration chromatography. Instead, following removal of the His-tag by thrombin digestion, the protein was passed over a metal affinity column coupled to a benzamidine column, as described (Werneburg et al., 2015). While this method is not as effective as a gel filtration column for the separation of dimers and monomers, it saved time and the majority of proteins reconstituted in liposomes are dimeric based on electrophysiological experiments. The purified protein product was stored in 20 mM Tris-HCl pH 8.0 buffer containing 120 mM NaCl and 5 mM LDAO detergent but lacked 25% glycerol compared to the protein preparations created by Gilles Phan. Preparations from the Waksman Lab tended to remain more stable over longer periods of time than those received from the Thanassi Lab by several months. It is believed that the addition of glycerol to the storage buffer may play a vital role in stabilizing PapC protein samples. These protein samples had a typical concentration ranging between 0.30-0.80 mg/ml and were delivered to our laboratory encased in either ice packs or dry ice for electrophysiological analysis and characterization primarily in patch-clamp. Prior to patch-clamp experiments, PapC protein was prepared via reconstitution into liposomes

described in section 2.3.2A.

The PapDG chaperone-adhesin complex was purified by Nadine Henderson in the Thanassi laboratory according to a published protocol (Henderson and Thanassi, 2013) and stored in a 20 mM 2-(N-morpholino)ethanesulfonic acid (MES) pH 5.8 buffer containing 250 mM NaCl. However, because it was eluted off of the chromatography column in a slope gradient, the NaCl concentration may vary by +/- 10 mM. Received samples were aliquoted and stored at 4° Celsius.

2.2.3 NSP4 Viroporin

A. Synthetic Peptides

The NSP4 viroporin was provided to our laboratory by Joseph Hyser at Baylor College of Medicine. Several constructs were designed and synthetic peptides were provided by LifeTein LLC as follows in Figure 2.1:

*(**1**) Short Peptide (47-90) encompassing the Viroporin Domain (VPD)*

*(**2**) Long Peptide (47-139) encompassing the VPD and Coiled-Coil Domain*

*(**3**) Full Length NSP4 (1-175)*

*(**4**) C63S/C71S Mutant Short Peptide (47-90)*

Peptides were provided lyophilized typically in aliquots of either 0.1 mg or 1 mg stored at -20° Celsius. Peptides were initially dissolved in a dimethyl sulfoxide (DMSO) solvent to achieve a stock concentration of 1-2 mg/ml. The resulting samples were stored at 4° Celsius. However, various issues arose from this particular method of preparation. It was discovered that peptides dissolved in DMSO were only functional for approximately one week. Initially it was believed that peptide storage in DMSO was rendering the

peptide inactive over time. In order to alleviate this, fresh aliquots of peptides were often resuspended in DMSO and used within the week. However, inconsistencies in reconstitution and observed channel activity still occurred after some time. It was then observed that DMSO as well could deteriorate quickly over time upon first exposure to air. To solve this issue, septum-sealed bottles of DMSO were used to prolong the shelf life of DMSO. It was also observed that storage in 4° Celsius led DMSO to crystallize possibly causing the peptide to precipitate out. Storage at room temperature resulted in more consistent reconstitution over the course of the week, however, deterioration of activity still occurred after a week. Because only minute amounts of peptide were required for each experiment, DMSO was a rather costly means of dissolving the viroporin. Consequently, several other different solvents were tested for a suitable means of long-term storage. The peptide dissolved well in n-n-dimethylformamide (DMF), but activity proved rather inconsistent relative to that seen with DMSO. Similar results were observed when the viroporin was dissolved in either 2,2,2-trifluoroethanol (TFE) or ethanol. Surprisingly, although particularly hydrophobic in nature, peptides dissolved quickly in water. Water-dissolved samples stored at room temperature remained active for several months and reconstituted just as well as freshly dissolved peptide in DMSO. Water was then chosen to be the solvent of choice for viroporin peptide. The table below summarizes all the different solvents used for each peptide (Table 2.1).

B. Microsome Preparations

Microsome fractions were prepared by Joseph Hyser from insect cells infected with a Baculovirus Expression Vector System for nuclear expression of NSP4 viroporin

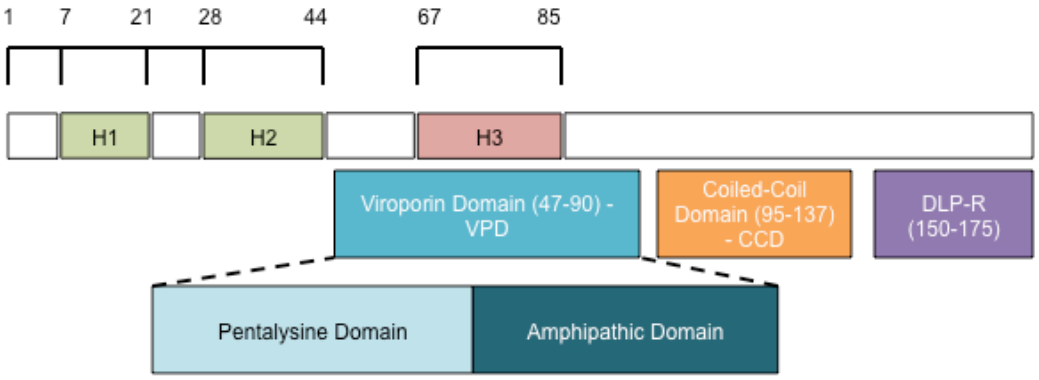

Figure 2.1. Structural domains within the NSP4 viroporin. *Characteristic regions within the NSP4 viroporin that were selected for peptide synthesis. H1, H2, and H3 are all hydrophobic domains within the viroporin. H1 is believed to protrude outward from the ER and H2, specifically, directs the insertion of the viroporin into the ER. H3 comprises an amphipathic α-helix presumed to line the wall in the oligomerized state of the VPD pore.*

Construct	*DMSO*	*DMF*	*TFE*	*OPOE*	*Water*	*Ethanol*
*Short Peptide (**1**)*	*X*	*X*	*X*	*X*	*X*	*X*
*Long Peptide (**2**)*	*X*	*X*	*X*			
*Full Length Peptide (**3**)*	*X*			*X*		
*C63S/C71S Short Peptide (**4**)*	*X*				*X*	

Table 2.1 NSP4 constructs and solvents used. *"X"s denote solvents that were attempted for the respective NSP4 constructs.*

(Viskovska et al., 2014). These microsomes were then resuspended in 50 mM KCl and 5 mM Hepes at pH 7.2 for reconstitution into liposomes suitable for patch-clamp. For liposome preparation, a stock solution of 10 mg/ml asolectin (1,2-Diacyl-*sn*-glycero-2-phosphocholine Type II-S) in 5 mM Tris buffer pH 7.2 was sonicated to clarity with a microtip sonicator probe. One-ml aliquots of this solution were frozen at -60° Celsius in an acetone bath and subsequently thawed at room temperature twice in order to form multilamellar liposomes. Microsomes were then added to 500 µl of freeze-thawed asolectin at the desired protein: lipid ratio (1:100 – 1:3000, w:w) prior to using the dehydration-rehydration method for reconstitution, as described in 2.3.2.

2.3 Electrophysiology

2.3.1 Materials and Buffers

Lipid asolectin (1,2-Diacyl-*sn*-glycero-2-phosphocholine Type II-S) was purchased from Sigma. Phosphatidylcholine, phosphatidylserine, and cholesterol in chloroform were obtained from Avanti Polar lipids. All salts (KCl, $MgCl_2$, $CaCl_2$, $BaCl_2$,

NaCl), Hepes, MOPs, K-EDTA, and sucrose were also obtained from Sigma Aldrich with at least >99.0% purity. Planar lipid bilayer chambers were custom-made in-house at the University of Houston. Polytetrafluoroethylene (PTFE, Teflon) film (Goodfellows) with 10 μm thickness was used between bilayer chambers. A High-Frequency Spark Tester PPM MK3 (Buckleys Ltd.) was used to puncture a hole in the teflon film. Hexadecane was obtained at TCI and pentane from high purity solvent grade from Burdik & Jackson. N-Octyl-oligo-oxyethylene (OPOE) from Alexis Inc. was utilized as a detergent for dilutions of purified protein.

A probe sonicator (Fisher Scientific 550 Sonic Dismembrator) was used for sonication of asolectin in Tris buffer. Biobeads were obtained from Biorad for detergent removal. Fisherfinest premium microscope slides (3" x 1" x 1.00 mm) were used for proteoliposome suspensions during the dehydration-rehydration reconstitution method. Petri dish filters for rehydration were obtained from VWR (size 9.0 cm, qualitative 413). Glass capillary tubes for patch-clamp obtained from Drummond Scientific were heated and pulled using a P87 pipette puller from Sutter Instruments to form micropipettes. The filament utilized in the pipette puller was a trough filament from Sutter Instruments.

The following are the composition of buffers used in planar lipid bilayer and patch-clamp experiments described below (Table 2.2 and 2.3):

2.3.2 Reconstitution Protocols

A. Dehydration-Rehydration Method

The dehydration-rehydration method for liposome formation was described

previously (Delcour et al., 1989). This method for protein reconstitution was primarily used to incorporate PapC into asolectin liposomes for patch-clamp analysis. Asolectin solution was prepared first by sonicating to clarity a mixture of 10-mg/ml asolectin in 5 mM Tris buffer pH 7.2 utilizing a microtip sonicator probe. Purified PapC protein was incubated in 500 µl (5 mg) of this asolectin solution at a protein:lipid ratio between 1:2000 and 1:3000 (w:w) for 1 hour on a test tube rotator. At the same time, biobeads were washed in a test tube with methanol by simple inversion. The methanol was decanted into waste disposal and beads were placed onto Kimwipes and blotted to absorb excess methanol. This was left to air-dry for 30-60 minutes to ensure all methanol had evaporated. Twenty mg of these biobeads were then added to the protein/lipid mixture in order to remove detergent and to promote the reconstitution of PapC into the liposome membrane. This incubation proceeded for 3 hours with rotation. Four-hundred fifty µl of this mixture per tube was then pelleted down in a Beckman Optima TL ultracentrifuge using a TLA100.2 rotor at 90,000 RPM (287,582 avg. RCF and 352,901 max RCF) for 15 minutes at 4° Celsius. Supernatant was discarded and the pellet resuspended in 50 µl of 10 mM MOPS buffer pH 7.2 supplemented with 5% ethylene glycol. The total volume was measured and aliquoted into 3 equal drops onto premium microscope slides that had been wiped with Kimwipes prior. These slides were placed within a dessicating unit containing blue-indicator drierite at 4° Celsius for 3.5-4 hours. Each droplet was rehydrated overnight in buffer A in an amount calculated such that the final lipid concentration equates to 90 mg/ml per drop. This final step induces swelling of large multilamellar liposomes. The next day, 5 µl of this droplet suspension can be added directly to the patch-clamp bath chamber for electrophysiological analysis.

Planar Lipid Bilayer	
Buffer	***Composition***
Buffer T	*1 M KCl, 5 mM Hepes, pH 7.2*
Buffer A	*150 mM KCl, 5 mM Hepes, pH 7.2*
Buffer CA	*75 mM $CaCl_2$, 5 mM Hepes, pH 7.2*

Table 2.2 Planar lipid bilayer buffers.

Patch-Clamp	
Buffer	***Composition***
Buffer B	*20 mM $MgCl_2$, 150 mM KCl, 5 mM Hepes, pH 7.2, 10 μM $CaCl_2$, 0.1 mM K-EDTA*
Buffer A	*150 mM KCl, 5 mM Hepes, pH 7.2, 10 μM $CaCl_2$, 0.1 mM K-EDTA*
Buffer CA	*75 mM $CaCl_2$, 5 mM Hepes, pH 7.2*
Buffer BA	*75 mM $BaCl_2$, 5 mM Hepes, pH 7.2*
Buffer NA	*150 mM NaCl, 5 mM Hepes, pH 7.2, 10 μM $CaCl_2$, 0.1 mM K-EDTA*

Table 2.3 Patch-clamp buffers. *The table above lists the most common buffers utilized in the patch-clamp technique. The $CaCl_2$ in buffer A, B, and NA is used to stiffen liposome bilayers for patching.*

B. Cloud Technique Method

This previously described technique (Battle et al., 2009) was modified for our use. Asolectin was dissolved in chloroform at a stock concentration of 10 mg/ml. Interestingly, it was observed that attempting to use the mixture immediately failed to produce a liposome cloud. Thus, the chloroform-lipid mixture was left at room temperature for 30-60 minutes under low-light settings. Two hundred µl of this stock solution (2 mg of lipid) were added to a 0.5 DRAM glass vial and dried under nitrogen stream to form a film along the inner walls of the DRAM. In order to produce an evenly distributed film along the lower walls of the DRAM, the vial was rotated slowly while directing the nitrogen stream at an angle (Figure 2.2).

An initial gas pressure of 0.4 bar provided a stable stream that could be directed at an angle against the wall of the vial without splashing the chloroform mixture. The pressure was increased to 0.6 bar once approximately half of the chloroform remained. Five µl of deionized water is then added to pre-wet the lipid film according to the published procedure (Battle et al., 2009). However, preparations made omitting this step produced perfectly functional proteoliposome clouds. This may have been because 5 µl of water was not a sufficient amount to pre-wet enough of the lipid film to make a substantial difference. One ml of 0.4 M sucrose in water was then added to this lipid film and incubated at 45° Celsius on an orbital water-bath shaker at 150 RPM for 3 hours. Temperatures below 45° Celsius resulted in very poor and suboptimal liposome cloud formations. It was observed, however, that phosphatidylserine lipids alone did not form a cloud of liposomes but rather a large ribbon within the DRAM, and liposomes from this ribbon did not blister. On the other hand, phosphatidylcholine lipids alone and

phosphatidylcholine lipids supplemented with 10% cholesterol were not able to form liposome clouds at all. Asolectin supplemented with 10% cholesterol tended to form larger than normal liposome clouds. Once a cloud of liposomes had swelled within the DRAM after the 3-hour incubation, protein was added at the desired protein: lipid ratio and further incubated overnight with shaking as above. The next morning, the DRAMs were removed from the orbital shaker and chilled at 4° Celsius for 2 hours in order to stiffen the liposomes for patch-clamp. Subsequently, 3 µl of liposomes were gently taken from the liposome cloud and added directly to the patch-clamp bath chamber for patch-clamp experiments.

For reconstitution of NSP4 viroporin, pure asolectin liposomes or asolectin liposomes supplemented with 10% cholesterol were used. The protein: lipid ratio ranged between 1:20 and 1:200 (w:w) using NSP4 dissolved in either DMSO or water at a stock concentration of 2 mg/ml. Thus, 50 µl or 5 µl, respectively, were added directly to the DRAM without disturbing the liposome cloud by dispensing the protein-solvent mixture against the wall away from the cloud. This was left to further incubate overnight. In the morning, the DRAM was removed from the orbital shaker and placed at 4° Celsius for 2 hours in order to stiffen the bilayers for patch-clamp analysis.

In the case that a protein dissolved in detergent is used for reconstitution, the cloud was first made by a 3-hour incubation in the orbital shaker following the method described above. The protein was then added and incubated for a further 2 hours for reconstitution. At the same time, biobeads were washed in a test tube with methanol by simple inversion. The methanol was decanted into waste disposal and beads were placed onto Kimwipes and blotted to absorb excess methanol. This was left to air-dry for 30-60

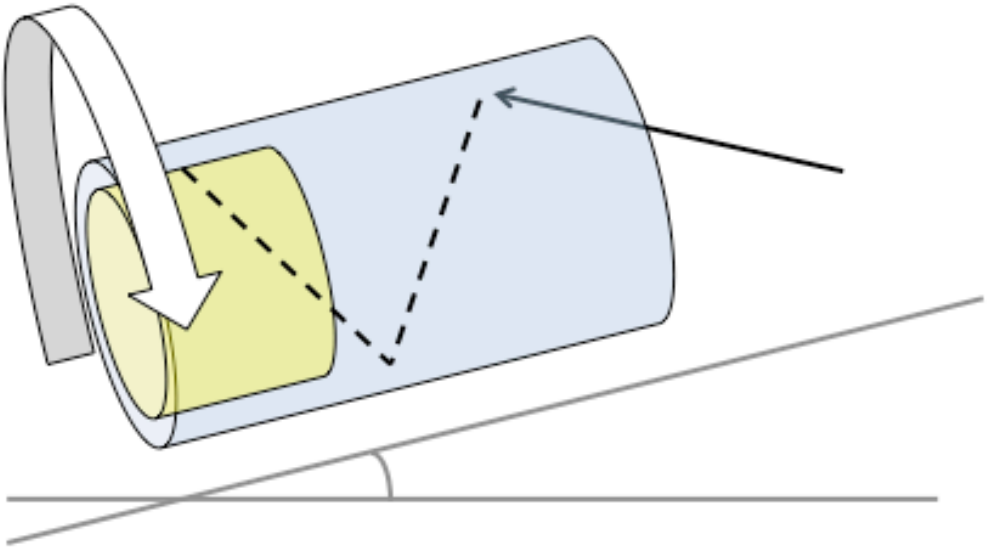

Figure 2.2 Drying chloroform-asolectin under nitrogen stream. *The blue cylinder represents the 0.5 DRAM vial used in the cloud-liposome method. The yellow cylinder inside represents the chloroform-lipid mixture. The DRAM must be rotated at an angle slowly while directing the nitrogen stream also at an angle against the wall. This causes the stream to swirl down the vial. As a result, it helps to prevent the nitrogen from splashing the chloroform-lipid mixture high up on the wall where the resuspension solution cannot come into contact with it. It also helps to dry the film evenly along the wall.*

minutes to ensure all methanol had evaporated. Twenty milligrams of these biobeads were then added to the DRAM in order to remove detergent. Care was taken in adding the biobeads as they could very easily destroy the liposome cloud. Biobeads were not removed and left incubated overnight. After overnight incubation, the DRAM was chilled at 4° Celsius for 2 hours in order to stiffen the bilayers. A 3-µl aliquot of liposomes was removed from the liposome cloud while taking care not to aspirate any biobeads into the pipette tip, and placed in the patch-clamp chamber.

2.3.3 Planar Lipid Bilayer

In the planar lipid bilayer technique for electrophysiological analysis, two halves of a chamber were separated by a 0.01 mm-thick Teflon film. Within the center of the Teflon film, an aperture measuring approximately 100 µm in diameter was created utilizing a High-Frequency Spark Tester PPM MK3 adjusted to 45 kV. A single lipid bilayer would be formed over this aperture. In order to create a hydrophobic interface to attract lipids, the aperture was treated with a 1% hexadecane in pentane solution and allowed to dry for 15 minutes. One and a half ml of buffer T or A was added to each half of the chamber as depicted in Figure 2.3A. Five µl of the asolectin mixture dissolved in pentane at a concentration of 5 mg/ml was added to the surface of the buffer on both sides. Electrodes attached the CV-4B headstage (Axon Instruments) were then inserted into holes pre-drilled into the chambers to come into contact with buffer (Figure 2.3C). The chamber-electrode configuration was then allowed to equilibrate for 10-15 minutes before adjusting the junction null on the amplifier to 0. Subsequently, lowering and raising the volume of the buffer-lipid mixture utilizing a 1 ml syringe in one of the half

chambers caused the spontaneous formation of a lipid bilayer over the aperture. The formation of a stable bilayer was indicated by an increase in resistance in the electric circuit. A transmembrane voltage of + or - 90 mV was then applied to check membrane stability for 10 minutes. This was also performed to ensure that there were no contaminations or channel-like activity prior to the addition of channel-forming protein. If contaminants or an unstable baseline were observed, the chamber was taken apart and cleaned for re-preparation. In cases where different proteins were investigated with the same chamber, the chamber was first thoroughly cleaned by soaking in a beaker containing a 10% ethanol solution. This was placed in sonicating bath for 1-hour in order to ensure that no contaminating protein or reagent remained adhered to the chamber. If the stability test showed no contaminants and a stable baseline, then protein was added to one half chamber, defined as the *cis* side. A membrane potential of + or - 90 mV and stirring of the *cis* side were typically used to promote insertion. Channel insertion was detected by the appearance of channel activity. Once channel activity was detected, stirring was stopped to limit further insertions.

An aliquot of the PapC WT or mutant sample containing 8 μg of protein was diluted 1:1 with a 1-2% OPOE solution in buffer T or A. This whole mixture was then added to one half of the chamber. The presence of extra detergent in the added protein sample typically helped the insertion process. NSP4, however, was added directly from its stock in quantities between 4.0-8.0 μg.

2.3.4 Patch-Clamp

In the patch-clamp electrophysiological technique, purified protein or peptides

were first reconstituted into asolectin liposomes at the desired protein to lipid ratio (see Sections 2.3.2 A and B above). These proteoliposomes were added to a bath chamber depicted in the figure below (Figure 2.4 A and B). This chamber contained a small inlet that allowed for the perfusion of bath solutions (Figure 2.4 A and B). It initially flowed into a smaller reservoir that served as a bubble trap in order to maintain a stable patch during perfusion. This trap communicated with the main bath chamber where proteoliposomes were added. A electrode holder containing 3 M KCl in water and an agar-bridge also made in 3 M KCl contacted the bath solution in the main bath chamber and acted as a reference electrode. In order to promote the formation of unilamellar blisters containing our reconstituted proteins, the proteoliposomes were incubated for approximately 15 minutes in a 20 mM $MgCl_2$-containing buffer, buffer B. A small capillary micropipette of 10-MΩ resistance was filled with buffer, typically buffer A. An Ag/AgCl electrode with pellet was then inserted into this micropipette such that buffer A covered just the pellet. The pipette was immersed in the bath with constant positive pressure and micro-manipulated to come into contact with the unilamellar blister. A seal was formed between the glass of the micropipette tip and the bilayer utilizing gentle suction to achieve a resistance between 1 - 10-GΩ. This patch of membrane that resided within the tip of the micropipette was brought into the air briefly to excise the patch and leave only a single bilayer at the tip of the micropipette. Low resistance seals were often indicative of either poor seal between the glass and the membrane or the presence of a large and predominantly open channel. On the other hand, extremely high seals often indicated that the patch was lacking in any reconstituted channel protein. Once the patch had been excised and channel activity observed, the bath solution was perfused out for

Figure 2.3 General concept behind planar lipid bilayer electrophysiology. *(**A**) Top view schematic of the two halves of a planar lipid bilayer chamber separated by a Teflon film with a 100-μm aperture. Each cylindrical half chamber and the walls of the half chamber are shown as black lined circles. These were the regions where buffer and lipids were placed is depicted in light blue. A stir bar was often used on the cis side of the chamber to promote insertions and is indicated by the white cylinder and rotating arrowheads. Pre-drilled holes in teal were locations for the electrodes to be inserted for contact with buffer. Pre-drilled holes in red were locations for 1 ml syringes for lowering and raising the chamber solution. A screw that clamps the chamber in place is depicted in green. A grounding wire with alligator clamps was always used between this screw and the faraday cage. (**B**) Side view schematic of two halves of a planar lipid bilayer chamber depicting the monolayer of lipids and the added protein on the cis side. The aperture is depicted in a zoomed view to showcase presumed bilayer formation. (**C**) Electronics configuration for planar lipid bilayer.*

A.

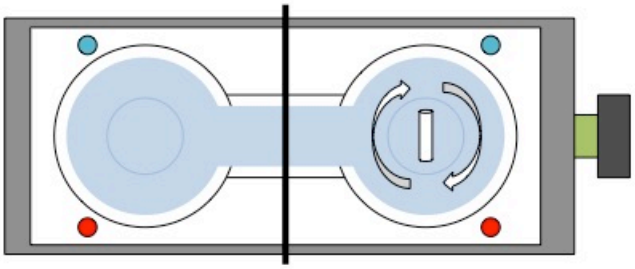

B.

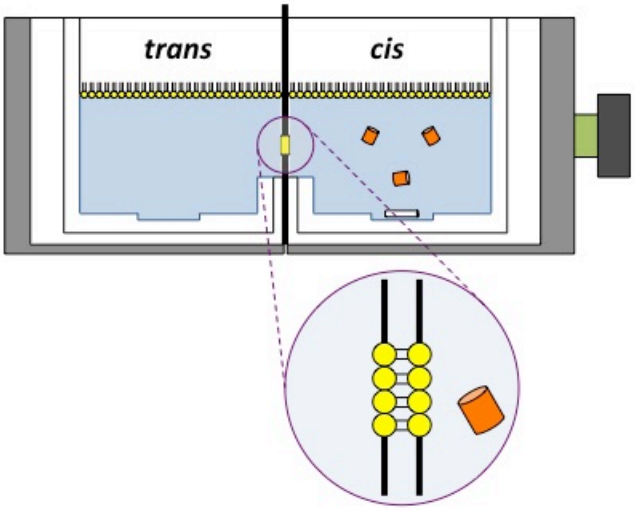
trans
cis

C.

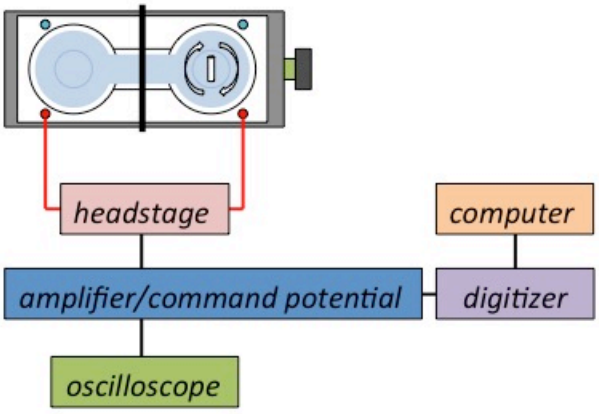
headstage
computer
amplifier/command potential
digitizer
oscilloscope

Figure 2.4 Patch-clamp electrophysiology. ***(A)*** *Patch-clamp chamber configuration depicts a solution filled inlet (blue) connecting the bubble trap reservoir with the main bath chamber reserved for proteoliposomes indicated in yellow.* ***(B)*** *Depiction of the reference electrode location within the main bath chamber (dotted red lines) and an enhanced view of micropipette contact with a unilamellar blister containing channel-forming proteins (dotted blue lines).* ***(C)*** *Representation of the electronic configuration used in patch-clamp.*

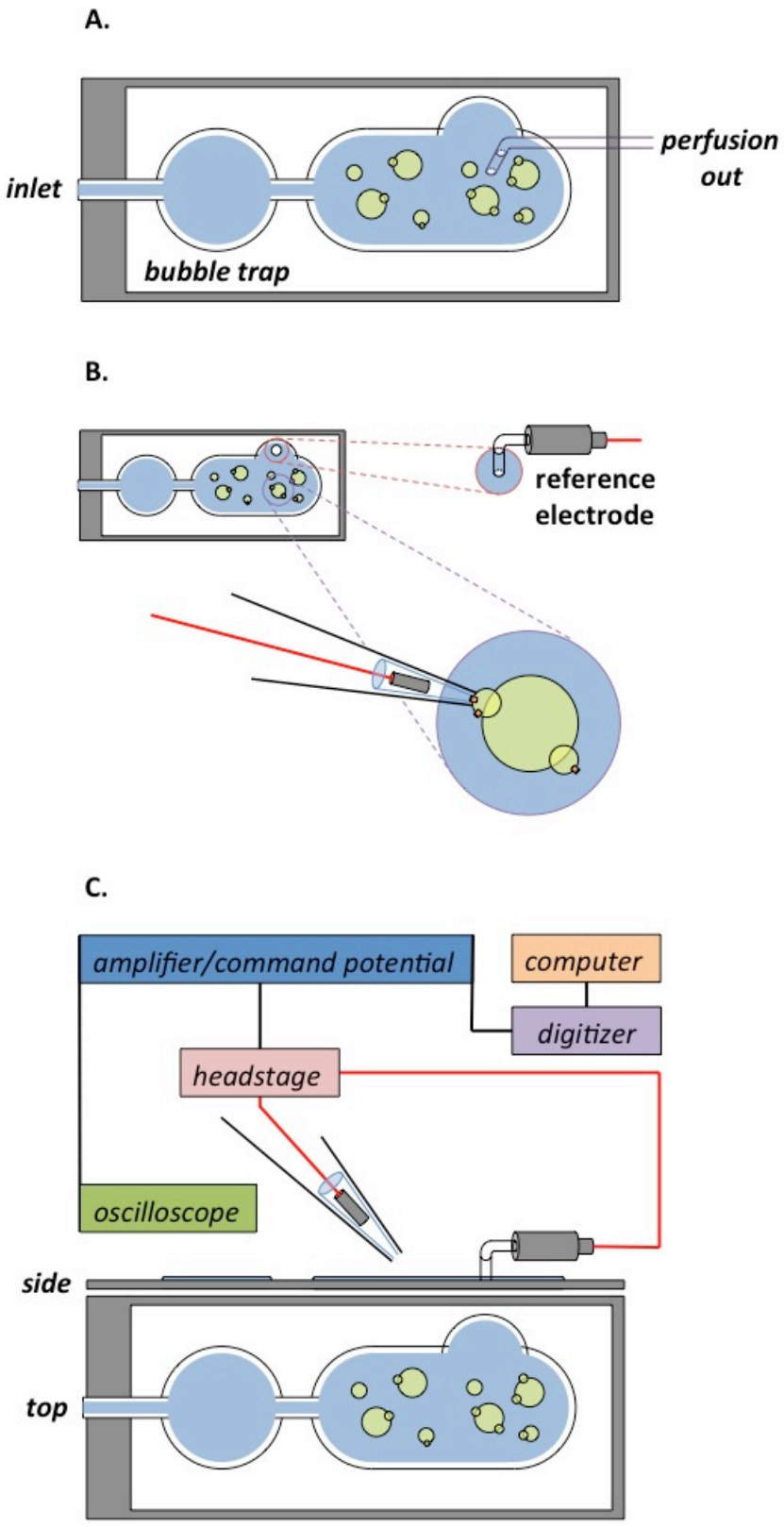
A.
inlet
perfusion
out
bubble trap
B.
reference
electrode
C.
amplifier/command potential
computer
digitizer
headstage
oscilloscope
side
top

buffer A in order to record in symmetric ionic conditions. In some cases, buffers CA, BA, and NA were used in the pipette; however, buffer B was always used to promote blistering.

2.3.5 Data Acquisition and Analysis

Recordings of electrophysiological traces were made by measuring currents under voltage-clamp. In planar lipid bilayer, the *trans* side is grounded. An Axopatch 1D amplifier (Axon Instruments) with a CV-4B headstage was used to record currents of inserted channels. The current was filtered at 500 Hz through a low-pass Bessel filter. For recordings up to 10 minutes, currents were digitized at 1.25-ms sampling intervals (ITC-18, Instrutech). For shorter high-resolution recordings of 1-2 minutes, the currents were filtered at 1 kHz and sampling at a rate of 100 μs sampling intervals. For patch-clamp experiments, the Axopatch 1D amplifier was used with a CV-4 headstage. The reference electrode (World Precision Instruments) was in contact with the bath solution via a 3 M KCl agar bridge. Currents were filtered at 1 kHz with a low-pass Bessel filter and sampled at 100 μs intervals for high-resolution single channel recordings. Electrophysiological recordings were digitized using the Acquire software version 5.0.1 (Bruxton). The raw data outputted by Acquire was then converted from digital units (DU) to current values utilizing Sigmaplot 11.0 using the following equation: $pA = (1000*DU)/(\alpha*\beta)$ where DU=Digital Units (raw data from Bruxton Acquire). Analysis of the electrophysiological traces was performed with the Clampfit program version 9.0 (Axon Instruments). Ohm's Law was used to calculate the channel conductance from the current of distinct channel opening events.

CHAPTER 3

Control of PapC Plug Displacement by an Allosteric Network of Residues

Parts of this chapter are published in:

Farabella, I et al. (2014) "Allosteric Signalling in the Outer Membrane Translocation Domain of PapC Usher", eLife 3: e03532.

3.1 Allosteric Network Identification

3.1.1 PapC Structure

The PapC usher is composed of a twin β-barrel imbedded within the outer membrane, and globular N-terminal and C-terminal domains facing the periplasm. Each monomeric β-barrel comprises twenty-four β strands, and a globular plug domain that gates the channel shut. The plug domain extends from two linker regions located at the base of the barrel wall and connecting with β-strands 6 and 7. Additional structural features of importance are a β5-6 hairpin, which constrains the plug domain in place, and an α-helix residing externally to the β5-6 hairpin and stabilizing it (Figure 3.1A). A remarkable snapshot of the translocation process has been provided by the X-ray crystal structure of the complex of the usher, the chaperone and the first pilus subunit of the *fim* system (Phan et al., 2011). The data reveals that the plug domain is displaced from the channel lumen towards the periplasmic side, where it makes extensive contact with the usher N-terminal domain. Thus, this suggests that, in order for pilus biogenesis to initiate, plug displacement must first occur. However, the exact molecular mechanism behind this complex event has yet to be elucidated.

3.1.2 Residue Interaction Networks and "Hot-Spot" Identification

Structural dynamics is the ability of proteins to undergo conformational changes in response to extrinsic stimuli, such as ligand binding, while maintaining a folded conformation. Such allosteric transitions are usually comprised of global motions, essentially dictated by the architecture of the protein and its secondary structure elements, complemented by local motions, such as residue side-chain movement (Liu and Bahar,

2012). Computational work has suggested that global conformational changes and allosteric communication are often associated with highly conserved and co-evolved residues (Tang et al., 2007; Suel et al., 2003; Liu and Bahar, 2012). Activation of the PapC usher requires the displacement of the plug domains in response to the binding of the first chaperone-subunit complex (the chaperone-adhesin complex) to the usher. Thus, in order to determine whether there exists an allosteric signal propagation pathway within the PapC usher, our collaborators in the laboratories of Gabriel Waksman and Maya Topf identified several distinct communities of key residues within the PapC usher postulated to modulate plug displacement, as described below (Farabella et al., 2014).

Previous studies utilizing cellular assays and electrophysiological analyses have shown that PapC mutants lacking the α-helix or β5-6 hairpin loop have significantly increased pore permeability reminiscent of the plugless PapC mutant (Volkan et al., 2013; Mapingire et al., 2009). In addition, they were also completely defective for pilus biogenesis (Mapingire et al., 2009). Thus, it was hypothesized that both secondary structural elements function to maintain the plug domain in a closed configuration in the wildtype usher (Volkan et al., 2013; Mapingire et al., 2009). In order to better understand their role in this process and identify a possible allosteric signaling network between these elements our collaborators, Maya Topf and Irene Farabella, constructed computer models of the PapC usher containing deletions of the α-helix, the β5-6 hairpin loop, or both.

Then, by using a hybrid computational approach, they combined sequence conservation and mutual information-based coevolution analysis in combination with all-atom molecular dynamics (AA-MD) to model a residue-residue interaction network

within the PapC usher. This computational modeling was conducted on the WT usher as well as mutant ushers lacking either the α-helix, the β5-6 hairpin loop, or both. Specifically, four independent simulations were analyzed. Each simulation identified a core set of strong residue-residue non-covalent interactions (NCI) (hydrogen bonds and salt bridges) within the β-barrel, and the network of residues linked by them (residue interaction network, or RIN). When simulations were conducted on the mutants, this core network of residue-residue NCIs was altered. Comparisons of the RINs from the WT and the mutants revealed that 24%, 22.6%, and 23.3% of the strong residue-residue interactions in the original RIN were weakened in the mutant lacking the hairpin, α-helix, or both, respectively. This indicated that the RIN within the WT usher was severely perturbed in the absence of the α-helix and/or β5-6 hairpin loop.

In order to further determine key residues, Topf and Farabella utilized multiple sequence alignment analysis to identify two regions of highly conserved residues on the PapC usher (Figure 3.1B): (**1**) the first region maps to the plug domain and plug linkers (3.1B - red oval), and the second (**2**) is localized to the region surrounding the α-helix and β5-6 hairpin loop interfaced with the barrel wall (Figure 3.1B - blue oval). In particular, the large majority of conserved residues identified were primarily located in the second region (Figure 3.1B - blue oval). Additionally, evolutionary analyses were conducted to identify coevolved residue-residue interactions within the usher. Among those identified, most of these coevolved residues mapped to the same regions as observed via sequence conservation analysis (Figure 3.1B). These analyses, in concert with the RIN obtained from molecular dynamics, allowed them to identify residues that are highly conserved, co-evolved and with weakened interactions in the mutants. These residues, which

represent 14% of all the residues in the translocation domain (i.e. the usher without the N- and C-terminal domains), were considered "hot-spots" or highly potential candidates functioning in allosteric signal propagation. In addition, they cluster relatively close to each other in a continuous area within PapC.

These key residues fell into 5 primary communities (Figure 3.2) located at the base of the plug linkers (Community 1 or **C1**); between the β5-6 hairpin loop and the conserved cluster at the base of the α-helix (**C2**); between β12-13 loop and plug linker 1 (**C3**); between the β5-6 hairpin loop, plug linker 2, and the plug domain (**C4**); at the tip of the plug domain (**C5**). Mutations of the residues in this 5th community did not alter cellular phenotypes, were considered less critical in the proposed allosteric signaling pathway, and were not considered for further study. From the first four communities, 15 residues, which linked one community to the next, were selected as the *core* "hot-spot" sub-network of residues postulated to participate in modulating plug displacement through an allosteric signaling mechanism (Figure 3.2). As seen in the figure, key residues were selected from each community and appear to form a physical pathway within the usher on which an allosteric signal could be propagated.

3.1.3 Cellular Assays of Core "Hot-Spot" Residues

Alanine substitution was constructed at the core "hot-spot" residues, in order to determine whether these residues indeed participate in an allosteric signaling network modulating plug displacement. Each of the mutant ushers was present at a similar level in the OM compared to the wild-type PapC usher, and the mutations did not affect the ability of the usher to form a stable β-barrel in the OM (Farabella et al., 2014). Three

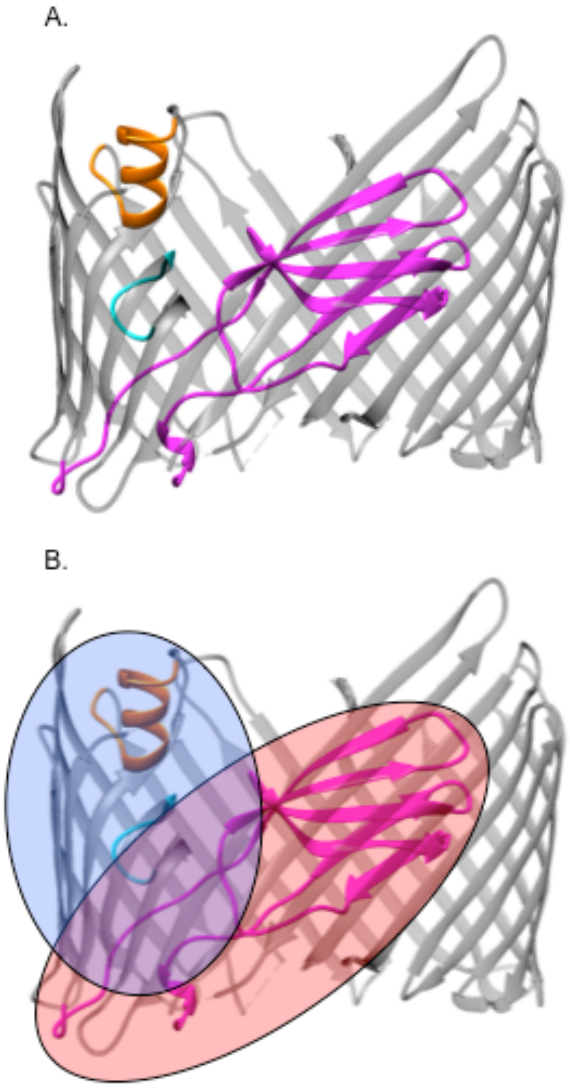

Figure 3.1 Evolutionary analysis of the PapC usher family identifies two regions of highly conserved residues. *(**A**) Cartoon representation of the PapC usher modeled in Chimera. The plug domain is shown in magenta, β5-6 hairpin loop in cyan, and α-helix in orange. (**B**) The red oval and blue ovals identify areas of highly conserved residues in the plug domain/barrel region and the interface of α-helix and β5-6 hairpin loop with the barrel wall, respectively.*

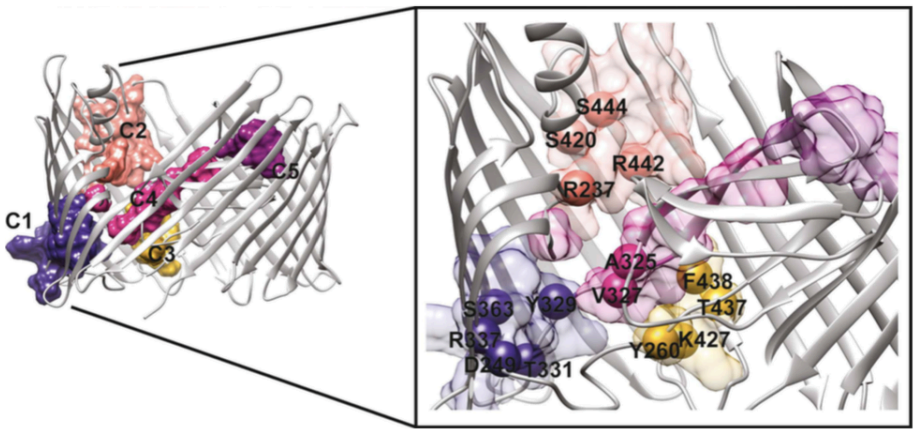

Figure 3.2 The core "hot-spot" residues link one community to the next in the proposed allosteric signaling pathway. *Cartoon model depicts the 5 primary communities identified (C1-5): C1 blue, C2 pink, C3 yellow, C4 magenta, and C5 purple. All communities comprise residues from several of the secondary structural elements within the translocation domain including the β-hairpin, plug linkers 1 and 2, and the α-helix. Fifteen key residues were postulated to form the core subset or "hot-spot" of residues implicated to link one community to the next in a proposed allosteric pathway for plug displacement.*

cellular assays were performed by Nadine Henderson in David Thanassi's laboratory. **(1)** A hemagglutination (HA) titer was used to assess the ability *E. coli* cells expressing the mutant usher to agglutinate red blood cells (RBCs). Because P pili serve as the agglutinating factor in this assay, this HA titer functions as a test for the ability of the usher to assemble functional pili. The WT HA titer was 64. This value represents the maximum-fold dilution of PapC expressing *E. coli* cells that are still able to agglutinate RBCs utilizing P pili. Consequently, lower HA titers demonstrate a reduced efficiency of the cells at agglutinating RBCs due to impaired pilus assembly. **(2)** Mutants were also assayed for their sensitivity to antibiotics. Antibiotic discs were added to PapC expressing *E. coli* cells grown on agar plates and observed for zones of clearing around each disc. Mutants showing zones of clearing that are larger than WT are more sensitive to the given antibiotic. This indicates that the particular PapC mutant presumably has a "leaky" usher or one with a higher propensity to be open allowing the influx of more antibiotics. These "leaky" phenotypes may be due to a more frequently open state due to plug displacement. **(3)** Gram-negative outer membranes are also resistant to detergent permeabilization. The detergent SDS was tested in order to determine whether PapC mutants had also become more permeable to detergents as well as antibiotics.

Collectively, mutations at 10 out of the core "hot-spot" residues selected demonstrated a cellular effect (Farabella et al., 2014). However, of these 10 mutated ushers, only 7 could be purified for electrophysiological analysis, and we are reporting only the results obtained with these mutants here. The locations of the mutated residues are shown in Figure 3.3. Table 3.1 summarizes the results of the cellular assays obtained for these 7 mutants. Most of mutants with the exception of R237A and V327 (HA titer of

64) were partially defective for pilus assembly. The K427A mutant was completely defective (HA titer of 0). In addition, PapC mutants T331A, F438A, and V327A showed a significantly increased sensitivity to antibiotics. None of the mutants showed reduced antibiotic sensitivity. With respect to SDS sensitivity, only the V327A mutant displayed increased permeability to SDS.

3.2 Electrophysiology of PapC WT and mutants

3.2.1 Characteristics of the WT PapC Usher

In order to determine the effect of these mutations on channel activity, we utilized the planar lipid bilayer technique for electrophysiological analysis. The insertion of either WT or mutant purified PapC was induced by applying a membrane potential of + or – 90 mV as described in Chapter 2. Promotion of insertion was also aided by the addition of a stir bar on the side of the bilayer chamber containing protein. The membrane potential was returned to 0 mV and stir bar stopped once an insertion event was observed to minimize further insertions. Electrophysiological analysis of WT PapC captured a characteristic kinetic signature at relatively low membrane potentials (< 100 mV). Experiments showed that the usher is a mostly closed channel indicated by prolonged times at low levels of current.

However, it can also be an extremely dynamic channel. As seen in the traces of Figure 3.4A and 3.4C, the WT channel exhibits frequent transient openings of small, but varying conductance (50-600 pS in 1 M KCl). These current fluctuations likely originate from ion movements through water-filled conduits that exist at the barrel-plug interface (Mapingire et al., 2009). Interruptions of the current might be due to thermal motion of

			Antibiotic Sensitivity			
PapC	***Community***	***HA Titer***	***SDS***	***Erythromycin***	***Vancomycin***	***PD Propensity***
WT		*64*	*15*	*6*	*6*	*57%*
T331A	*C1*	*24*	*15*	*15*	*10*	*86%*
S444A	*C2*	*24*	*14*	*6*	*6*	*15%*
R237A	*C2*	*64*	*16*	*6*	*15*	*35%*
K427A	*C3*	*0*	*14*	*6*	*6*	*23%*
F438A	*C3*	*32*	*14*	*12*	*6*	*75%*
T437A	*C3*	*24*	*14*	*6*	*6*	*50%*
V327A	*C4*	*64*	*20*	*14*	*16*	*87%*

Table 3.1 Cellular and electrophysiological phenotypes of PapC WT and allosteric network mutants. *The table lists all of the PapC mutants accompanied by their cellular phenotypes prepared for electrophysiological analysis. Each residue was categorized into communities C1-C4 within PapC. Community 5 is excluded for reasons given above. A hemagglutination (HA) titer was utilized to assay for functional pilus assembly, and the antibiotic sensitivity assay was performed by adding filter discs containing either antibiotic or detergent to growths of PapC expressing E. coli. Zones of clearing around the disc (in mm) represent sensitivity to the antibiotic (erythromycin 15 μg or vancoymycin 20 μg) or detergent (SDS 750 μg). Larger relative zones of clearing compared to the WT indicate that the PapC mutant has a more "leaky" usher, resulting in more antibiotic influx. "PD propensity" refers to plug displacement frequency as observed via planar lipid bilayer experiments at +/- 90 mV (see Fig. 3.7).*

the plug within the channel lumen or spontaneous conformational changes of the barrel or the periplasmic domains leading to transient occlusions of these small pathways observed by occasional periods at the closed level. The channel could occasionally have opening events of extremely large conductance (~ 3 nS in 1 M KCl) at + or – 50 mV (Fig. 3.4B). Previous studies of domain mutants demonstrated that removal of the plug domain

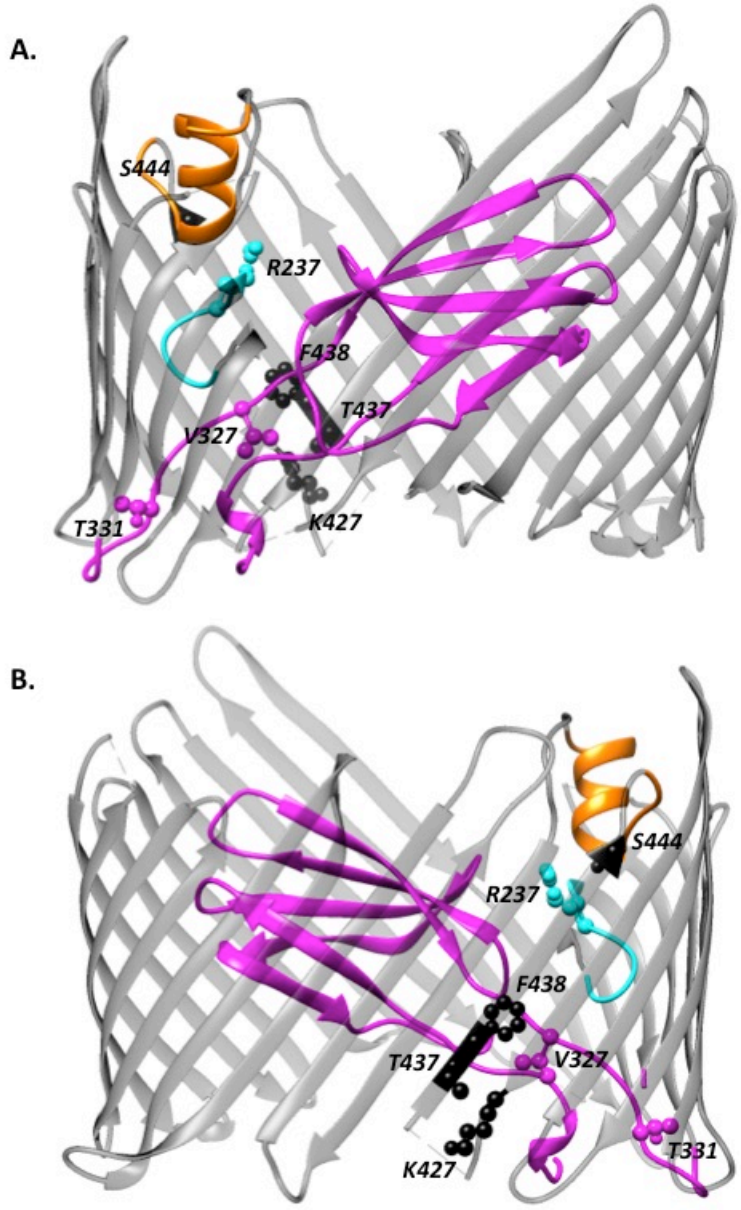

Figure 3.3 Location of core "hot-spot" residues analyzed via electrophysiology. *The plug domain is depicted in magenta, α-helix in orange, β5-6 hairpin loop in cyan, and barrel wall in gray. Residues are colored according to their region. Model was displayed using Chimera. The structure in the bottom panel (**B**) is rotated 180 degrees from the top panel (**A**).*

generates a pore with a very similar conductance, which surprisingly, still displays a highly dynamic behavior (Mapingire et al., 2009). As a result, these large current events are believed to correspond to spontaneous plug displacement events in one of the monomers of the PapC usher. Interestingly, when membrane potentials were increased to +90 mV (Figure 3.4C-D) or -90 mV, the frequency of observing these displacement events increased (Figure 3.6). Some events did not quite reach the 3-4 nS level of conductance that is attributed to a plug displacement event. In these cases, it is believed that these events are partial displacements.

3.2.2 Characteristics of Allosteric Network Mutants

PapC mutants with increased antibiotic sensitivity (Table 3.1) exhibited high propensities for plug displacement relative to WT when analyzed in planar lipid bilayer, in accordance with a more "leaky" usher phenotype conferring increased antibiotic entry. Representative traces for these mutants (T331A, V327A, and F438A) are seen in Figure 3.5. All 3 mutants displayed very active kinetics with frequent spontaneous plug displacements. In contrast, mutants impaired in their ability to form functional pili displayed very low propensities for plug displacement, as expected (Figure 3.6). The K427A mutant usher, which is completely defective in pilus assembly (Table 3.1) had almost no dynamic activity and displayed a very closed kinetic phenotype (Figure 3.6A).

Although all allosteric network residue mutants were able to show signs of plug displacement, the propensity of observing these events was varied. Because the electrophysiological behavior of PapC is quite variable, and in attempt to quantify the propensity of spontaneous plug displacement events, we have counted the number of 10-

Figure 3.4 Electrophysiological characteristics of WT PapC. *Traces of WT PapC activity recorded in planar lipid bilayer using buffer T. Insertions were obtained at +90 mV. Subsequently, (**A-B**) the membrane potential was clamped to +50 mV, or (**C-D**) to +90 mV as indicated. Each experiment was recorded for 10 minutes with 50 seconds shown here. Recordings could be observed with or without plug displacement events at either voltage. Channel kinetics often displayed transient openings to the 50-600 pS levels of conductance but could occasionally spike to large levels representing spontaneous plug displacement events. The "C" denotes the closed level of the channel and "M" the monomeric conductance level (~3 nS).*

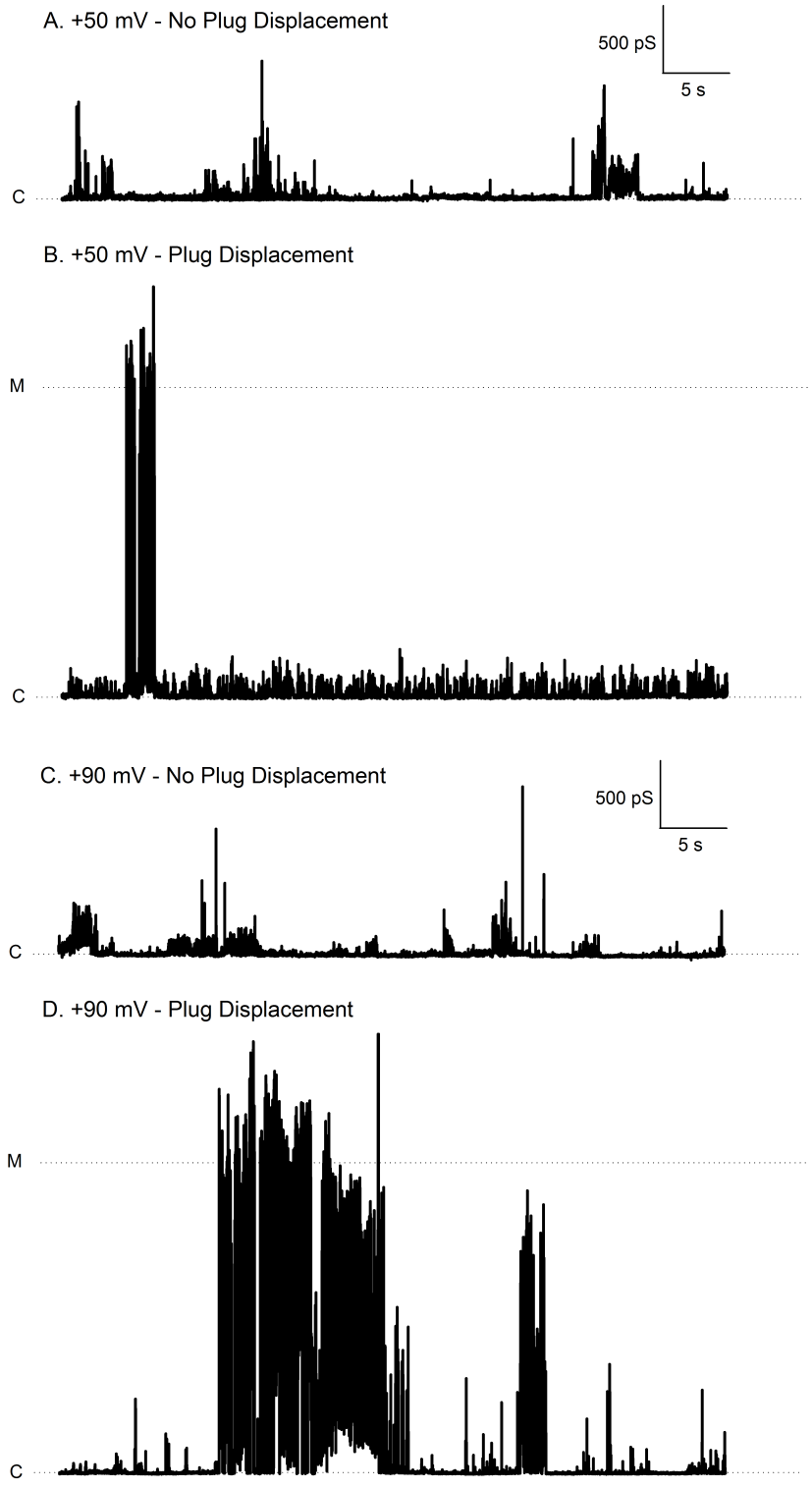
A. +50 mV - No Plug Displacement
500 pS
5 s
C
B. +50 mV - Plug Displacement
M
C
C. +90 mV - No Plug Displacement
500 pS
5 s
C
D. +90 mV - Plug Displacement
M
C

min long recordings (sweeps) that show plug displacements. Each experiment or individual bilayer formed with inserted PapC protein was subjected to four 10-minute recordings each at +50, -50, +90, and -90 mV. Figure 3.7 shows the frequency of observing plug displacement at 50 or 90 mV (positive and negative potentials combined). The frequency of observing these plug displacement events in the WT usher is ~ 20% at + or - 50 mV. However, at + or - 90 mV the frequency of triggering plug displacement increased to ~ 60%. V327A, T331A, and F438A, which all displayed "leaky" cellular phenotypes indicated by increased levels antibiotic sensitivity, showed a much higher propensity for plug displacement relative to the WT at + or – 90 mV, with frequencies nearing 80%. On the other hand, allosteric network mutants defective in their ability to form functional pili, such as K427A and S444A, usher mutants had greatly diminished frequencies for plug displacement relative to the WT usher, even at + or – 90 mV. Although the effects are not as prominent at + or – 50 mV, we believe that the application of a larger transmembrane voltage disrupts the interactions between key residues involved in keeping the plug in place, thus allowing us to better differentiate between the mutants and WT. Finally, some mutants (R237A and T437A) showed propensity at plug displacement similar to WT. These mutants showed mixed effects in their cellular phenotypes. Overall, the electrophysiological analyses are consistent with the cellular phenotypes observed.

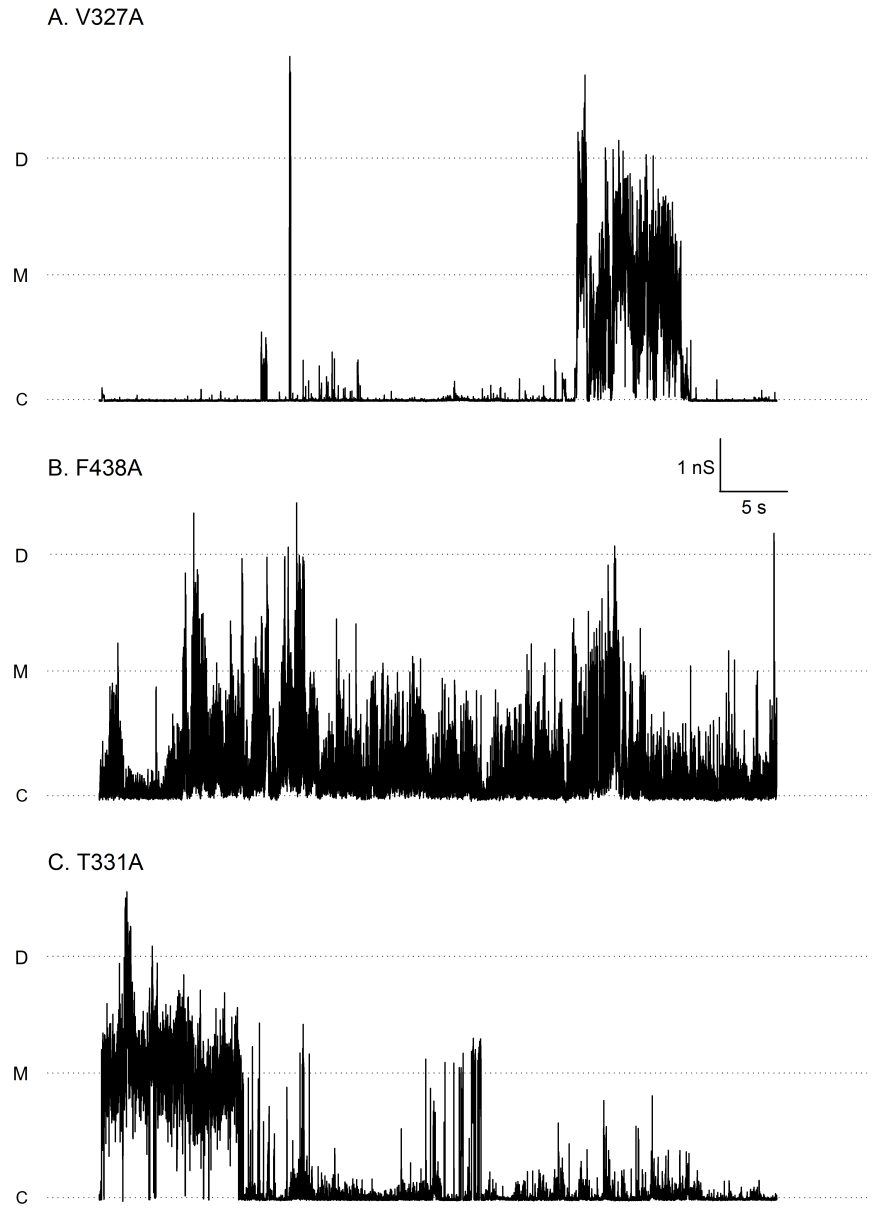

Figure 3.5 Representative traces of allosteric mutants with increased sensitivity to antibiotics. *Traces were obtained in buffer T for mutants V327A, F438A, and T331A, as indicated. Each experiment was 10 minutes in length with 50 seconds displayed. The membrane potential was +90 mV. The "C" level denotes the closed level of the usher, "M" signifies the monomeric level of conductance (~3 nS), and "D" the dimeric level of conductance (~6-7 nS).*

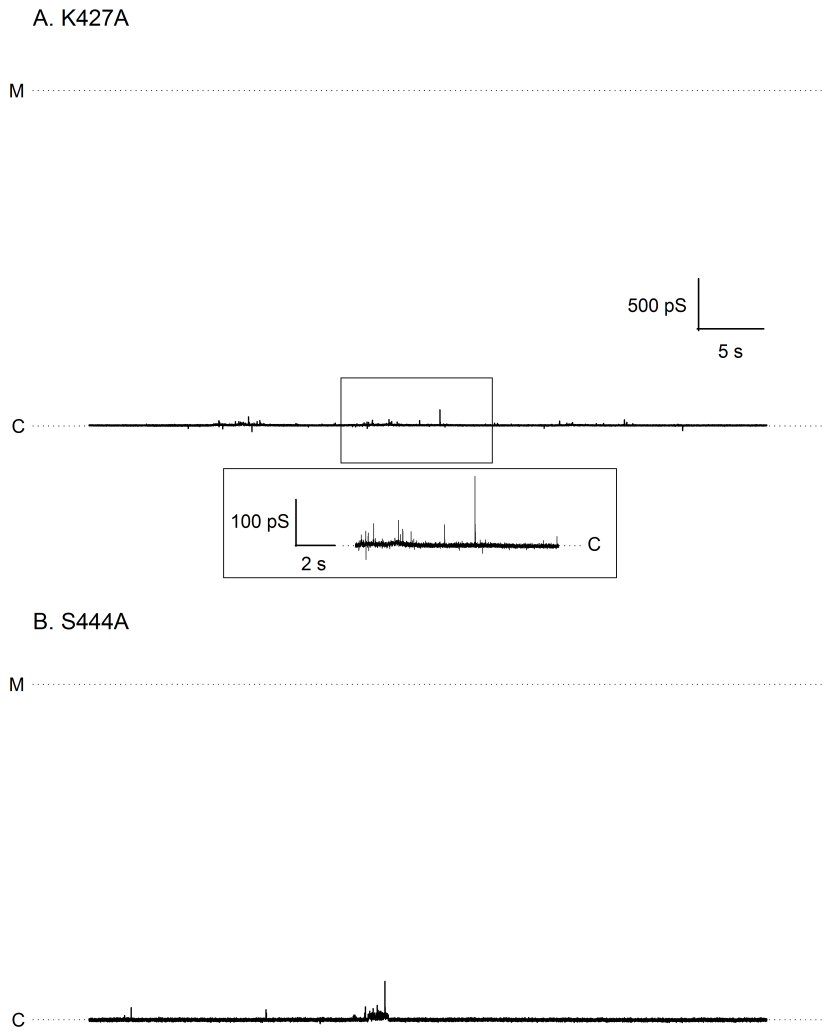

Figure 3.6 Representative traces of allosteric mutants with severe defects in pilus assembly and WT antibiotic sensitivities. *Traces were obtained in buffer T and are representative for mutants K427A and S444A, as indicated. Each experiment was 10 minutes in length with 50 seconds displayed. The membrane potential was +90 mV. The "C" level denotes the closed level of the usher and "M" signifies the monomeric level of conductance (~3 nS). Traces were plotted onto a Y scale large enough to mark the monomeric level of conductance, in order to highlight the complete lack of plug displacement events. The boxed segment under trace A represents a stretch of data shown at an expanded time scale to allow visualization of small openings.*

3.3 Discussion

The PapC usher is critical for the assembly and translocation of the P pilus across the outer membrane of UPEC. In order for assembly to initiate, the plug domain that occludes the usher must first displace towards the periplasm in order to provide incoming pilus subunits access to the barrel lumen. As studied previously and demonstrated in our experiments, the WT usher has a highly dynamic channel kinetic characterized by short and transient openings of varying levels of conductance (50-600 pS in buffer T) (Volkan et al., 2013; Mapingire et al., 2009). The α-helix and β5-6 hairpin have been shown to be critical for maintaining the plug domain in a closed configuration (Volkan et al., 2013; Mapingire et al., 2009). Although strong and stable interactions exist between the α-helix or β5-6 hairpin and the plug domain, residue-residue interactions between the plug domain with the rest of the usher are weak (Farabella et al., 2014). This will allow for release of the plug domain once interactions between the secondary structural elements (the α-helix or β5-6 hairpin) and the plug have been destabilized due to the first chaperone-subunit binding. Furthermore, the computational analyses conducted by Irene Farabella and Maya Topf show that both the α-helix and β5-6 hairpin loop are key components in this proposed allosteric gating mechanism (Farabella et al., 2014). Although only 14% of all residues comprising the translocation domain of the usher were considered as potential candidates in this allosteric network, "hot-spot" residues were identified and clustered in 5 communities. Of these, a core set of "hot-spot" residues was selected among communities C1 to C4, based on their interconnectedness between communities, which may be critical for an allosteric signal to be propagated for triggering plug displacement. Of the 15 mutants made at these core "hot-spot" residues, 10

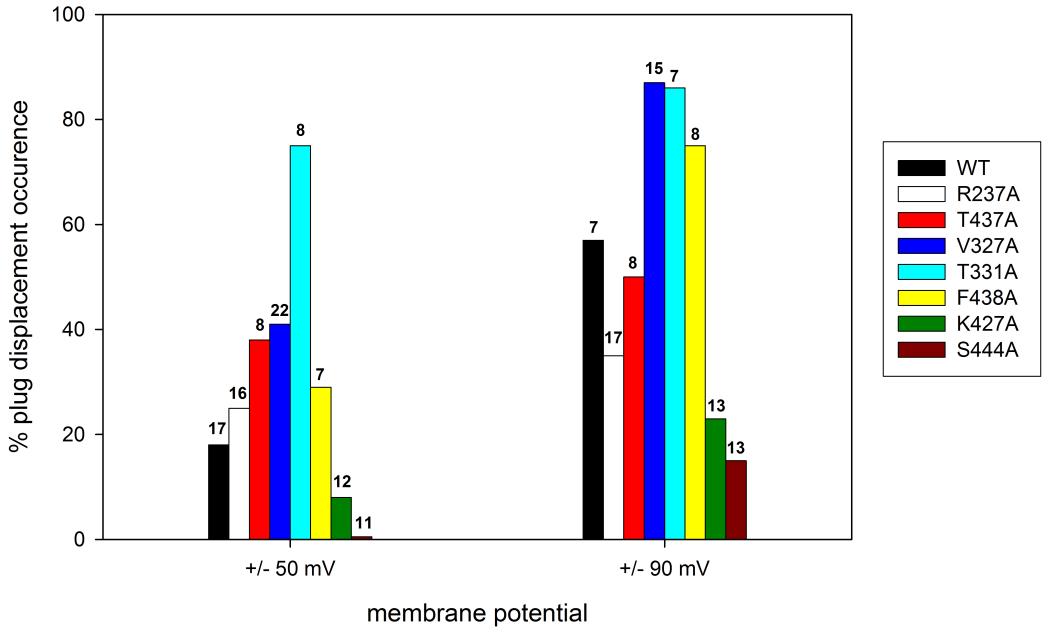

Figure 3.7 Plug displacement propensity in WT and allosteric mutants of PapC. *Probability for plug displacement in planar lipid bilayer experiments at the indicated membrane potentials. WT PapC and allosteric network mutants are color-coded. The number of experiments (n) corresponding to each individual bilayer with a new population of inserted PapC ushers is given above each bar.*

displayed cellular phenotypes (**1**) defective in their ability to form functional pili or (**2**) characterized by increased permeability to antibiotics presumably due to a "leaky" usher. These affected mutants span the 4 communities. In particular, core "hot-spot" residues in C1-C3 displayed defects in pilus assembly as indicated by their low HA titers. This indicates that the C1-C3 set of communities is key for proper pilus assembly and thereby usher function.

In addition, electrophysiological analyses on these allosteric network mutants showed results consistent with the observed cellular phenotypes. Specifically, as observed in Figure 3.7, at membrane potentials of + or – 90 mV in planar lipid bilayer, PapC mutants severely defective in their ability to assemble pili (K427A and S444A) were characterized by a decreased propensity for plug displacement. This suggests that the mutation of these residues to alanine stabilized the closed conformation. Thus, in the native WT usher, residues K427 and S444 function to promote plug displacement. In contrast, residues T331, V327, and F438 when mutated displayed varying degrees of defects for pilus assembly. However, these mutants also showed an increased sensitivity to antibiotics and their electrophysiological characteristics were consistent with this observation. At membrane potentials of + or – 90 mV, each of these mutants displayed a significantly higher propensity for plug displacement relative to the WT (Figure 3.7).

Figure 3.8 summarizes, in a cartoon fashion, the electrophysiological and cellular phenotypes obtained for mutants with strong effects in electrophysiology. The S444A and K427A mutated PapC have a low propensity of plug displacement. When mutated at S444, the usher displays only a pilus assembly defect, without increased leakiness. S444 is localized to the region at the interface between the extracellular-facing portions of the

plug domain with the barrel wall. However, when mutated at K427, the usher displayed both pilus assembly defects as well as increased antibiotic flux. K427 is localized to a highly conserved patch of residues located at the base of the barrel on the β12 strand interfaced with the plug domain. Thus, these two residues, which flank the extracellular and periplasmic sides of the plug domain, appear to be responsible for promoting plug displacement in the WT usher.

Residues T331, V327, and F438 are localized to the interface between the plug domain and both plug linkers. The mutations of these residues to alanine result in significantly increased propensities for plug displacement. This suggests a role for these residues in the native usher in maintaining the plug domain in a closed configuration, as their mutants appear to destabilize the plug. Overall, a good correlation has been found between the cellular and electrophysiological phenotypes.

Altogether, the results of this study suggested that an allosteric pathway connecting residues close to the periplasmic and the extracellular sides of the usher might control the gating of the plug domain. These key residues are clustered in four communities localized on different secondary structural elements: plug linkers, β-hairpin, plug domain, and β-barrel wall. A 5^{th} community, with residues all clustered on the plug domain, does not seem to be involved, because mutations in this community did not lead to variations in cellular phenotype relative to the WT. In addition, there appears to be interconnectedness between one community and the next within the C1 to C4 communities. Therefore, one can conceive of an allosteric signal travelling along this network of residues to induce plug displacement upon the first chaperone-subunit binding. This pathway includes conserved elements located on the β13 strand, the plug

linkers, and the periplasmic loop linking β12 and β13 strands. Interestingly the β12 and β13 strands comprise a loop believed to be a "latch" (β12/13 "latch") maintaining the plug domain in a closed conformation. Previous studies show that the "latch" can adopt different conformations in the open and closed states of the *fim* system (Phan et al., 2011). This suggested that the "latch" itself also plays some role in the modulation of plug displacement. Interestingly, both S444 and K127 of PapC, located on the β-12/13 conserved patch and β-12/13 latch, respectively, show strong closed phenotypes when mutated to alanine, in agreement with the observations on the *fim* system.

Electrostatic interactions also exist at the interface of the plug domain with the α-helix, β5-6 hairpin, and barrel wall, and may participate in maintaining the plug in place. Collectively, allosteric interactions and electrostatic interactions may work together to modulate plug displacement. In chapter 4, we focus on the electrostatic interactions.

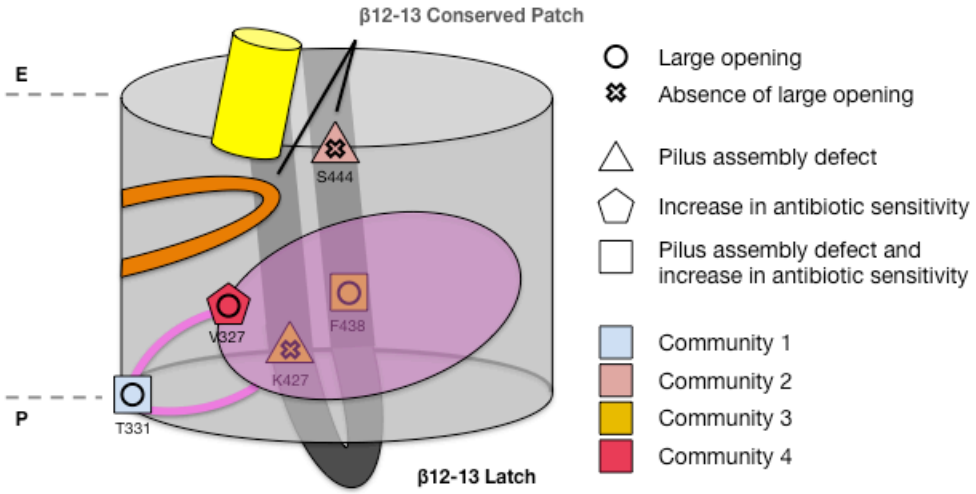

Figure 3.8 Allosteric network summary. *The cartoon is a depiction of the PapC usher, summarizing the electrophysiological and cellular phenotypes at the most affected residues. "E" denotes the extracellular-facing side and "P" denotes the periplasmic-facing side of the usher. The α-helix is show in yellow. The β5-6 hairpin loop is depicted in orange, and the plug-domain is shown in dark pink. The β-12/13 conserved patch of residues observed in the fim system is depicted in black along the back of the barrel wall behind the plug domain in this view. The β-12/13 latch extends from this patch to cover the periplasmic base of the barrel in the closed conformation. Cellular phenotypes are represented as different shapes, and the key is given in the figure. An X or O within the shape indicates a decreased or increased occurrence of spontaneous plug displacement relative to WT, respectively, as observed by electrophysiology.*

CHAPTER 4

An Electrostatic Network of Residues Modulates Plug Displacement

Parts of this chapter are published in:

Pham T et al. (2015) "Electrostatic Networks Control Plug Stabilization in the PapC Usher", Molecular Membrane Biology, 32:198-207.

Pham T et al. (2016) "Effect of Chaperone-Adhesin Complex on Plug Release by the PapC Usher", FEBS Letters, in press.

4.1 Electrostatic Interactions in Channel Gating

4.1.1 Electrostatic Interactions

Electrostatic interactions are a sub-classification of non-covalent interactions and often play important roles in protein structure, function, and stability (Perutz, 1978; Waldburger et al., 1995; Yang et al., 1992). These interactions comprise three distinct types of bonding interactions: (**1**) Ionic bonding occurs between residues of opposite charges, and is also commonly referred to as a salt bridge. This interaction is potent because it can nearly reach the strength of covalent bonds. (**2**) Hydrogen bonding is another common electrostatic interaction that exists between a hydrogen and a highly electronegative atom. (**3**) An electrostatic interaction can occur between a charged residue and the oxygen atom central to water molecules. Most charged molecules are found on the protein surface. Here, these residues can interact with the surrounding solvent to induce the formation of water shells around each charged side-group. This often serves to both stabilize as well as solubilize the protein.

4.1.2 Electrostatics Governing Channel Gating

Previous studies have shown that electrostatic interactions consisting of attractive or repulsive forces between residues can function to gate a channel-forming protein (Hong et al., 2006). Electrostatic interactions were assessed thermodynamically in computational studies of OmpA (Hong et al., 2006). OmpA is an 8-stranded β-barrel located in the OM of Gram-negative bacteria. There it forms a small pore that is permeant to both ions and amino acids (Sugawara and Nikaido, 1992; Sugawara and Nikaido, 1994). However, within the central lumen of OmpA is a cluster of electrostatic

interactions. In particular, the closed configuration of the channel is a result of salt bridge formation between a glutamate located on one side of the lumen with an arginine residue on the opposite side, Glu52-Arg138. This functions to block the pore and gate the channel closed. However, beneath these two residues are a lysine (Lys82) and glutamate (Glu128), respectively. Thus in order to displace the interaction between Glu52-Arg138 gating the channel closed, Lys82 moves forward to form an electrostatic salt bridge with Glu128 to stabilize the open configuration (Hong et al., 2006). Unfortunately, these findings *in silico* have not been confirmed by electrophysiological analyses on this protein.

Other channel-forming proteins utilize a network of electrostatic interactions to modulate pore gating, such as the proton channel Hv1 (Chamberlin et al., 2014; Chamberlin et al., 2015; Castillo et al., 2015b), and voltage-gated potassium channels such as BK. While these latter channels are activated by voltage and intracellular calcium, their lumens also host a network of electrostatic interactions that aid in channel gating (Castillo et al., 2015a; Yang et al., 2013; Zhang et al., 2014). The outer membrane protein, OmpF, is another such channel that utilizes electrostatic interactions in order to govern conductance and ion selectivity (Delcour, 2003). These channels are aqueous porins that are located in the outer membrane of *E. coli*. Their primary purpose is to facilitate the diffusion of small and vital solutes across the membrane such as amino acids and sugars (Delcour, 2003; Koebnik et al., 2000). In regards to structure, these porins exist as trimeric entities within the outer membrane. Each monomer within this complex forms a β-barrel comprised of 16 antiparallel β-sheets (Cowan et al., 1992). In particular, each monomer contains an L3 loop folded into its lumen forming a constriction zone that

regulates solute influx and efflux (Delcour, 2003; Nikaido, 2003). This L3 loop is comprised of acidic residues that confer an electrostatic field to the eyelet region, and their studies showed that mutants causing a shift in charge distribution across the L3 loop resulted in a change of diffusion characteristics through the channel (Delcour, 2003).

4.2 Electrostatic Networks Clustered at the Plug Domain Interface in PapC

In the PapC usher, several residues that form key components of electrostatic networks possibly modulating plug displacement have been identified previously (Remaut et al., 2008). These networks are localized primarily to the regions at the plug domain interface with the barrel wall, α-helix, or β5-6 hairpin loop. In particular, there are three networks of residues that utilize these electrostatic interactions:

(1) R237-R305-D323-E467 (R-Quad Network)

(2) D234-R303-K339-E361 (D-Quad Network)

(3) R237-R256-R305-R332 (R-Pairs Network)

a. R237-R305 (R-Single Pair Extracellular Side "RSP-OUT")

b. R256-R332 (R-Single Pair Periplasmic Side "RSP-IN")

(**1**) The R-Quad network is at the interface between the α-helix and β5-6 hairpin with the plug-domain (Figure 4.1A). This particular network consists of a series of attractive residue-residue interactions that are postulated to modulate plug displacement. (**2**) The D-Quad network of electrostatic residues is localized to the region surrounding the base of the β5-6 hairpin loop interfaced with the barrel wall on one side and the plug domain on the other (Figure 4.1B). Specifically, residue R303 on the plug domain and E361-K339 on the barrel wall sandwich D234 located on the β5-6 hairpin loop (Figure 4.1B).

Collectively, this network also forms attractive interactions between opposite charge residues. (**3**) Whereas the R-Quad and D-Quad networks of residues consist of residue-residue interactions between opposite charges or attractive forces, there is one electrostatic network that involves repulsive interactions between arginines (R-Pairs). This network is located at (**a**) the plug-domain interfaced with the β5-6 hairpin and (**b**) the interface between plug-domain linkers 1 and 2 (Figure 4.1C). Individually, additional analysis later in this chapter details the findings of each individual arginine-arginine pair and their total contribution to the R-Pairs network. In particular, residues R305-R237 (RSP-OUT) form the repulsive pair towards the extracellular side of the usher, and arginine pair R332-R256 (RSP-IN) forms the other repulsive arginine-arginine interaction between plug-linkers 1 and 2 (Figure 4.1C). In order to confirm that residues were within a close enough proximity for an electrostatic interaction, we measured the distance between residues in each of the three electrostatic networks. This was performed in Chimera and confirmed that the residues of each proposed network are indeed within appropriate distances for electrostatic interactions (Table 4.1).

In order to determine whether these electrostatic networks were at all critical for proper usher function, a series of cellular assays were performed by the Thanassi laboratory as described previously (Henderson et al., 2011). Mutant PapC was constructed for each of the three networks. In each case, the residues comprising each network were mutated to alanines. All of the PapC mutants had WT-like expression in *E. coli* (data not shown). A hemagglutination (HA) titer was used to assess the ability *E. coli* cells expressing the mutant usher to agglutinate red blood cells. Because P pili serve as the agglutinating factor in this assay, this HA titer functions as a test for the ability of the

Figure 4.1 Molecular model of the electrostatic networks of residues analyzed via electrophysiology. *Molecular model of PapC rendered with the PDB ID: 2VQI in Chimera. Gray represents the barrel wall of the PapC usher. Yellow represents the α-helix and indicates the side of the usher facing the extracellular space. The α-helix caps the β5-6 hairpin depicted in orange, and the plug domain and plug-linkers are shown in magenta. Residues were mutated to alanine and selected based on their cellular phenotypes by the Thanassi Laboratory. A zoomed-in view of each respective electrostatic network is provided adjacent to each panel in a box (dashed-line border). (**A**) R237-E467-R305-D323 or R-Quad electrostatic network of attractive interactions at the interface between the β5-6 hairpin and α-helix with the plug domain. (**B**) D234-K339-E361-R303 or D-Quad electrostatic network of attractive interactions comprising the region around the β5-6 hairpin loop. (**C**) The R237-R305-R332-R256 network comprises two pairs of arginine-arginine repulsive interactions clustered on (**1: RSP-IN**) the plug linkers and (**2: RSP-OUT**) plug domain.*

A. R-quad

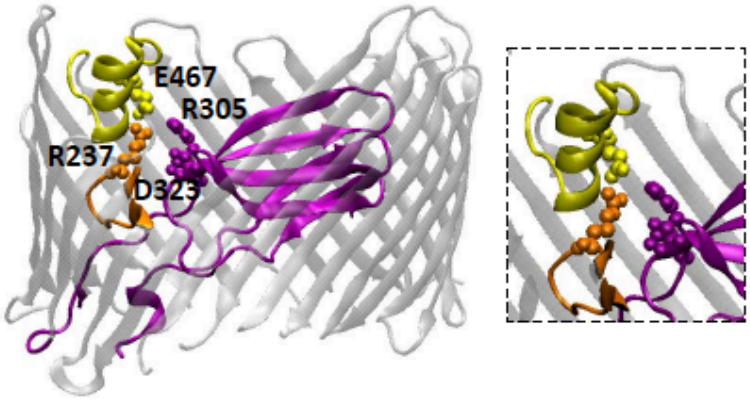

B. D-quad

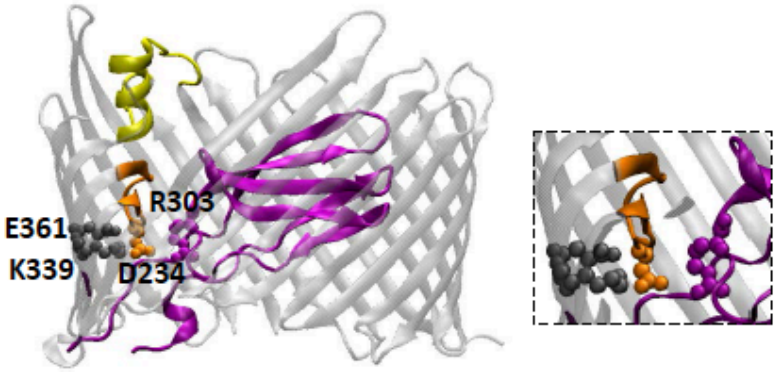

C. R-pairs

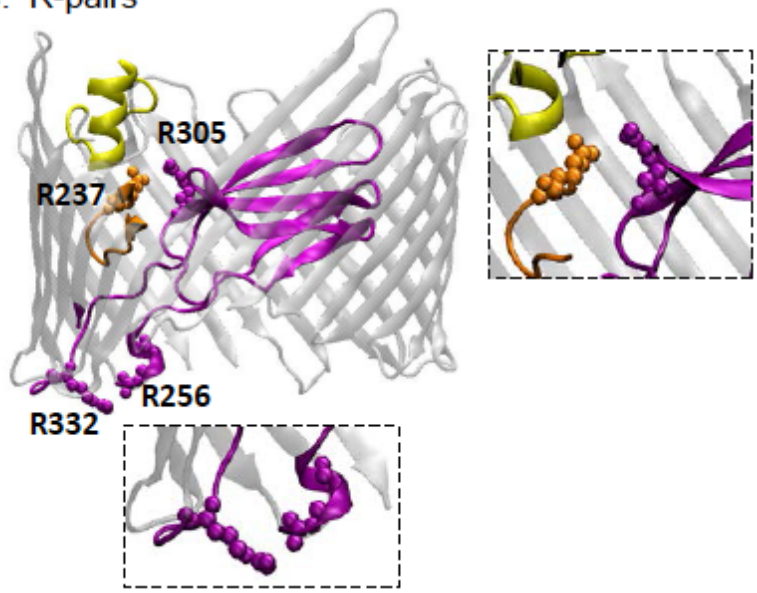

usher to assemble functional pili. The Thanassi laboratory established a WT HA titer of 64. This represents the maximum-fold dilution of PapC expressing *E. coli* cells that are still able to agglutinate red blood cells (RBCs) utilizing P pili. Consequently, lower HA titers demonstrate a reduced efficiency of the cells at agglutinating RBCs due to impaired pilus assembly. The D-quad mutant had a WT phenotype for pilus assembly (HA titer of 64), whereas the R-quad mutant was deficient (HA titer of 21). The R-pairs mutant, however, was completely defective for pilus assembly (HA titer of 0).

4.3 Electrophysiological Analysis of Electrostatic Network Mutants

4.3.1 PapC WT and Plug Displacement

As shown previously in planar lipid bilayer experiments (Mapingire et al., 2009), the WT PapC usher exists in a primarily closed state with very transient openings of small conductance attributed to the presence of water-filled conduits between the barrel wall and the plug domain. However, occasionally large conductance events could be observed. The conductance of these events corresponded to the monomeric size of a PapC mutant lacking its plug domain. Hence, these events were believed to represent spontaneous plug displacement. As previously discussed in Chapter 3, the frequency of observing these plug displacement events increases with membrane potential (Chapter 3) (Farabella et al., 2014). However, membrane potentials beyond + or – 90 mV were never tested in these studies.

Utilizing patch-clamp electrophysiology, single-channel recordings of WT PapC also show that the channel is indeed in a mostly closed state with very transient openings of small conductance (50-600 pS in 150 mM KCl) (Figure 4.2A). The channel appears to

PapC Residues	***Locations***	***Distances (Å)***
R-Quad		
R237-E467	*Hairpin-Helix*	*2.70*
E467-R305	*Helix-Plug domain*	*3.69*
R305-D323	*Plug domain - Plug domain*	*5.23*
D-Quad		
E361-K339	*Barrel-Barrel*	*2.92*
K339-D234	*Barrel-Hairpin*	*2.64*
D234-R303	*Hairpin-Plug domain*	*5.24*
R-Pairs		
R256-R332	*Plug Linker 1-Plug Linker 2*	*3.81*
R237-R305	*Hairpin-Plug domain*	*3.71*

Table 4.1 Locations and distances of residue side-groups in each electrostatic network. *Chimera was used to measure atom-atom distances between the functional side groups of each residue within its network.*

be more closed at positive membrane potentials than at negative ones. However, at high membrane potentials, large openings from the closed level could be triggered (Figure 4.2B), reaching the dimeric level of conductance, as seen on the expanded trace. This conductance was assigned to the dimeric level (1.2 nS in buffer A) because it corresponds to the maximum conductance obtained from plugless variants of PapC, previously shown to undergo monomeric and dimeric transitions (Mapingire et al., 2009). Therefore, these large and sharp increases in conductance were attributed to spontaneous plug displacements in the two monomers of the dimer. These plug displacement events are highly reproducible and have a very characteristic signature. Following its initial peak, the current is often observed to quickly relax to monomeric or smaller amplitudes. Once closed or while in the process of closing, the channels can also undergo spontaneous re-displacement of the plug domains after the initial displacement. We were

able to observe such an event in the second half of the experiment seen in Figure 4.2B whereupon a second prolonged excursion to the dimeric level of conductance occurs followed by relaxation.

Initially, we believed that these relaxations in conductance that followed plug displacement were presumably the result of plug re-entry. In order to determine whether or not this was the case, we assayed the PapC usher mutant containing a plug domain deletion (Δplug) in patch-clamp. We observed that upon immediate onset of pipette voltage, there was an immediate excursion to the dimeric level of conductance, because the channel is already open, followed by rapid relaxation (Figure 4.3). Because this was an usher mutant lacking the plug domain, the relaxation event in this instance cannot be the result of plug re-entry. Rather, we believed that it was caused by three possible scenarios: (**1**) the relaxation event in the Δplug PapC mutant is a result of barrel instability or collapse, (**2**) it could also be a result of N-terminal globular domain occlusion, or (**3**) likewise, it could be caused by the movement of the C-terminal globular domain into the barrel lumen to occlude the pore.

In order to examine this relaxation event in the Δplug PapC mutant further and consequently determine the cause of the relaxation event in the WT usher, we attempted to examine mutant constructs lacking either the N-terminal (ΔN) or C-terminal (ΔC) globular domains, or both (ΔNC). However, we were unable to reconstitute any of the mutant ushers into liposomes for patch-clamp analysis. This suggested that the globular domains might be important for promoting proper insertion into lipid membranes *in vitro*. Ultimately, we were unable to firmly establish that the relaxation event following plug displacement in the WT PapC usher is a result of plug re-entry. While it is most likely the

case since we were able to observe re-displacements within the same experimental recording, it could also involve barrel collapse, N-terminal or C-terminal globular domain occlusion of the pore, or any combination.

An important aspect of these observations is the existence of a "threshold" voltage to trigger plug displacement. We will take advantage of this in our analysis of the electrostatic network mutants.

4.3.2 Electrostatic Network Mutants in PapC

In order to assess whether specific electrostatic networks within the usher are responsible for modulating plug displacement required for pilus assembly, we investigated the D-Quad, R-Quad, and R-Pairs mutants individually in patch-clamp. At voltages below the threshold required to trigger plug displacement, all of the mutants displayed an electrophysiological signature similar to that of WT PapC (compare Figure 4.2 with Figures 4.4 to 4.6).

Also similarly to the WT PapC usher, we were able to induce plug displacement in all electrostatic network mutants. Interestingly, the unique signature of the plug displacement event and subsequent relaxation is also similar to that of the WT for most of the mutants. The exception to this is the R-Pairs mutant (Figure 4.6). In contrast to the D-Quad and R-Quad mutants which had an average threshold voltage similar to that of WT (Figures 4.4 and 4.5), the threshold voltage required to trigger plug displacement in the R-pairs mutant was ~ 40 mV lower than in the WT (Figure 4.6). In addition, while the WT activity typically returns to normal when low voltages are again applied after plug displacement, the R-Pairs mutant often retained a very active kinetic mode even when

Figure 4.2 Patch-clamp analysis of WT PapC usher. *The figure showcases representative single channel recordings of WT PapC in patch-clamp. The "C" denotes the current level for the closed channel, "M" the monomeric current level, and "D" the dimeric current level (correlating to plug displacement in both monomers of the PapC dimer). (**A**) At +140 mV, small transient deflections represent thermal fluctuations at small water-filled conduits at the plug domain interfaced with the barrel wall, perhaps due to "jiggling" of the plug-domain and other structural elements within the lumen. Some larger deflections are seen, but none reach the monomeric level of current indicated. (**B**) At -140 mV, some time after application of the voltage (typically 10-20 seconds), a large displacement event is observed that peaks at the dimeric level of current before relaxing, and represents a plug displacement event. The (*) represents the region of the trace that has been enhanced below on a shorter time span. The arrow in each panel points to the time point at which voltage was applied to the patch.*

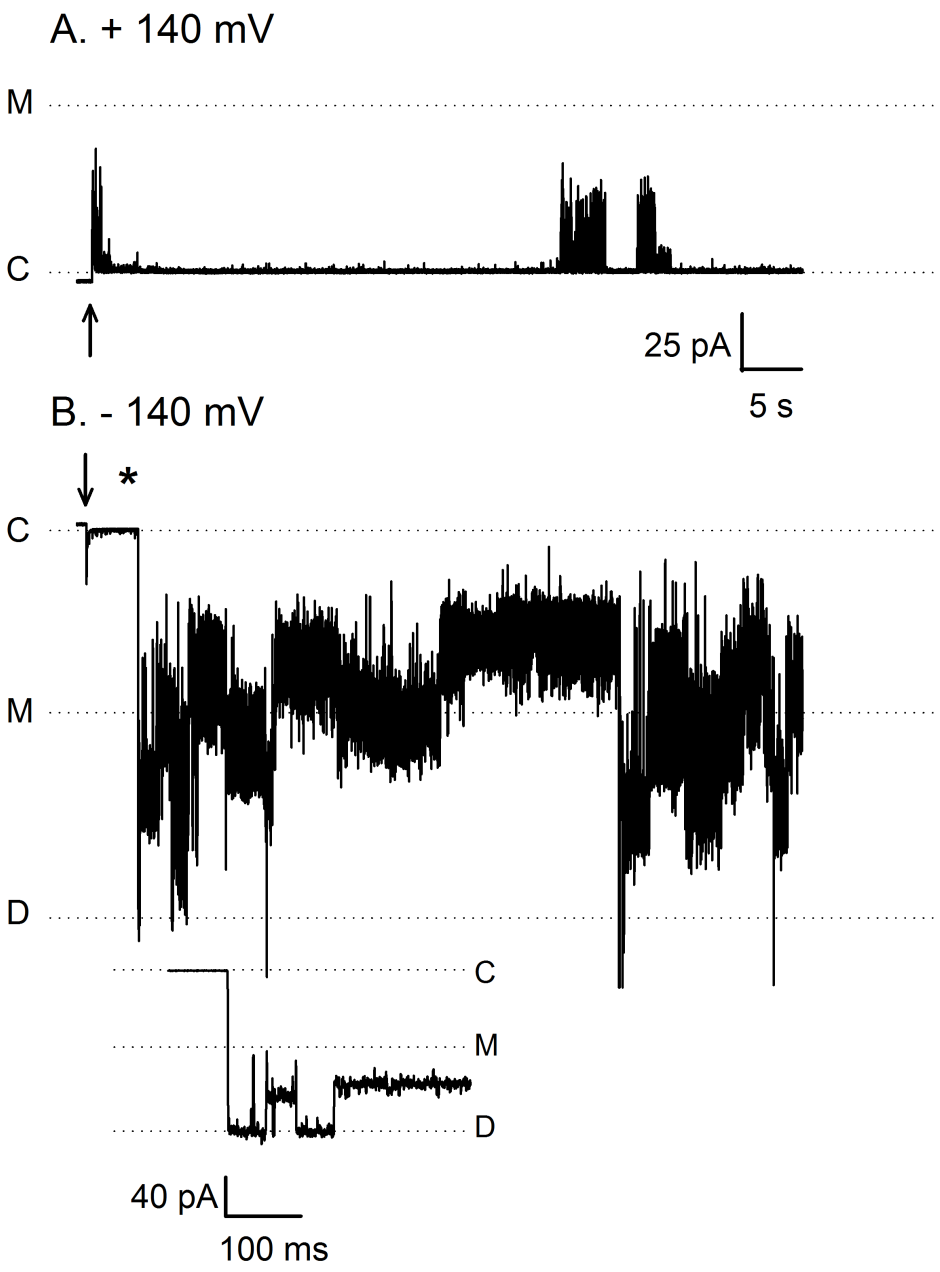
A. + 140 mV
M
C
25 pA
5 s
B. - 140 mV
*
C
M
D
C
M
D
40 pA
100 ms

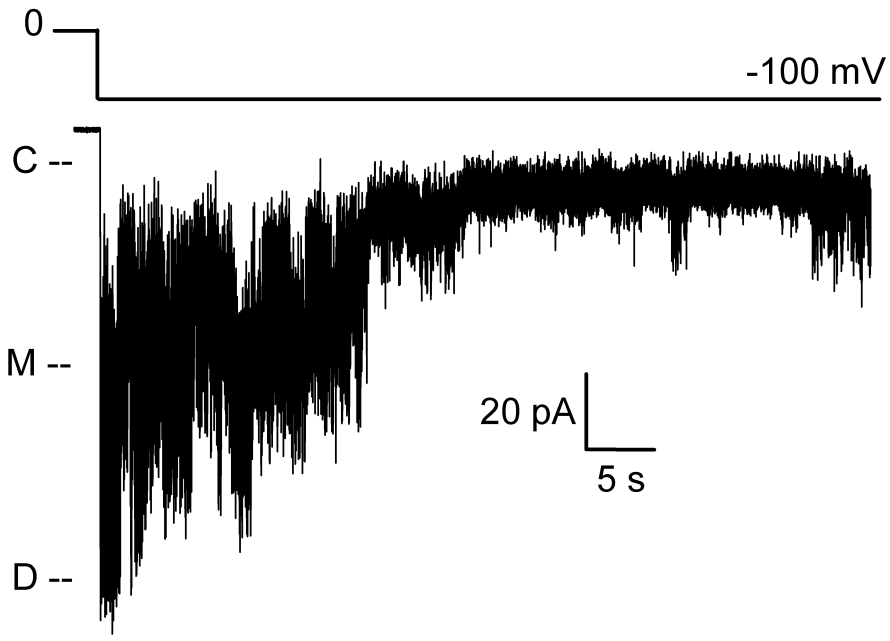

Figure 4.3 Current relaxation in the absence of plug domains. *A representative trace of the plugless PapC mutant shows an immediate dimeric current when a voltage is applied because the channel is fully already open. A relaxation of the current still occurs, perhaps due to barrel collapse and/or pore occlusion by the N- and C-terminal domains. The line above the trace indicates the voltage protocol. "C", "M", and "D" represent the closed, monomeric, and dimeric current levels, respectively.*

returned to low membrane potentials applied prior to plug displacement, as depicted in Figure 4.6 (compare traces of Figure 4.6A and 4.6C).

In order to quantify the effect of these mutations on channel gating, experiments were analyzed with respect to frequency of plug displacement occurrence and the required threshold voltage to trigger such events (Figure 4.7). Plug displacement was observed in 11 out of 15 experiments on WT channels, with an average displacement voltage of -134 mV. Plug displacement in the D-Quad mutant occurred much less frequently that the WT (3 out of 7 experiments). However, the voltage required to trigger these events in the D-Quad matched that of the WT. Likewise, the R-Quad mutant was also similar to WT. The most significantly affected mutant was the R-Pairs mutant with an average threshold voltage for plug displacement of -104 mV (Figure 4.7).

As mentioned previously, the R-Pairs electrostatic network is comprised of two pairs of arginine-arginine repulsive interactions, RSP-OUT (R237-R305 located towards the extracellular side of the usher) and RSP-IN (R256-R332 located at the base of the plug linkers at the periplasmic side of the usher). Thus, in order to determine which pair of arginine-arginine interactions contributed more to this reduced threshold for plug displacement, we also assayed each of the R-Pairs individually (Figure 4.8). The voltage required to trigger plug displacement in the RSP-IN mutant was most similar to that of the R-Pairs mutant (-106 mV) (Figure 4.7 and 4.8). In contrast, the threshold voltage of the RSP-OUT mutant was slightly less reduced compared to WT (-116 mV), but still significantly different from WT (Figures 4.7 and 4.9). Both mutants also had an increased frequency for plug displacement relative to WT. They also had the propensity to remain in an active state after plug displacement even at lower voltages, as seen for the R-Pairs

mutant (Figure 4.6C).

4.3.3 Gating Modes

As mentioned previously in respect to the R-Pairs mutant, plug displacement is typically followed by periods of high activity when returning to pre-displacement voltages. These are seen most often in the R-Pairs mutant and the other electrostatic network mutants but also in the WT usher, albeit to a lesser extent. This post-plug displacement period of activity is often characterized by a large amount of current transitions with distinctive kinetic signatures, open probabilities, and conductance levels, corresponding to different gating modes. Figure 4.10 shows examples of modal gating, where the channels appeared to spontaneously oscillate between different gating modes. We initially sought to categorize these different modes that we believed could be attributed to specific voltages or some other condition. However, we were unable to successfully identify any real correlation between gating mode and mutant type. Rather, we believed that mutations in the electrostatic networks helped the channel attain a level of dynamic activity following plug displacement that makes the gating modes more easily observable.

4.4 Effect of Chaperone-Adhesin Complex on PapC

In vivo, plug displacement and subsequently pilus biogenesis through PapC are initiated by the binding of the first subunit complex to the usher. This complex is comprised of PapD (chaperone) and the adhesive tip subunit, PapG, subsequently

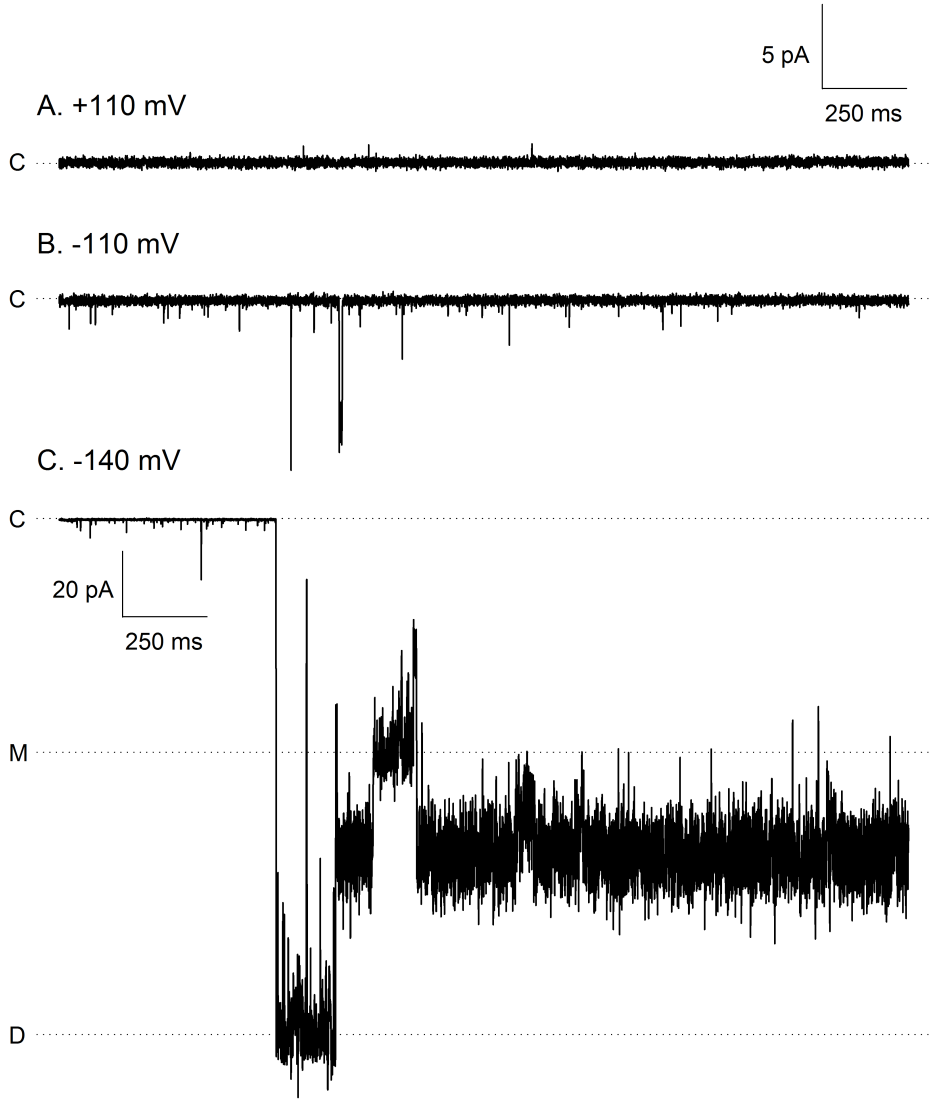

Figure 4.4 Representative traces of PapC D-Quad mutant. *The above are representative traces of PapC D-Quad mutant in patch-clamp from a single experiment at the indicated voltages. A plug displacement event is seen at -140 mV. "C", "M", and "D" represent the closed, monomeric, and dimeric current levels, respectively. Levels of conductance observed between "M" and "D" could possibly correspond to partial plug re-entry into one of the barrel monomers.*

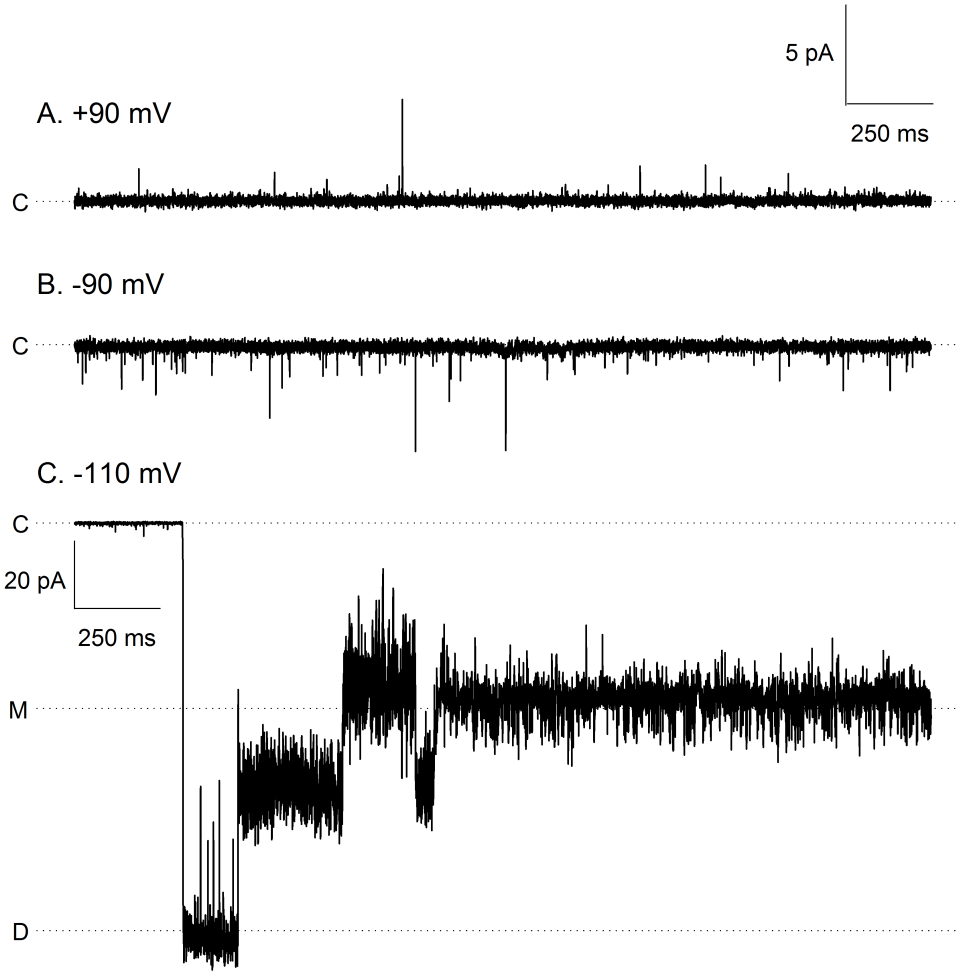

Figure 4.5 Representative traces of PapC R-Quad mutant in patch-clamp. *These traces showcase the activity of PapC R-Quad mutant from a single experiment at the voltages indicated. Small deflections of low conductance are transiently seen at + or – 90 mV. A plug displacement event is observed at – 110 mV. "C", "M", and "D" represent the closed, monomeric, and dimeric current levels, respectively. Levels of conductance observed between "M" and "D" could possibly correspond to partial plug re-entry into one of the barrel monomers.*

Figure 4.6 Representative traces of the PapC R-pairs mutant in patch-clamp. *These representative traces were obtained from a single experiment at the voltages indicated. (**A**) At -50 mV, the channel displays its typical quiet kinetic signature with small transient deflections of low conductance. (**B**) Increase in voltage to -100 mV triggers plug displacement. (**C**) When the voltage is returned to -50 mV after plug displacement, the R-pairs mutant is still highly active with distinct monomeric and dimeric levels of conductance, as highlighted in the expanded view. The (*) indicates the region of each main trace expanded below. "C", "M", and "D" represent the closed, monomeric, and dimeric current levels, respectively. Levels of conductance observed between "M" and "D" could possibly correspond to a full displacement from one barrel monomer and partial displacement from the other, however, this remains unclear.*

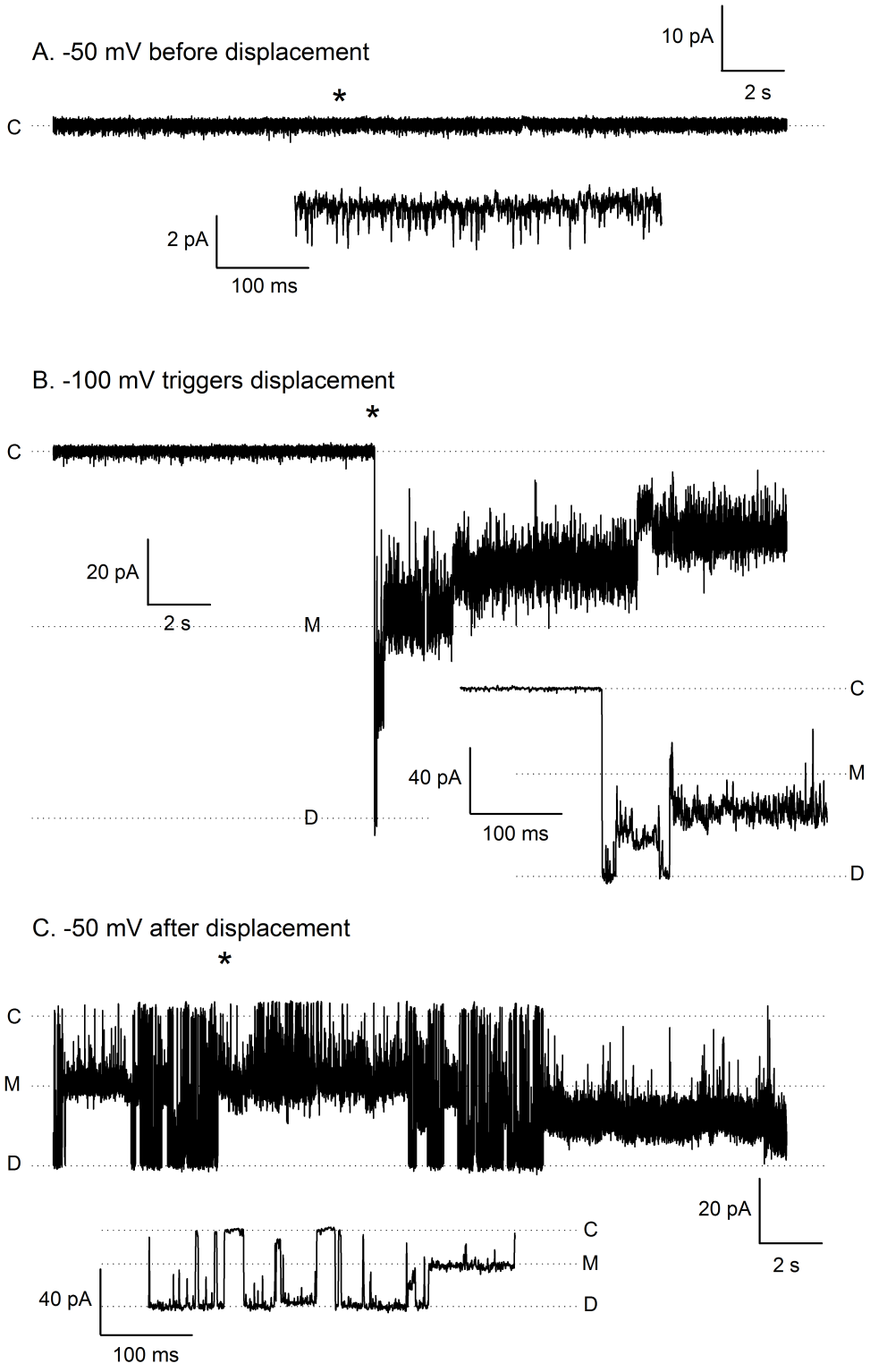
A. -50 mV before displacement
10 pA
2 s
*
C
2 pA
100 ms
B. -100 mV triggers displacement
*
C
20 pA
2 s
M
D
C
40 pA
M
100 ms
D
C. -50 mV after displacement
*
C
M
D
20 pA
2 s
C
M
40 pA
D
100 ms

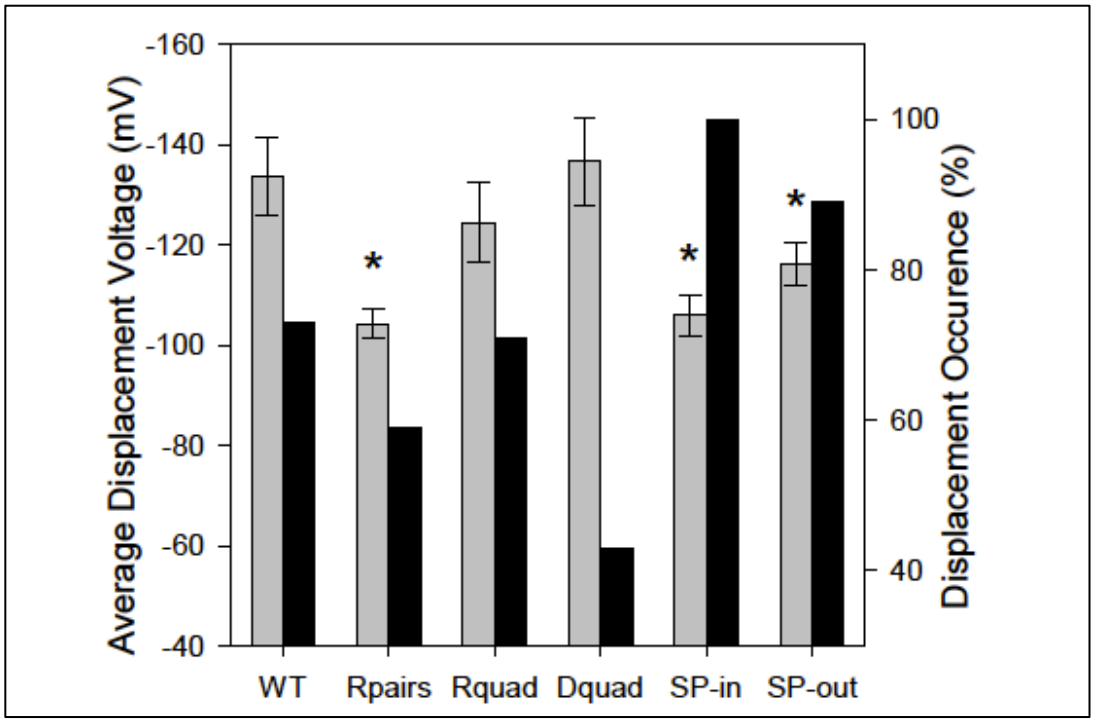

Figure 4.7 Plug displacement parameters in WT and mutant PapC. *The chart displays the average voltage required to trigger plug displacement as well as the frequency of occurrence for WT PapC and each of the mutants. (*) designate statistically significant results compared to WT PapC at the p=0.05 level. Error bars are s.e.m. The numbers (N) of samples used for the average displacement voltage are: 11 for WT, 7 for R-pairs, 9 for R-quad, 3 for D-quad, 5 for SP-in and 8 for SP-out. There are no error bars for the % occurrence, since this is not an average, but a value computed from all the experiments.*

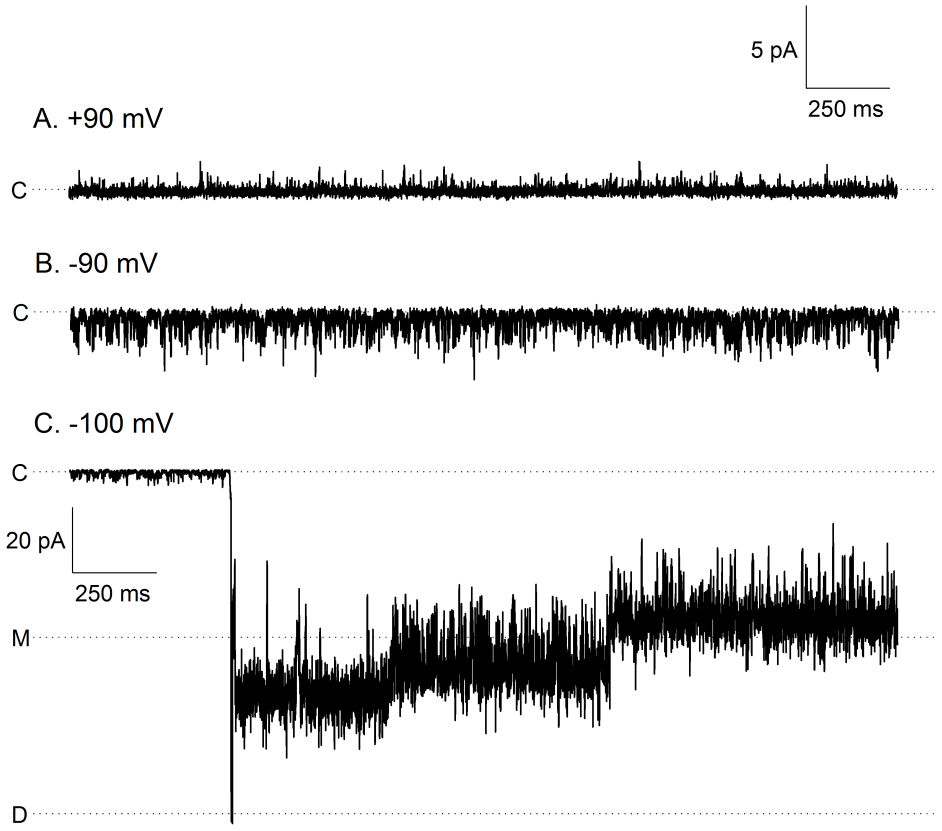

Figure 4.8 Representative traces of PapC RSP-IN mutant. *These traces showcase the activity of PapC R-Pair IN mutant from a single experiment at the voltages indicated. Small deflections of low conductance are transiently seen at + or – 90 mV, sometimes with increased kinetics as observed here. A plug displacement event is observed at – 100 mV. "C", "M", and "D" represent the closed, monomeric, and dimeric current levels, respectively. Levels of conductance observed between "M" and "D" could possibly correspond to partial plug re-entry into one of the barrel monomers.*

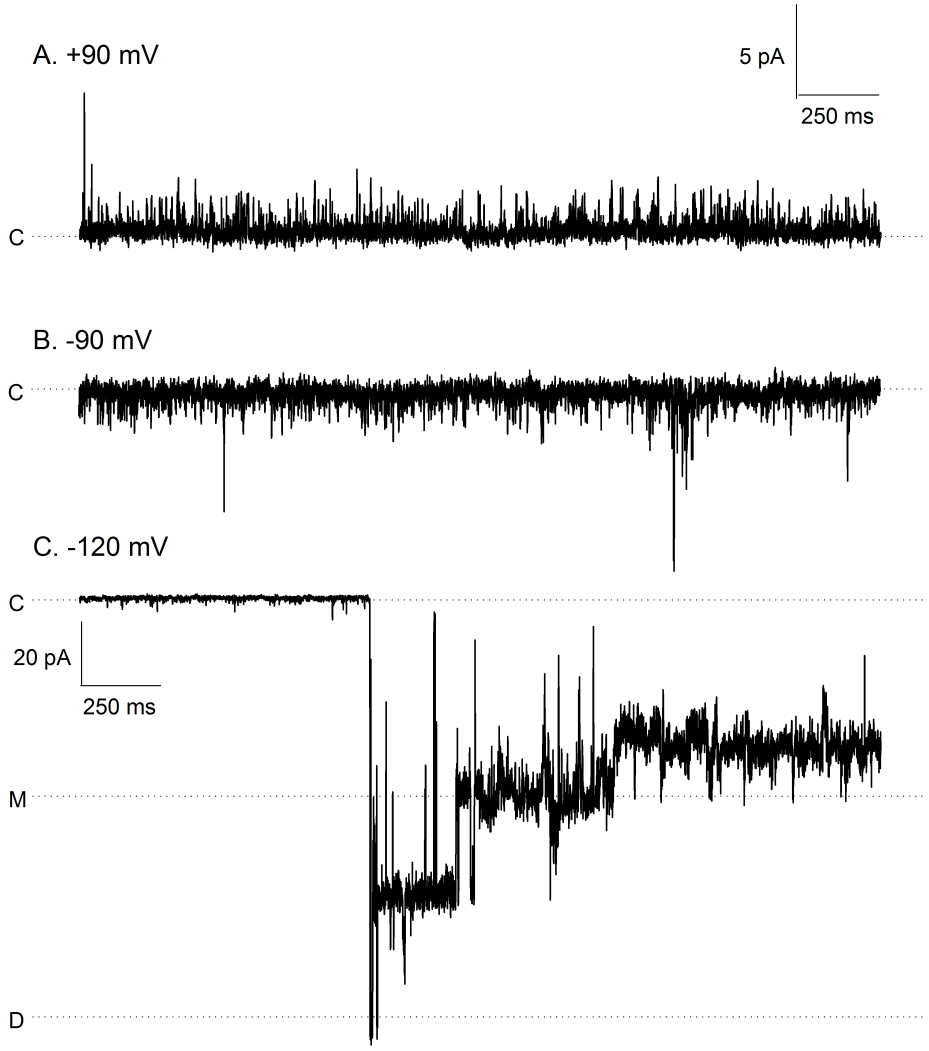

Figure 4.9 Representative traces of PapC RSP-OUT mutant. *The above traces showcase the activity of the PapC R-Pair OUT mutant at the voltages indicated. A plug displacement event is seen at – 120 mV, channel kinetics are frequent but still small in conductance. "C", "M", and "D" represent the closed, monomeric, and dimeric current levels, respectively. Levels of conductance observed between "C", "M", and "D" could possibly correspond to partial plug re-entry into the barrel monomers.*

referred to as PapDG. Because we thought that the initial chaperone-subunit binding to the usher triggers a large global conformational change that results in the displacement of the plug domain, we sought to determine the effects of this initial chaperone-adhesin complex on PapC usher activity. We observed during our plug-displacement experiments that we could re-trigger displacement once the channel closed. We could achieve this by applying a pipette potential at the threshold voltage or slightly higher, and this could often be repeated multiple times. Also, because the R-Pairs mutant could displace the plug domain at lower threshold voltages compared to the WT, this indicated that the value of the threshold voltage could be used to indicate the propensity for the usher to displace the plug domain. Thus, we recorded WT PapC activity in patch clamp, and obtained the channel threshold voltage for plug displacement. In the same patch, we subsequently added 325 nM of PapDG to the bath (an amount ~ 5 times higher than the K_d required for PapDG binding to PapC) (Li et al., 2010; Saulino et al., 1998) and re-triggered plug displacement. We observed that exposure to PapDG resulted in a 30% decrease in threshold voltage required for plug displacement (Figure 4.11A). Therefore, this indicated that the WT PapC usher had an increased propensity for plug displacement in the presence of PapDG. Re-triggering plug displacement revealed that the decrease in voltage threshold remains consistent as long as PapDG was in the bath. However, upon the removal of the chaperone-adhesin complex from the bath via perfusion, the threshold voltage required for displacement returned to similar levels seen prior to PapDG exposure. PapDG did not appear to alter the kinetics of the channel during plug displacement or relaxation, although this may be masked by the high level of dynamic activity during these events. When the same experiments were performed with the R-

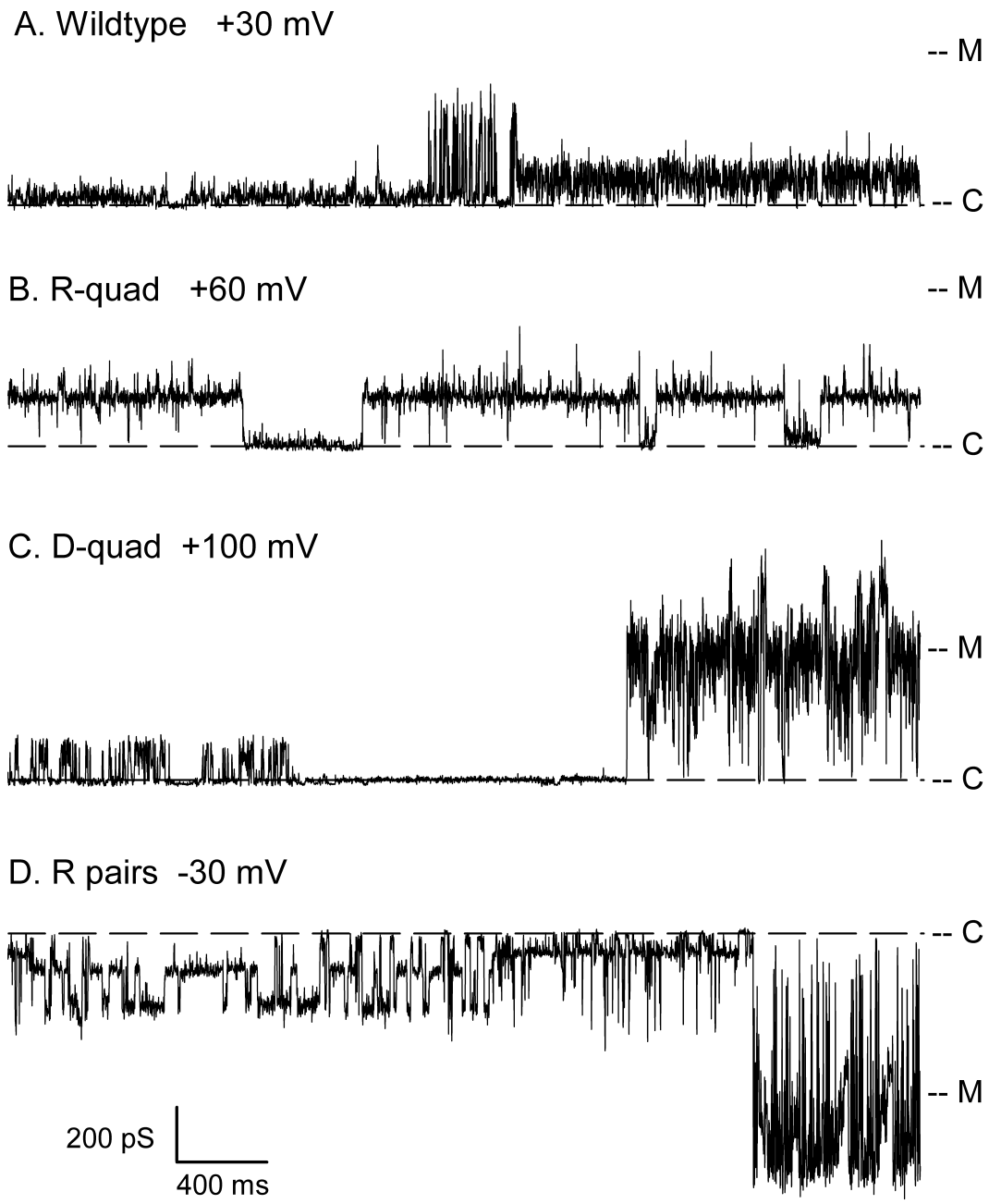

Figure 4.10 Modal gating of the WT and electrostatic network mutants. *The figure showcases representative recordings of modal gating in the WT and electrostatic network mutants. The "C" denotes the current level of the closed channel, and "M" signifies the monomeric current level. The recordings were obtained at the indicated pipette voltages.*

Pairs mutant, we observed no effect on the average voltage threshold required to displace the plug domain (Figure 4.11B). Thus, this *lack* of an effect substantiates the earlier observation that the R-Pairs network indeed functions to modulate plug domain activity.

Although plug-displacement events still occurred for WT ushers in the presence of PapDG, we observed that the conductance of such events was significantly reduced in those conditions (Figure 4.12). The effect was fully reversible upon PapDG washout. Interestingly, the reduced conductance appeared when the plug displacement was triggered not the 1st time, but the 2nd time in the presence of PapDG, and subsequently until PapDG was washed out. It is possible that the reduced conductance is due to a reversible block of one of the usher β-barrels by a delivered PapG subunit. A possible scenario is that the first plug displacement event occurred in both monomers of the dimer, allowing PapG to start moving inside one of the open pores, as shown in structural studies (Phan et al., 2011). Subsequent displacements would originate from the remaining non-occupied pore, with a conductance ~ 60% of the dimeric one. It is not surprising that the conductance of the remaining pore is not exactly half of the dimeric conductance, since the monomeric conductances of the plugless PapC and *Vibrio cholerae* OmpT porin, for example, have been reported not to be exactly the same for all the monomers of the respective oligomers (Duret and Delcour, 2006; Mapingire et al., 2009). Since the effect is fully reversible, the PapG subunit must be able to dissociate from the usher pore upon wash-out of the PapDG complex. This is consistent with the measured dissociation rates of chaperone-adhesin complexes from the usher in the absence of other subunits required for pilus assembly (Saulino et al., 1998). Interestingly, the reduced conductance was not observed in the R-pairs mutant (Figure 4.12).

Figure 4.11 Effect of PapDG on threshold voltage for plug displacement*. The threshold voltage for plug displacement was determined for WT PapC (**A**) and the R-pairs mutant (**B**). The graphs plot the ratio of this voltage in each condition to the threshold voltage in the initial condition prior to application of PapDG (PRE 1), with the PRE 1 voltage set to 100%. The dashed line marks the 100% level. For both graphs, the conditions were: 1st and 2nd measurements prior to PapDG application (PRE 1 and PRE 2); 1st to 5th measurement in the presence of 325 nM PapDG (DG 1 to DG 5); 1st and 2nd measurement after perfusion of PapDG out of the bath (OUT 1 and OUT 2). The data points represent averages ± s.e.m. of 9 and 5 measurements for WT and R-pairs mutant, respectively. Note that the number of measurements taken into the average varies for each time point, because it was not always possible to maintain the patch for the whole series of measurements.*

A. WT

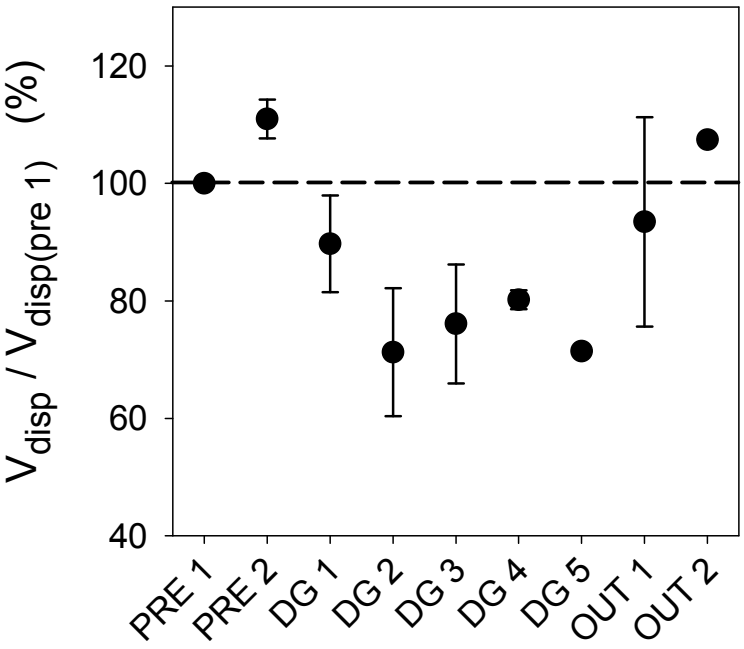

B. R-pairs mutant

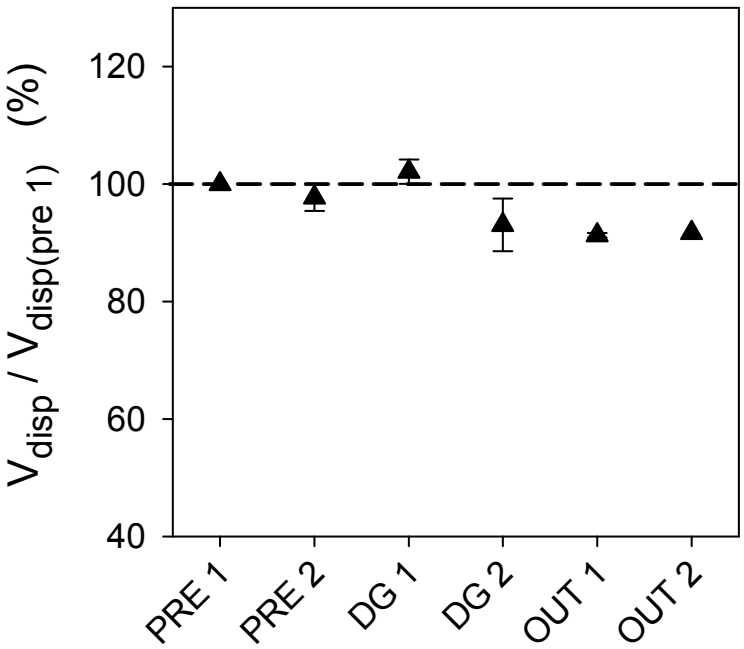

Figure 4.12 Effect of PapDG on conductance*. The immediate peak conductance reached upon plug displacement was measured for WT PapC (A) and the R-pairs mutant (B). For both graphs, the conditions were: 1st and 2nd measurements prior to PapDG application (PRE 1 and PRE 2); 1st to 5th measurement in the presence of 325 nM PapDG (DG 1 to DG 5); 1st and 2nd measurement after perfusion of PapDG out of the bath (OUT 1 and OUT 2). The data points represent averages ± s.e.m. of 7 and 5 measurements for WT and R-pairs mutant, respectively. Note that the number of measurements taken into the average varies for each time point, because it was not always possible to maintain the patch for the whole series of measurements.*

A. WT

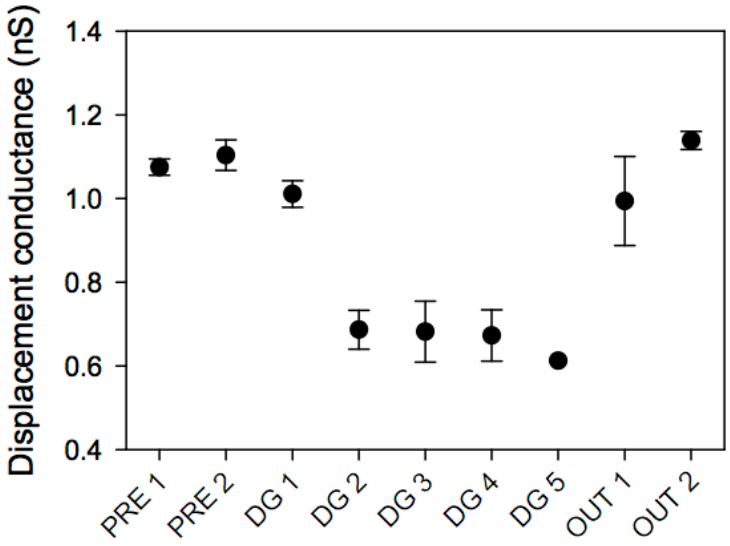

B. R-pairs mutant

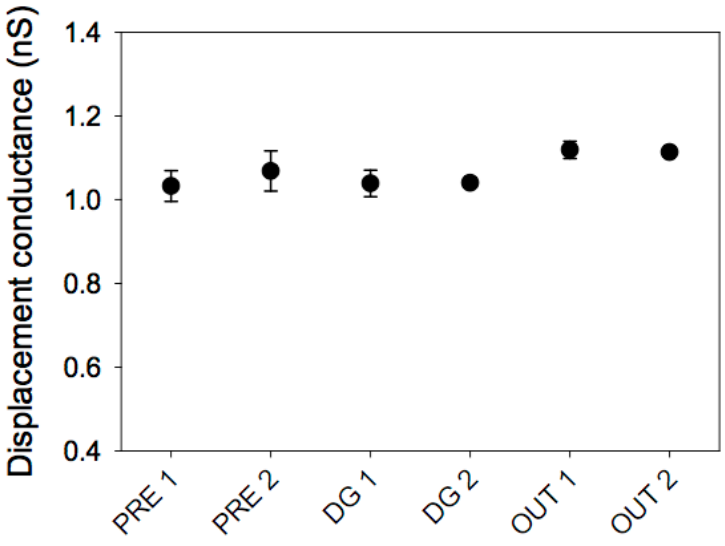

4.5 Discussion

The PapC usher functions to assemble P pili at the bacterial cell surface, which are responsible for promoting host cell adhesion. Previous electrophysiological studies using planar lipid bilayer techniques on this usher established that the channel has a highly dynamic behavior (Mapingire et al., 2009). In the conserved *fim* system, Phan et al. were able to obtain the resolved crystal structure of the complex of the usher with a bound chaperone-adhesin complex, providing a snapshot of the fimbriae biogenesis process (Phan et al., 2011). It revealed that the plug domain is displaced towards the periplasmic side during fimbriae translocation. Thus, this plug displacement step is critical in the process for pilus biogenesis. We identified three distinct electrostatic networks at the interfaces of the plug domain with various structural elements within PapC and postulated that one or more of these networks may function to modulate gating of the plug domain. We were able to trigger plug displacement in the PapC usher reproducibly in our electrophysiological experiments, by using high membrane potentials. This provided us with a reliable method by which to determine whether a particular electrostatic network was critical for usher function. These characteristic plug displacement events were observed for the WT PapC usher as well as each mutant tested.

We expected that salt bridges might play an important role in stabilizing the plug domain in the channel lumen. Interestingly, no statistically significant effect was observed in the D-Quad and R-Quad mutants, both of which have disruptions in salt bridges. However, as seen in Table 4.1, the distances between the R305-D323 pair (mutated in the R-Quad mutant), and the D234-R303 pair (mutated in the D-Quad mutant) are slightly larger than is appropriate for salt-bridge formation. This may be the

reason why no significant differences were observed in these mutants.

The most significant results were observed in the R-Pairs mutant. This is interesting because the R-Pairs electrostatic network is comprised of two arginine-arginine pairs that are postulated to generate a repulsive force at the interface between the plug domain with the β5-6 hairpin (RSP-OUT) and between plug-linker 1 and plug-linker 2 at the base of the barrel towards the periplasmic side (RSP-IN). Attractive interactions between the stacked parallel guanidinium groups of arginines have been reported when the guanidinium groups are in close proximity (< 4 Å) (Vondrasek et al., 2009). In proteins with known crystal structures, there is ~ 10% occurrence of guanidinium groups located within 6 Å of each other, and 40% of these are parallel (Lee et al., 2013). Our analysis of the distances between the C_ζ atoms of the guanidinium groups and the angle between the guanidinium groups are 6.9 Å and 50.1^o for R256/R332, and 4.3 Å and 74.3^o for R237/R305 (Figure 4.13). Therefore, attractive forces between these arginine pairs are unlikely.

Notably, as illustrated in Figure 4.8, the RSP-IN mutant appeared to contribute most of the increased sensitivity observed in the R-Pairs quadruple mutant relative to the RSP-OUT mutant (Figure 4.9, compare RSP-IN vs. RSP-OUT in Figure 4.7). In addition, the HA titer for the RSP-IN mutant was 0 (as in the R-pairs mutant), while it was as WT for the RSP-OUT mutant. Therefore, it appears that the cellular and electrophysiological phenotypes of the R-pairs mutant are best recapitulated in the RSP-IN mutant, suggesting a prime role of the repulsive interaction between R256 and R332 in controlling the stability of the plug, and the ability of the usher to assemble a functional pilus.

The R-pairs mutant was also insensitive to the effect of the chaperone-adhesin

complex PapDG. The lack of effect confirms the involvement of these two pairs of arginines in the molecular mechanism underlying the plug displacement event, and substantiates the conclusion that PapDG does indeed promote plug release. Essentially, since the mutations have already enhanced the ability of the channel to release the plug, the application of PapDG does not further contribute to plug displacement in such a mutant. These results suggest that one mechanism by which PapDG promotes plug release in the WT usher is to weaken the repulsive interactions between the arginines of the pairs R237-R305 and R256-R332, as mimicked by the alanine mutations at these sites.

In addition, we have observed that the presence of PapDG does not affect the conductance of the R-pairs mutant. We infer that the mere displacement of the plug domain, which also occurs in the R-pairs mutant albeit in a non-PapDG dependent way, is not sufficient for PapG to move inside the pore and block it. This entry of PapG in the pore must require a productive association of PapDG with the usher that leads to a PapDG initiated plug release, rather than one that occurs simply because the plug domain has been released. This observation is consistent with the complete defect in pilus biogenesis of the R-pairs mutant, as well as of plugless PapC mutant (Henderson & Thanassi, unpublished).

In summary, we believe that *in vivo*, binding of the chaperone-subunit complex to PapC results in a series of local conformational changes that translates into a large global conformational change triggering release of the plug domain towards the periplasm. This displacement would then allow pilus subunits access to the lumen for translocation and pilus biogenesis. Interestingly, this conformational change must somehow disrupt the

repulsive interactions within the RSP-IN and RSP-OUT arginine pairs in order to accomplish this, and perhaps impact RSP-IN even more since it is closer to the PapDG binding site on the periplasmic N-terminal domain. In our *in vitro* system, applying a high membrane potential appeared to mimic the conformational changes that would result from chaperone-subunit binding (Figure 4.14). Indeed a lower threshold voltage is required to activate a mutant usher (the R-pairs mutant) already primed to open due to the weakened repulsive forces between key arginine pairs. We can imagine that the repulsive interaction between the arginines located on the two P-linkers (R256 and R332) may act as a wedge keeping the two linkers apart and preventing the plug from exiting the barrel lumen. It is easily conceivable that the two linkers must indeed move relative to each other when the plug relocates towards the periplasmic side. This relative movement may be facilitated when the repulsive interaction between these residues is disrupted by the alanine substitutions, or by productive interactions of PapDG with the usher.

Finally, we noted that plug displacement was always observed at negative membrane potentials and never at positive ones, even up to +200 mV. This indicates that the purified PapC protein always reconstitutes in the same orientation. This may be due to the presence of the globular N-terminal and C-terminal domains, although we have no concrete evidence. Unfortunately ΔN, ΔC, and ΔNC mutants did not reconstitute efficiently into liposomes, preventing us to directly test the role of these domains in determining the orientation of the reconstituted protein. However, it is likely that these globular domains may play important role in guiding insertion of the usher into the membrane in our reconstitution system.

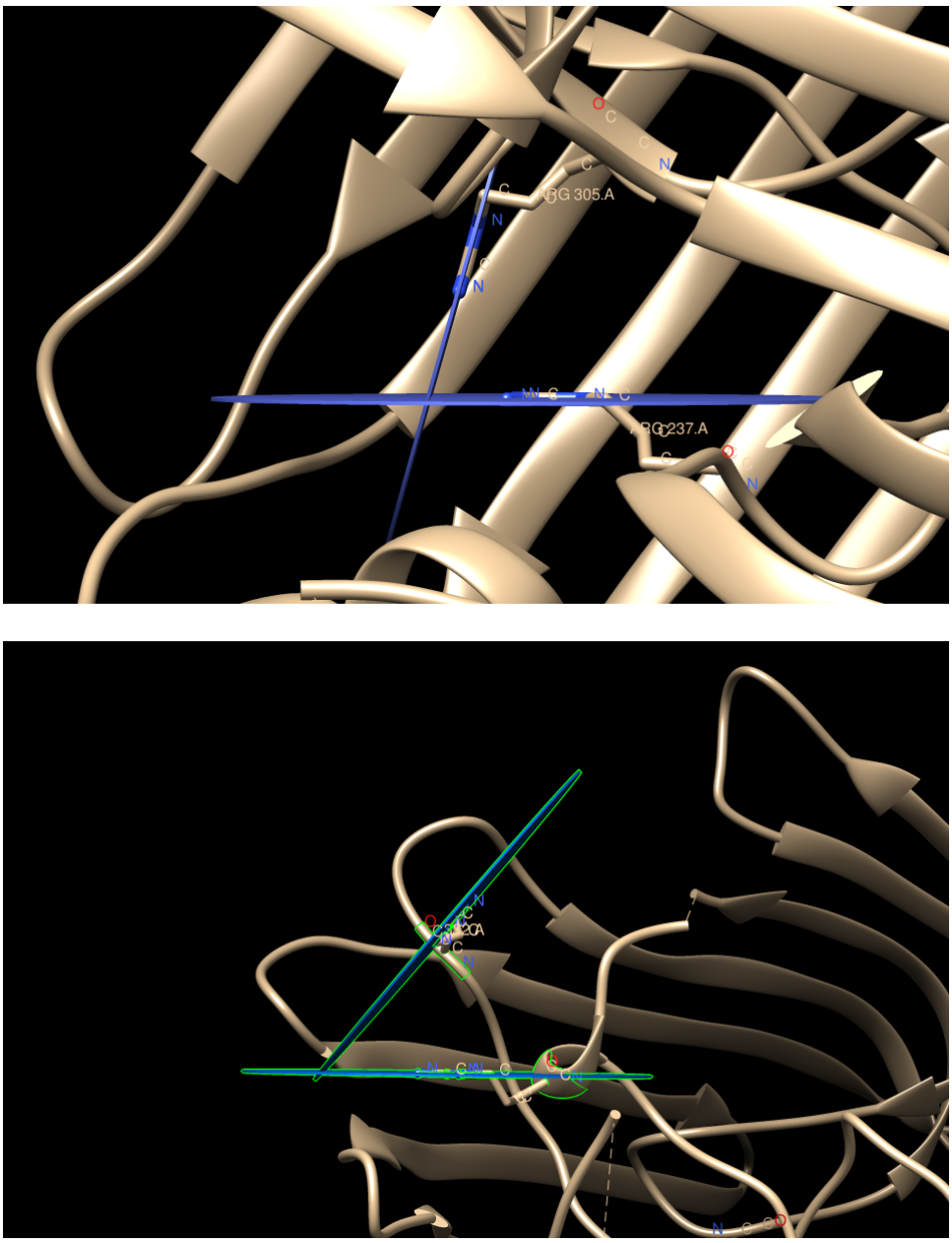

Figure 4.13 Chimera analysis of arginine-arginine side groups. *Chimera was used to determine whether each R-Pair formed base stacking interactions. The top panel is RSP-OUT, and the bottom panel is RSP-IN. The RSP-OUT angle was 74.3^{o} and the RSP-IN angel was 50.1^{o}.*

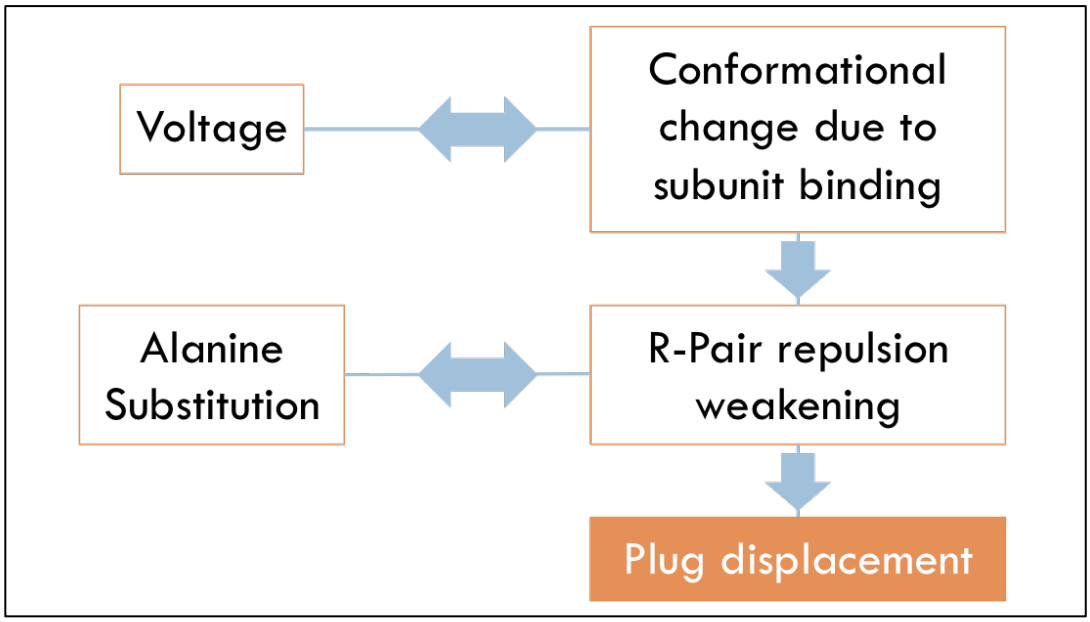

Figure 4.14 Proposed model of a pathway for plug displacement. *Right-hand side: In vivo, chaperone-subunit binding results in a conformational change that leads to weakened repulsive interactions at the R256-R332 and R237-R305 pairs. This in turn destabilizes the plug and allows it to be displaced to open the channel. Left-hand side: High transmembrane voltage induces a conformational change that mimics the one triggered by PapDG binding. Alanine mutagenesis weakens the repulsive interactions at the arginines in a similar way to the weakening triggered by the conformational change.*

CHAPTER 5

Rotavirus Viroporin NSP4

In collaboration with Dr. Joseph Hyser at Baylor College of Medicine

5.1 Introduction

5.1.1 Viroporins

Viruses are parasites that subjugate host cell machinery in order to fuel their replication cycle and propagate. In order to aid in this process, many viruses utilize pore-forming proteins inserted within intracellular host membranes, specifically the ER (Martinez-Gil and Mingarro, 2015; Nieva et al., 2012). This provides the virus with the ability to manipulate the ionic gradients to their strategic advantage (Royle et al., 2015). These proteins are collectively known as viral-encoded pore-forming proteins, or viroporins. In fact, many major human pathogens employ these viroporins, such as picornaviruses (Nieva et al., 2003; OuYang and Chou, 2014; Scott and Griffin, 2015; Nieto-Torres et al., 2015), paramyxoviruses (Royle et al., 2015), and human immunodeficiency virus (HIV) type-1 (Gonzalez, 2015; Martinez-Gil and Mingarro, 2015; Nieto-Torres et al., 2015), to name a few. Although still considered a relatively new field of research, studies into viroporins over the years have shown that these viral proteins are indeed channels capable of conducting the passage of ions (Delcour, 2015; Nieva et al., 2012; Scott and Griffin, 2015; Hyser, 2015). Abolishing the activity of these viroporins through knockdowns results in diminished virulence and as such is considered an important field of study (Giorda and Hebert, 2013; Nieva et al., 2012). A current challenge in the viroporin field is the identification of novel viroporins due to a distinct lack of sequence homology between those currently known. However, viroporins share a common structural motif, which defines the family, the viroporin domain (see below), although it is difficult to identify using strictly sequence information. A limitation is also the paucity of resolved high-resolution crystal structures for most of the viroporins (Gan

et al., 2012; Madan and Bartenschlager, 2015; OuYang and Chou, 2014; Pervushin et al., 2009). Fortunately, a novel bioinformatics approach has been successful in identifying key structural characteristics in viroporins lacking a resolved crystal structure (Scott and Griffin, 2015; Wetherill et al., 2012).

5.1.2 Structural Characteristics of Viroporins

The size of viroporins ranges between 60-270 amino acids in length (Royle et al., 2015), making them relatively small among ion channels. As typical ion channels, they are comprised of transmembrane domains, including amphipathic α-helices to form the channel wall (Gonzalez and Carrasco, 2003). The signature motif of the family, the viroporin domain (VPD) includes a cluster of basic residues, such as arginine and lysine, in close proximity to an amphipathic α-helix, which will be one of the transmembrane domains. Although unproven, it is believed that these charged residues promote association with the lipid membrane and subsequent insertion of the VPD (Gonzalez and Carrasco, 2003). To create a channel, the viroporins must oligomerize to bring the α-helical bundles in close proximity to form the channel wall (Gonzalez and Carrasco, 2003). The oligomer is typically at least a tetramer (for example, the M2 viroporin of influenza A virus; (Sakaguchi, 1997b; Sakaguchi, 1997a; Sakaguchi et al., 1997)), but can range up to a heptamer (for example, the p7 viroporin of hepatitis C virus; (Clarke et al., 2006; Madan and Bartenschlager, 2015)).

Because of the lack of sequence homology and conservation, viroporins are currently categorized according to their membrane topology (Nieva et al., 2012). For example, the number of transmembrane domains required to form the pore classifies the

channel as either a Class I or Class II viroporin (1 or 2 transmembrane domains, respectively) (Nieva et al., 2012). In addition, the location of the N-terminus of the protein, whether it be in the lumen of the intracellular compartment or outward into the cytoplasmic space, further groups these channels into subcategories A and B, respectively (Nieva et al., 2012). However, the primary criticism of this viroporin classification scheme is that it is unable to categorize (**1**) viroporins containing three transmembrane domains, (**2**) structurally similar viroporins with different functions, and (**3**) the ability of some viroporins to flip their C-terminal domains to the other side of the membrane under unique environmental conditions (Isherwood and Patel, 2005). Despite these caveats, however, this method is still currently the best means by which to categorize novel viroporins.

5.1.3 Electrophysiology of Viroporins

Current viroporin literature is often contradictory in regards to the channel characteristics (Scott and Griffin, 2015). Ultimately, it is believed that viroporins are very simplistic ion channels unlike the stereotypical voltage- or ligand-gated ion channels, which are highly regulated and with well-defined electrophysiological properties. Conflicting data from different investigators concerning ion specificity has resulted in the current skepticism within the scientific community about whether viroporins are actually *bona fide* channels or simply non-specific pores (Scott and Griffin, 2015). Because there is a distinct lack of sequence homology between viroporins, initial assays primarily focused on the ability of these viral-encoded proteins to either cause cell lysis or make

liposomes (*in vitro*) and bacterial cells (*in vivo*) permeable to fluorescent dyes. Subsequently, electrophysiological assays utilizing either planar lipid bilayer or patch-clamp techniques sought to refine in detail the characteristics of viroporins such as ion selectivity or specific conductance. However, some have criticized planar lipid bilayer experiments involving viroporins and the inability to assign a unitary level of conductance to the channel, because detergents or solvents involved in the channel purification or the technique itself could cause the appearance of channel-like artifacts (Kelly et al., 2003). An example is the Hepatitis C virus p7 viroporin whose electrophysiological signature could alternate between kinetics with well-defined unitary levels of conductance and a "bursting" behavior with frequent transient current fluctuations (Chew et al., 2009; Clarke et al., 2006; Griffin et al., 2003; Pavlovic et al., 2003; Premkumar et al., 2004; Whitfield et al., 2011). However, the "bursting" behavior observed with the planar lipid bilayer technique could in some instances merely be a result of too many channel insertions. Nevertheless, in order to prove a viroporin as a *bona fide* ion channel, studies must often combine both planar lipid bilayer and patch-clamp techniques to capture the kinetic signature of the channel (Hyser, 2015). The addition of a known chemical or ion inhibitor of that viroporin then helps to solidify the channel as *bona fide* (Hyser, 2015). In our study, we sought to employ a combination of the aforementioned in order to establish the viroporin NSP4 as a viral calcium channel.

5.1.4 The Rotavirus Viroporin NSP4

The infectious process of rotavirus results in a disruption of intracellular calcium

through an increase in cytosolic calcium concentration as a result of (**1**) increased cellular uptake of calcium and (**2**) depletion of ER calcium store (Berkova et al., 2006; Michelangeli et al., 1991; Perez et al., 1998; Zambrano et al., 2008). Interestingly, expression of rotavirus NSP4 viroporin alone can cause these effects (Berkova et al., 2003; Diaz et al., 2008; Tian et al., 1995). In addition it was shown that the NSP4 viroporin is the cause of calcium homeostasis disruption (Hyser et al., 2010). Therefore, we set out to study NSP4 electrophysiologically to (**1**) establish that it is indeed an ion channel, and (**2**) investigate whether it is a calcium-selective channel, or at least a channel permeable to calcium ions.

NSP4 oligomerizes as a tetramer in the membrane environment (Maass and Atkinson, 1990). Structurally, rotavirus NSP4 viroporin is unique in that it cannot be categorized into the current viroporin classification scheme because each monomer is predicted to contain three transmembrane domains (Hyser et al., 2010). Figure 5.1 depicts a cartoon of the domain organization of NSP4. The entire monomer spans 175 amino acids (aa) in length with the first 44 containing hydrophobic domains 1 and 2 (H1 and H2, respectively). Because H1 carries two putative high-mannose glycosylation sites, it is believed not to be a transmembrane segment, but rather to be oriented towards the ER lumen. H2 acts as an uncleaved signal sequence and is believed to be embedded in the membrane. It is followed by a viroporin domain (VPD) composed of a pentalysine domain and an amphipathic α -helical domain. This domain also houses two conserved cysteine residues (C63 and C71). Finally, the C-terminal region of the polypeptide includes a coiled-coil domain (CCD), and the double-layered particle receptor domain (DLP-R). In the model proposed by Hyser et al. (2010) (Hyser et al., 2010), the first

transmembrane segment, H2, directs the initial insertion of a NSP4 viroporin monomer such that H1 protrudes outward into the ER lumen. The VPD is proposed to insert as an α-helical hairpin with the pentalysine domain forming the 2nd transmembrane segment and the amphipathic domain of the VPD becoming the 3rd transmembrane segment, thus ultimately generating a three-pass transmembrane peptide. Upon oligomerization, the amphipathic domains of the VPD of the four monomers are proposed to from the inner lumen of the pore. This topological model then places the CCD and DLP-R as extruding out into the cytoplasmic space. Interestingly, the resolved crystal structure of the CCD shows it to contain a calcium-binding site, which may play a role in the cation selectivity to this viroporin (Viskovska et al., 2014) (PDB ID: 4WB4). In addition, the presence of bound calcium in the resolved structure of the CCD depends on the oligomeric composition of the domain: tetrameric conformation with a bound Ca2+ ion coordinated by residues E120 and Q123 (Bowman et al., 2000; Deepa et al., 2007; Sastri et al., 2014), or a pentameric structure lacking bound Ca2+ (Chacko et al., 2011). This might be of physiological significance, since a tetramer-to-pentamer transition can occur in the CCD upon lowering the pH (Sastri et al., 2014).

5.2 Electrophysiology of Viroporin NSP4

5.2.1 General Channel Kinetics

We utilized both planar lipid bilayer and patch-clamp techniques as described in Chapter 2 in order to assay viroporin NSP4. For the majority of our experiments, a lyophilized NSP4 synthetic peptide of the VPD (NSP4 VPD) was dissolved in various solvents including DMSO, water, TFE, ethanol, DMF, and OPOE detergent. This was

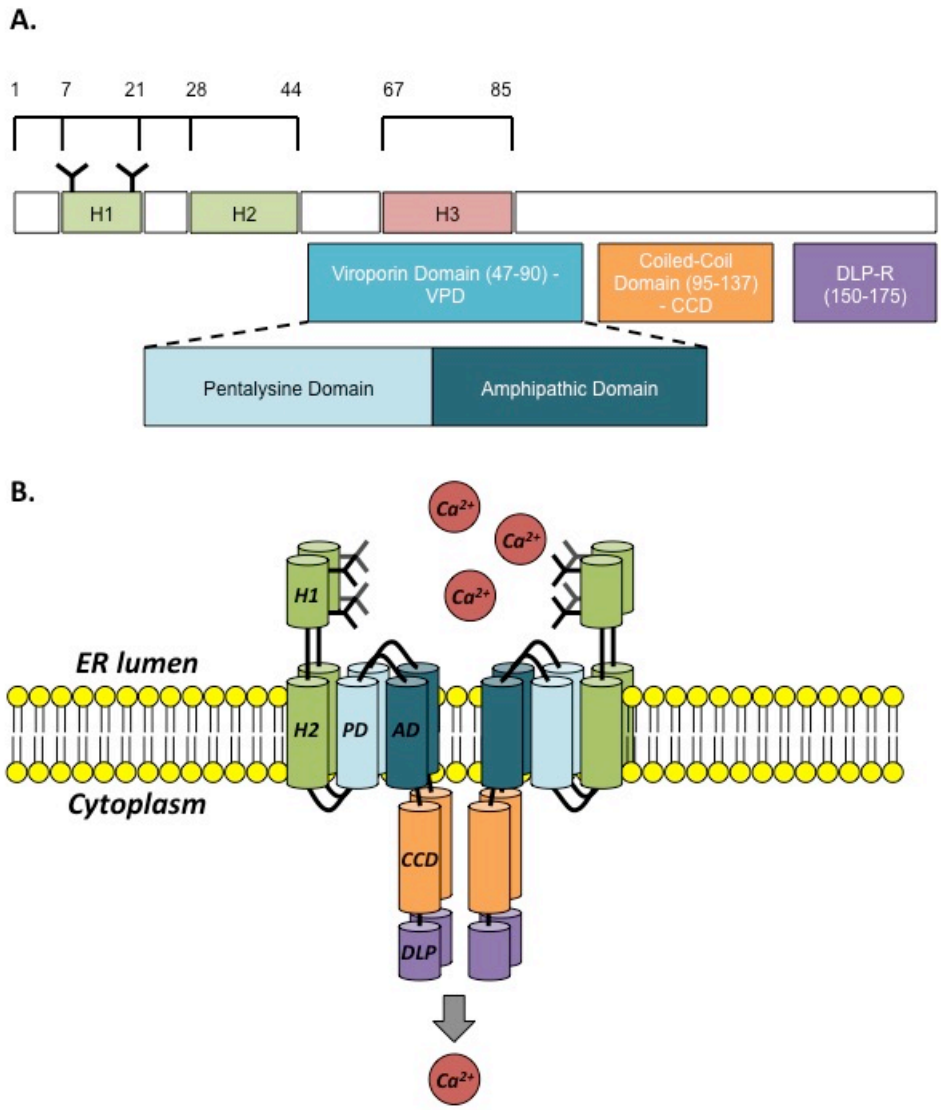

Figure 5.1: Cartoon representation of the NSP4 domains and the putative membrane topology of the tetramer. *Domains are color-coded as follows: H1 and H2, green; VPD, cyan; pentalysine domain (PD), light blue; amphipathic domain (AD), dark blue; CCD, orange; DLP-R, purple. The "Y" shapes represent putative glycosylation sites.* ***(A)*** *Domain schematic of NSP4.* ***(B)*** *Proposed topology for NSP4 being represented here as a tetramer, where calcium ions (red) flow from the ER lumen into the cytoplasm resulting in intracellular calcium increase. Modified from (Hyser et al., 2010).*

then either added directly to the *cis* chamber of a planar lipid bilayer set-up or reconstituted into liposomes for patch-clamp analysis. In both techniques, we captured two distinct electrophysiological signatures that characterize the NSP4 VPD peptide. Figure 5.2 shows that NSP4 VPD could display canonical well-defined opening events that measured approximately 70 pS in symmetric buffer conditions of 150 mM KCl with both techniques. These canonical "square-top" events are similar to those displayed by classical voltage or ligand-gated ion channels. In regards to this particular electrophysiological signature, the channel could be captured in a predominantly closed state with occasional opening events (Figure 5.2A), or it could be observed in a more actively open state defined by longer open times and occasional closing events (Figure 5.2B). Electrophysiological technique held no bearing on which state was captured.

In a large majority of the experiments, a second electrophysiological signature was characteristic of the NSP4 VPD. In this case, NSP4 VPD could adopt very fast kinetics that could be described as a particularly "spiky" behavior (Figure 5.3). In Figure 5.3A, NSP4 VPD was added to the *cis* side of the bilayer chamber and allowed to insert. The kinetics is characterized by very transient and frequent excursions in the downward or opening direction (Figure 5.3A). The high frequency of openings may be due to the concerted kinetics of multiple inserted NSP4 VPD oligomers in the lipid bilayer resulting in bursts of channel openings with very fast kinetics. However, when NSP4 VPD was reconstituted into liposomes and assayed by patch-clamp, it was also captured frequently in this predominantly "spiky" state (Figure 5.3B), even though it is likely that the patches contained fewer channels than the bilayer, simply because their surface areas are about 10

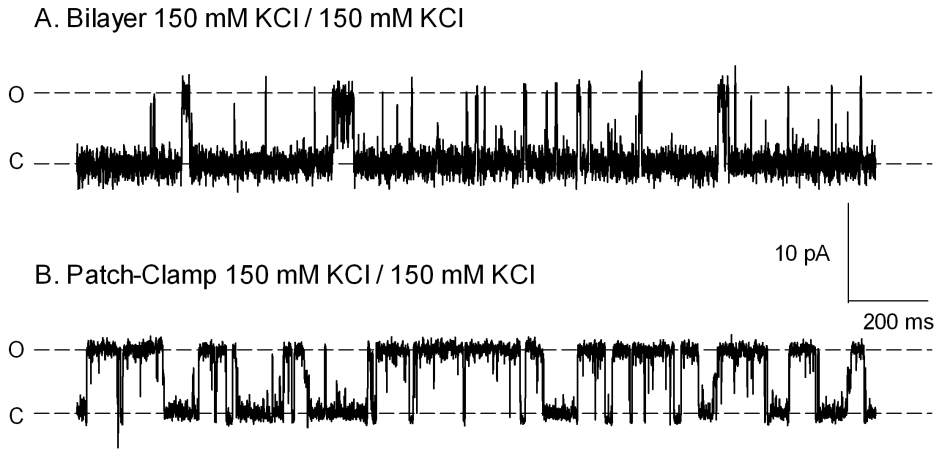

Figure 5.2 Kinetics of viroporin NSP4 VPD with well-defined openings. *The traces above are representative traces of NSP4 VPD in either (A) planar lipid bilayer or (B) patch-clamp with defined opening events and levels of conductance. The voltage used in both conditions was +90 mV in symmetric buffer conditions as indicated. The "c" denotes the closed level of conductance for the channel, and the "o" denotes the open level. These traces were both sampled at 100 μs intervals. (**A**) 2.5 μg of NSP4 VPD dissolved in DMSO was added to the cis side of the bilayer. In this experiment, the channel displays canonical well-defined opening events with a conductance of 70 pS. Such activity with square-top events was observed in less than 1 % of the bilayers. (**B**) NSP4 VPD dissolved in DMSO was reconstituted into multilamellar liposomes at a 1:3000 protein-to-lipid ratio (w:w) using the dehydration/rehydration method. The open level of conductance measured 70 pS.*

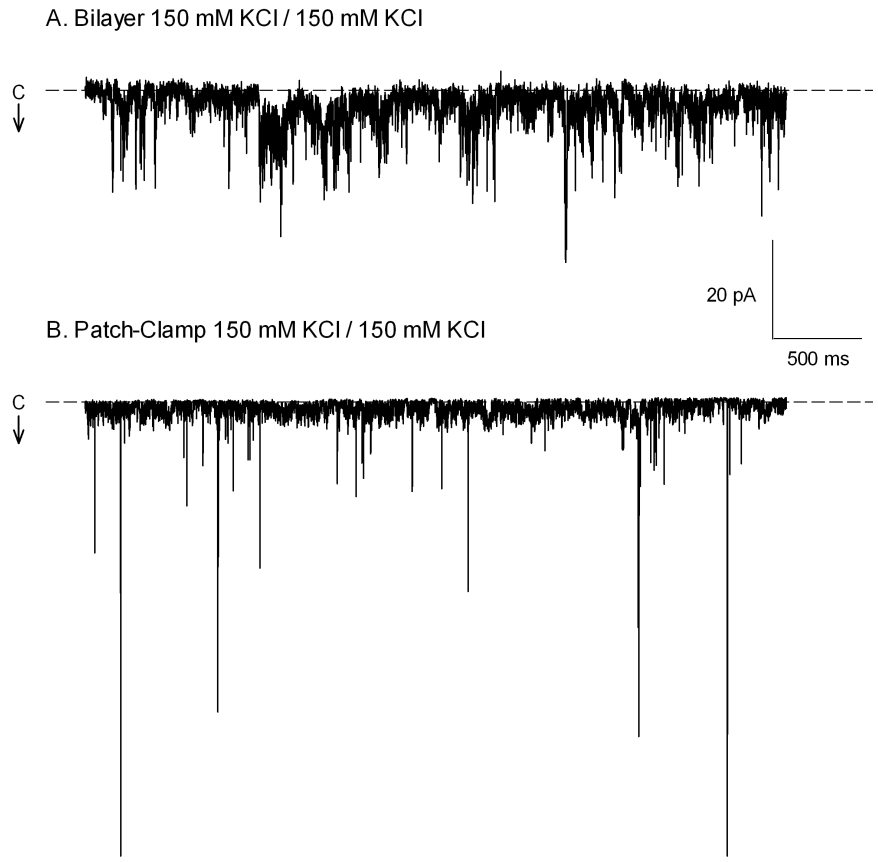

Figure 5.3 Kinetics of NSP4 VPD can also be fast. *Representative traces of rapid current fluctuations of NSP4 VPD in either (A) planar lipid bilayer or (B) patch-clamp with lack of discrete levels of conductance. The voltage used in both conditions was -60 mV in symmetric buffer conditions as indicated. The "c" denotes the closed level of conductance for the channel, and the arrow represents the direction of opening. These traces were both sampled at 100 μs intervals. (**A**) 3 μg of NSP4 VPD dissolved in DMSO was added to the cis side of the bilayer. In this experiment, the channel displayed current fluctuations of varied conductance represented by rapid and transient excursions in the downward direction. (**B**) NSP4 VPD dissolved in DMSO was reconstituted into multilamellar liposomes at a 1:200 protein-to-lipid ratio (w:w) using the rehydration/dehydration method.*

times smaller. Because the kinetics of this state were so rapid, we were unable to identify any well-defined and measurable levels of conductance.

Interestingly, the two types of kinetic behaviors could be seen within the same recording, as if NSP4 VPD is able to shift between the two electrophysiological signatures, "square-tops" and "spiky". Figure 5.4 shows a recording of the activity of NSP4 VPD dissolved in DMSO and reconstituted into liposomes utilizing the cloud method (see Materials and Methods), that illustrates that NSP4 VPD could shift states in the same experiment. As seen in the expanded segment highlighted by the red box, the reconstituted channel first displayed openings with a well-defined level of conductance measuring approximately 50 pS. However, within 500 milliseconds, the channel transitioned to the "spiky" state observed in a majority of our experiments. Similarly to Figure 5.3, due the rapid kinetics seen, we were unable to identify a unitary level of conductance when the channel is in the "spiky" state. Since we do not know how many channels are in the patch, we cannot ascertain whether the two distinct behaviors originate from two populations of channels (perhaps reconstituted differently) or from a single channel oscillating between two kinetic modes.

5.2.2 Calcium Conductance

Thus far, we have established that NSP4 VPD, which consists of only residues 47-90 comprising the conserved pentalysine domain and amphipathic α-helix, is indeed a channel capable of conducting ions in KCl solutions. The primary goal of this study was to determine whether NSP4 viroporin was indeed not only an ion channel, but one capable of conducting calcium as predicted by Hyser et al. (2010). Given that most

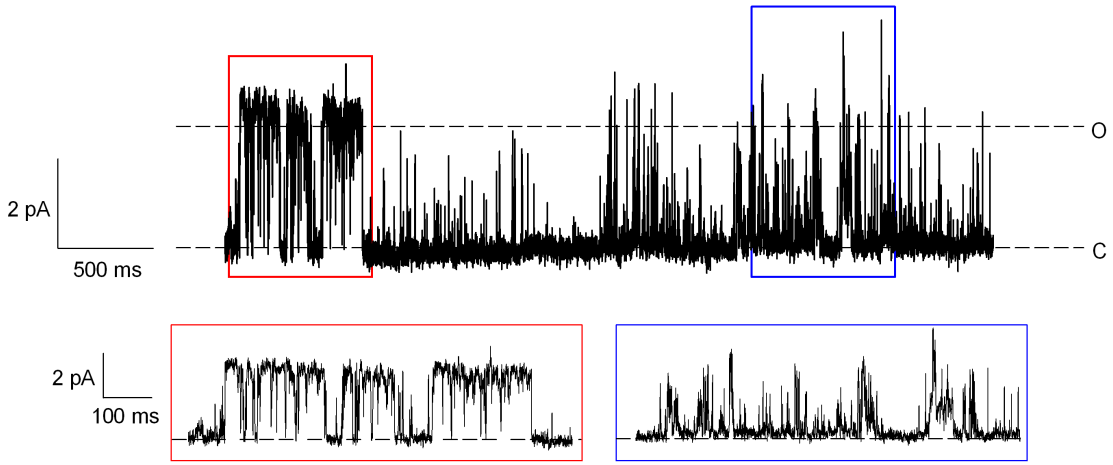

Figure 5.4 The kinetics of NSP4 VPD can vary within the same recording. *NSP4 VPD dissolved in DMSO was reconstituted into multilamellar liposomes at a 1:200 protein-to-lipid ratio (w:w) using the cloud method. The trace was obtained at +50 mV in patch-clamp in symmetric buffer conditions of 150 mM KCl (buffer A). The "c" denotes the closed level of conductance, and the "o" represents the open level of the channel obtained from well-defined openings. The red and blue boxes indicate the regions of the trace that are expanded below. The expanded segment in the red box has a conductance level measuring 50 pS. However, the expanded segment in the blue box has ill-defined conductance levels due to its highly transient and rapid kinetics.*

viroporins studied by electrophysiology to date are cation-selective channels (Hyser, 2015), and that a strong correlation has been established between NSP4 and intracellular Ca2+ flux, we made the assumption that NSP4 is indeed a cation-selective channel. This was later confirmed by Joe Hyser who determined that NSP4 VPD is 20 times more permeable to potassium than chloride (unpublished results). In our patch-clamp configuration, we were then able to test that the channel conducts Ca2+ ions by perfusing buffer CA (75 mM $CaCl_2$, 5 mM Hepes, pH 7.2) into the bath after capturing a patch in symmetric buffer A (150 mM KCl, 5 mM Hepes, pH 7.2) as a control. When a negative pipette voltage was applied to draw calcium into the pipette either one of two scenarios could occur: (**1**) No current fluctuation would be observed because the channel could not conduct calcium, or (**2**) current fluctuations would be observed indicative of calcium flux from the bath buffer into the pipette. Figure 5.5 illustrates that the latter was the case.

Utilizing the patch-clamp technique with the pipette voltage clamped to +70 mV, we observed well-defined levels of conductance measuring 42 pS in symmetric buffer A conditions (Figure 5.5A). Occasionally a 13 pS substate could also be observed (marked by the arrow in the figure). When the pipette voltage was clamped to -70 mV, we also observed a similar "square-top" kinetics (Figure 5.5B). When buffer CA was perfused into the bath, we continued to observe well-defined channel openings at both positive and negative voltages, indicating that the channel is indeed permeable to calcium, the sole cation able to sustain a current at negative pipette potentials (Figure 5.5C and D). The conductance, however, was slightly reduced (29 pS vs 42 pS, Figure 5.6), and the kinetics appears a bit faster, but given the variability, we observed in kinetic signatures, it is hard to ascertain whether this is due to the presence of calcium or not. Current-voltage

relationships obtained from these recordings (Figure 5.6) showed that the reversal potential shifted only slightly (by ~13 mV) in asymmetric conditions. Therefore, the channel does not appear to be more selective for potassium than calcium. However, these experiments indicated that the NSP4 VPD alone is not only capable of conducting potassium ions but also calcium ions, as predicted.

5.2.3 Barium and Other Salts

Although we were able to show that the NSP4 VPD was capable of conducting calcium ions, a persistent issue was the difficulty to obtain a high frequency of reconstituted bilayers or patches with consistent "square-top" activity. In addition, spurred by the idea that NSP4 could be a *bona fide* calcium channel, we had seen in previous literature that canonical calcium channels could conduct barium ions (Ferreira et al., 1997; Tsien and Tsien, 1990). Interestingly, when known calcium channels are introduced into a $BaCl_2$ containing buffer, not only can they conduct the barium ions, but also they do so with a larger conductance. Consequently, in hopes of establishing a higher frequency of observed "square-top" behavior as well as seeking to determine whether or not NSP4 VPD could conduct barium ions at a larger level of conductance similarly to canonical calcium channels, we introduced buffer BA (75 mM $BaCl_2$, 5 mM Hepes, pH7.2) into our patch-clamp configuration in symmetric conditions. Figure 5.7 illustrates that channel activity is indeed detectable in symmetric barium conditions, indicating that the channel can also conduct barium. Unfortunately, these conditions did not improve the frequency of observing channel kinetics with predominantly well-defined openings. We were also unable to perfuse buffer CA into the bath without triggering a rupture of the

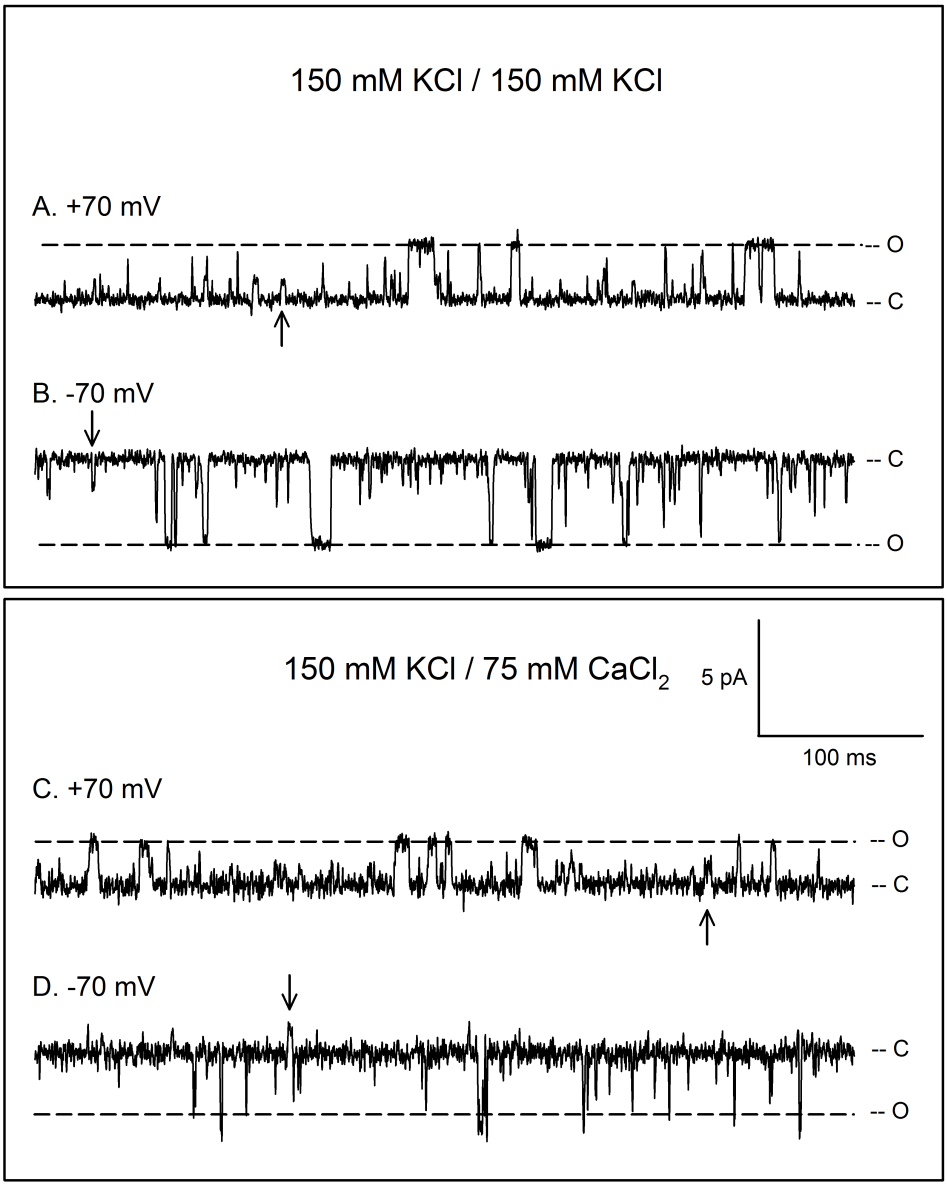

Figure 5.5 NSP4 VPD can conduct K+ and Ca2+ in patch-clamp experiments. *The peptide was dissolved in DMSO and reconstituted with the dehydration/rehydration method at a protein:lipid ratio of 1:3000 (w:w). The traces were obtained at the indicated voltages in symmetric buffer A or asymmetric conditions of buffer A in the pipette and buffer CA in the bath. The conductance of the main state was 42 pS in symmetric buffer A (**A-B**), and 29 pS with buffer CA in the bath (**C-D**), as determined from I/V plots made from the well-defined openings observed in this experiment (see Figure 5.6). The conductance of the substate (arrow) was 13 pS in both conditions.*

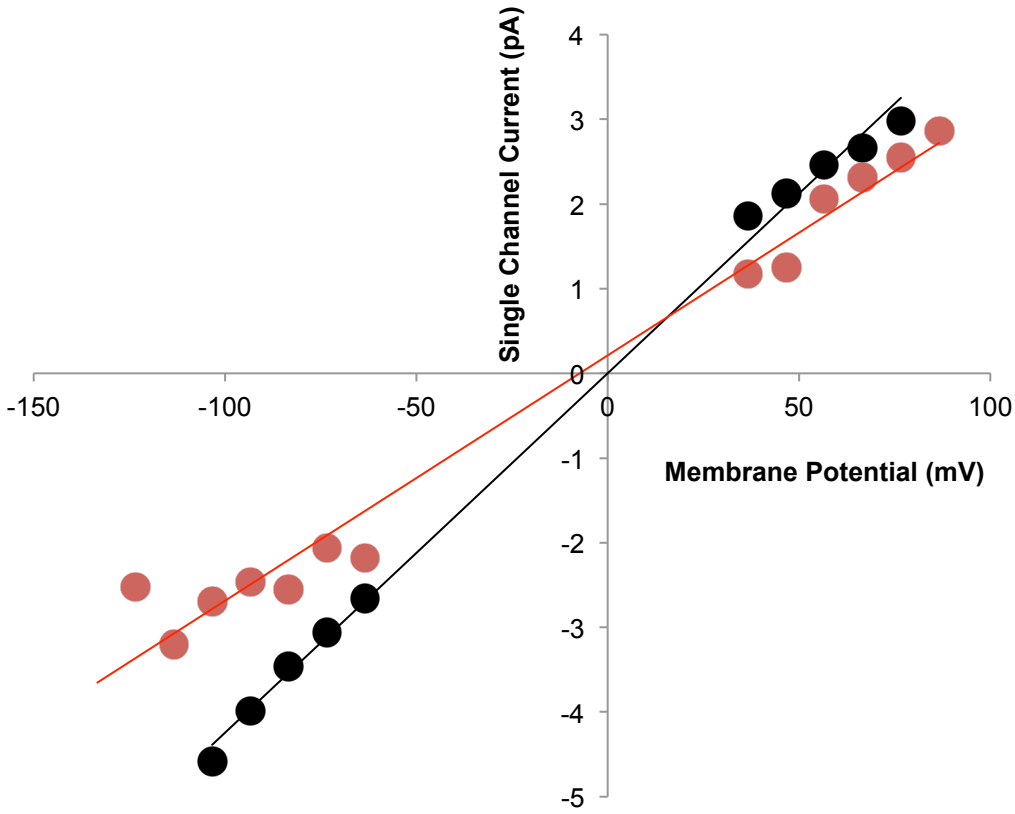

Figure 5.6 Current-voltage relationships of NSP4 VPD. *The current of well-defined openings were measured at several voltages in symmetric buffer A (black circles) and asymmetric buffer A/buffer CA (red circles) solutions. There was a ~13 mV offset potential in symmetric buffer A. Therefore all membrane potentials were corrected by the same offset in symmetric and asymmetric conditions. The lines represent the linear regressions through the data points. After correction of the offset in symmetric conditions, the linear regression passes through 0, as expected. The slopes of the linear regressions are the conductances of the channel in the different conditions, and we calculated to be 42 pS in symmetric buffer A and 29 pS in buffer A/CA.*

patch. Consequently, we were unable to determine whether or not barium conductance was larger relative to calcium in the same patch. Interestingly, perfusion of buffer A into the bath resulted in similar levels of conductance as observed in buffer BA (Figure 5.7B).

Finally, we turned to the use of known calcium channel blockers/inhibitors, such as cadmium and nickel ions, to assess whether NSP4 VPD shares this property with *bona fide* calcium channels. Thus, utilizing symmetric buffer BA conditions as a control (Figure 5.7A), we perfused the bath with buffer BA supplemented with to 2 mM cadmium chloride (Figure 5.7C) or 1 mM nickel chloride (Figure 5.7D). There appeared to be a slight decrease in conductance in the presence of 2 mM cadmium chloride (58 pS vs 63 pS in symmetric barium conditions without cadmium ions), as a well as a reduction in the open probability and average open time. In this experiment, prior to the addition of potentially inhibitory ions, the open probability for the channel was approximately ~36% with a mean open time of ~2.17 ms (Figure 5.7A, Table 5.1). However, upon the perfusion of buffer BA into the bath supplemented with 2 mM cadmium chloride, the open probability of the channel reduced to ~11% with a mean open time of ~1.53 ms (Figure 5.7C, Table 5.1). Interestingly, in the presence of 1 mM nickel chloride, well-defined openings were rarely seen, and the open probability and average open times were further decreased to ~7% and ~0.91 ms, respectively (Figure 5.7D, Table 5.1). In both conditions, the number of opening events was also substantially reduced. This indeed shows that these ions have some inhibitory effects on NSP4. Unfortunately, we were not able to replicate this experiment to confirm these findings due to difficulty in maintaining well-behaved patches long enough to survive multiple perfusions without rupturing the patch.

Bath Solution	*P_o*	*Average Open Time (ms)*	*# of Events*
BA	*36%*	*2.17*	*5160*
A	*24%*	*2.31*	*3712*
BA + 2 mM $CdCl_2$	*11%*	*1.53*	*2753*
BA + 1 mM $NiCl_2$	*7%*	*0.91*	*2688*

Table 5.1 Effect of $CdCl_2$ and $NiCl_2$ on NSP4 kinetics. *The kinetic parameters were obtained from 30 seconds of the same recordings as shown in Figure 5.7. P_o is the open probability, and # of Events is the number of openings. The pipette solution was buffer BA and pipette voltage was -50 mV.*

5.2.4 Native Disulfide Bond within NSP4

NSP4 VPD contains two conserved cysteines at residues 63 and 71. Previous data suggest the existence of native disulfide bond(s), most likely between adjacent monomers of the oligomer, since high molecular weights bands collapse into the monomeric band on SDS-PAGE in reducing conditions (Hyser et al., 2010). Because the structure of NSP4 is unknown, others strategies could be used to determine the membrane topology of the viroporin, such as scanning cysteine accessibility mutagenesis (SCAM) (Zhu and Casey, 2007). Such strategy is based on the introduction of engineered cysteines at precise locations, and thus, necessitates a cysteine-less construct as a control. In order to verify that such construct still retains ion channel activity, a cysteine-less double mutant VPD peptide, C63S/C71S, was obtained from Joseph Hyser for electrophysiological analysis. We dissolved the mutant VPD in water and reconstituted the channel into liposomes via the cloud method for patch-clamp analysis. As shown in Figure 5.8, the double cysteine mutant still retains channel activity and kinetics characteristic of the wild-type NSP4 VPD. Although the experiment captured “spiky” kinetics, a well-defined level was

Figure 5.7 NSP4 VPD can also conduct Ba+ in patch-clamp experiments. *The peptide was dissolved in water and reconstituted with the cloud method at a protein:lipid ratio of 1:200 (w:w). The traces were obtained at – 50 mV in symmetric buffer BA with and without potential channel-blocking salts (cadmium chloride and nickel chloride) in the bath. In our patch-clamp configuration, negative voltage pulled cadmium or nickel ions into the pipette. Traces were also obtained in asymmetric conditions of buffer BA in the pipette and buffer A in the bath as a control. The "c" denotes the closed level of conductance for the channel, and the "o" denotes the open level. These traces were all sampled at 100 μs intervals.*

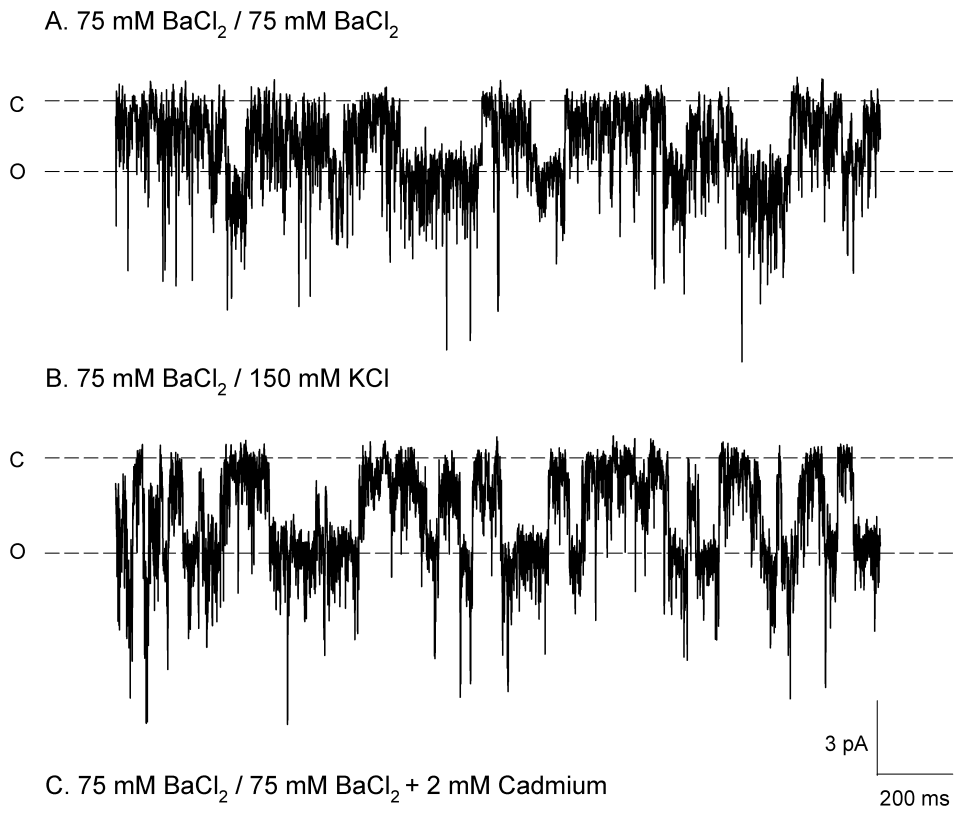
A. 75 mM $BaCl_2$ / 75 mM $BaCl_2$
C
O
B. 75 mM $BaCl_2$ / 150 mM KCl
C
O
3 pA
200 ms
C. 75 mM $BaCl_2$ / 75 mM $BaCl_2$ + 2 mM Cadmium
C
O
D. 75 mM $BaCl_2$ / 75 mM $BaCl_2$ + 1 mM Nickel
C

observed allowing us to measure a conductance of ~50 pS for the open state (indicate the "O" level in Figure 5.8). As a result, we show that the native disulfide bond(s) involving residues C63 and C71 in NSP4 VPD is not required for channel activity. Thus, future studies to establish the membrane topology of the NSP4 VPD can be envisaged using SCAM in this cysteine-less background.

5.3 Reconstitution of Viroporin NSP4

5.3.1 Planar Lipid Bilayer: The Solvent Issue

We had issues initially with retaining functionally active NSP4 VPD peptide. It was observed that we had the greatest success in reconstitution yield when the peptide was freshly suspended in DMSO and stored at 4^{o} C. We subsequently discovered that over time, DMSO could oxidize into methylsulfonylmethane (MSM) and thus the solvent may have been rendering our peptide inactive over time. We sought to use septum-sealed bottles of DMSO in order to rectify this issue, however, it was soon discovered that it did not help. Thus, we attempted to test other solvents that would fully dissolve the peptide, provide functionally active bilayers or patches, and not deteriorate rapidly over time. At the same time, we were also using this process to perhaps find a solvent that would promote reconstitution of NSP4 VPD in such a way as to yield higher frequencies of observing canonical "square-top" kinetics. Neither DMF, TFE, ethanol, nor OPOE detergent were more successful than DMSO. It was observed, however, that peptide dissolved in DMSO and stored in 4^{o} C appeared to be forming crystals, perhaps resulting in the precipitation of the peptide out of the solvent and causing our peptide preparations to deteriorate over time. Although highly hydrophobic, NSP4 VPD peptide was found to

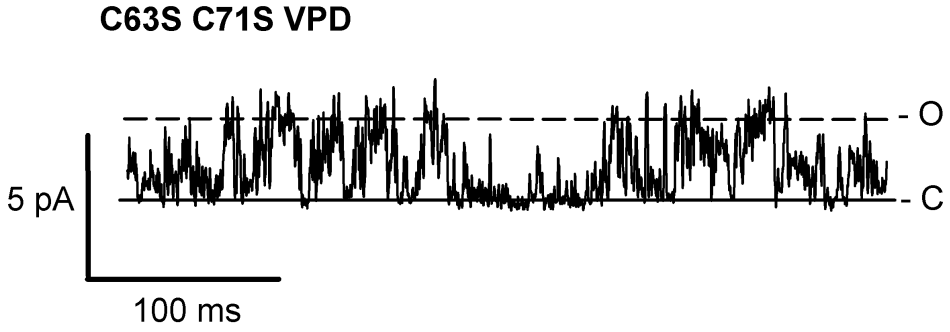

Figure 5.8 The double cysteine mutant NSP4 VPD C63S/C71S shows channel activity. *The mutated peptide dissolved in water was reconstituted with the cloud method at a protein-to-lipid ratio of 1:20 (w:w). The recording was made in symmetric buffer A at a pipette voltage of + 50 mV. The "c" denotes the closed level of conductance for the channel, and the "o" denotes the open level, with ~50 pS conductance. The trace was sampled at 100 μs intervals.*

dissolve perfectly in water. Even more so, the peptide dissolved in water could be stored at room temperature for months at a time and still retain functional activity levels when reconstituted into either bilayer or liposomes for patch-clamp analysis. Thus we were able to solve our long-term storage issues by switching from DMSO to water as a solvent.

Interestingly, we observed in planar lipid bilayer that the solvent we used to dissolve the synthetic peptide played an important role in the kinetics of the NSP4 VPD. In fact, "square-top" kinetics were *only* seen in planar lipid bilayers when the peptide was dissolved in DMSO (Table 5.2). However, it should be noted that we also observed "square-top" kinetics in patch-clamp with water-dissolved peptide. Perhaps the "square-top" kinetics were missed in bilayers with peptide dissolved in water, simply because our number of experiments with such aqueous solution of peptide is relatively low (15). With a 4% rate of occurrence of "square-top" behavior (see Table 5.2), 15 bilayers would not be enough to capture this type of kinetics. Altogether, we studied a total of 238 bilayers formed; of those, 54% did not yield any activity after waiting between 30 minutes to upwards of 12 hours (overnight incubation). Only 3% of the total bilayers formed had channels with "square-top" kinetics, and these bilayers were only seen with NSP4 VPD peptide that had been dissolved in DMSO. The remaining 43% of bilayers showed NSP4 VPD in a state of rapidly fluctuating kinetics or "spiky" activity.

5.3.2 Patch-Clamp: Dehydration/Rehydration vs. Clouds

In patch-clamp, we initially utilized DMSO as the solvent, but switched to water once we discovered that it solved our long-term storage issues and allowed the peptide to remain functionally active. Similarly, we sought different ways to try to capture NSP4

Solvent	*# Bilayers with Square-Top Kinetics*	*# Bilayers with Spiky Kinetics*	*# Empty Bilayers*	*Total Bilayers*
TFE	*0*	*12*	*1*	*13*
50% Ethanol	*0*	*2*	*1*	*3*
Water	*0*	*9*	*6*	*15*
DMSO	*7*	*64*	*93*	*164*
DMF	*0*	*6*	*7*	*13*
1-2% OPOE	*0*	*9*	*21*	*30*

Table 5.2 Summary of solvents used in dissolving NSP4 VPD. *The table lists all of the solvents used to dissolve NSP4 VPD tested in planar lipid bilayer experiments. Each bilayer was then analyzed based on whether it contained channels with well-defined openings or "spiky" kinetics as illustrated in Figures 5.2 and 5.3, respectively. A total of 238 bilayers were formed.*

VPD in its "square-top" kinetic state and to achieve a higher reconstitution efficiency. One of the methods by which we attempted to achieve this was through a different protocol for liposome reconstitution. We believed that perhaps the synthetic peptide did not respond well to the dehydration step during the dehydration/rehydration method. We had first attempted to utilize microsome fractions from transfected insect cells expressing NSP4. These fractions were fused to multilamellar liposomes for patch-clamp analysis, but it was discovered that there appeared to be very large channels with a conductance far exceeding that expected for NSP4, that were attributed to contaminating endogenous channels. Battle et al. (2009), however, devised an interesting method for reconstitution that utilizes swelling of the liposomes in a sucrose containing solution (as described in Chapter 2). Because the swollen liposomes appear as a "cloud" in the sucrose solution, we refer to this technique as the "cloud method". We utilized this method to reconstitute both water- and DMSO-dissolved NSP4 VPD peptide, assuming that the method might

allow for slower and gentler reconstitution compared to the dehydration/rehydration method. However, when we assayed patches containing NSP4 VPD reconstituted via the cloud method, we found that the kinetics of the channel were largely unaffected by the reconstitution method (Figure 5.9). "Spiky" kinetics could be observed in patches obtained from liposomes reconstituted via either the dehydration/dehydration (Figure 5.9A) or cloud (Figure 5.9C) methods. Likewise, "square-top" behavior could be seen from peptide reconstituted via either reconstitution method (Figure 5.9B and D). In the experiment shown, the conductance of the "square-top" events were ~34 pS (Figure 5.9B) and ~49 pS (Figure 5.9D) in patches obtained from liposomes made with the dehydration/rehydration method or the cloud method, respectively. This difference in conductance may not be of significance since variability in conductance has been observed frequently, and we have not been able to identify a single unitary conductance consistent across all experiments. Perhaps this is due to the fact that we are working with a NSP4 VPD synthetic peptide. Multiple levels of conductance might depend on the number of VPD monomers that come together and oligomerize in the membrane. Because the VPD peptide is lacking the CCD, which is responsible for oligomerizing the viroporin *in vivo*, oligomerization may be unregulated, and oligomers with varying numbers of monomers may assemble. This might in turn impact the size of the channel formed at the interface of the monomers. For example, observing "square-top" events of 40 pS conductance in one experiment and 60 pS in another may simply be due to the difference between a tetrameric and hexameric oligomer. However, this is only speculation, since we have not been able to examine full-length NSP4 in our patch-clamp experiments.

Although we were unable to observe more of the "square-top" kinetics from the NSP4 VPD by utilizing the cloud method for reconstitution, we had hoped to achieve a higher reconstitution efficiency as it could take upwards of 10-12 patches in a single day, even with a large range of protein:lipid dilution ratios (1:20 – 1:3250), before we were able to capture even a single patch with viroporin activity. However, regardless of the reconstitution method, the reconstitution efficiency was approximately 10% (Table 5.3).

The number of patches of NSP4 VPD obtained with *both* methods totaled 544. Next, we categorized our patches into 3 groups, according to the kinetic activity displayed throughout the experiment: "square-top" only, "spiky" only, and mixed (meaning presence of both behaviors in the same experiment). Table 5.3 shows that, while more patches with "square-top" only activity were obtained via the dehydration/rehydration method, more patches with the "mixed" activity were present using the cloud method. As a result, collectively, we observed "square-top" events in 64% of the *active* patches with the dehydration/rehydration method (25% "mixed" + 39% "square-top"), but in 73% (46% "mixed" + 27% "square-top") of the *active* patches with the cloud method (Figure 5.10). Therefore, the cloud method might be a slightly superior method for reconstitution NSP4 VPD peptide over the dehydration/rehydration method. Although the reconstitution rate was not better, it appeared that the channel had more of the well-defined openings using the cloud method.

5.4 Summary and conclusions

Collectively, we have shown that NSP4 VPD is indeed a *bona fide* ion channel, since it displays discrete levels of conductance. It is capable of conducting potassium,

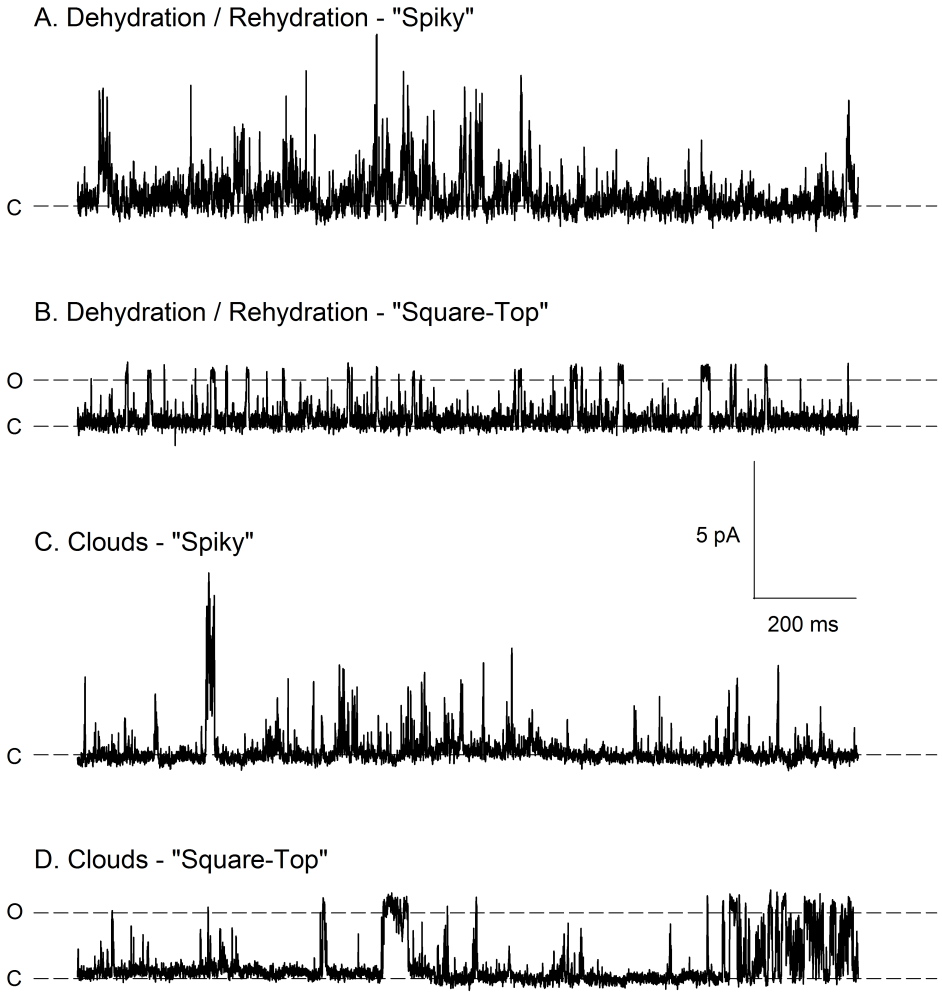

Figure 5.9 Similar kinetic signatures were observed regardless of reconstitution method. *NSP4 VPD peptide was dissolved in DMSO and reconstituted with either the dehydration-rehydration method at a protein:lipid ratio of* ***(A)*** *1:3250 (w:w),* ***(B)*** *1:3000 (w:w) or the cloud method at a protein:lipid ratio of* ***(C-D)*** *1:200 (w:w). The traces were obtained at +50 mV in symmetric buffer A. The conductance of the open state was 34 pS* ***(B)*** *and 49 pS* ***(D)****. In* ***A & C****, the conductance could not be determined due to a lack of a defined level of activity.*

NSP4 VPD - DHRH	
Empty Patches	*240*
Square-Top only	*11*
Spiky only	*10*
Mixed	*7*
Total Patches	***268***
Reconstitution Efficiency	*10.45%*

NSP4 VPD - Clouds	
Empty Patches	*250*
Square-Top only	*7*
Spiky only	*7*
Mixed	*12*
Total Patches	***276***
Reconstitution Efficiency	*9.42%*

Table 5.3 Reconstitution efficiency and number of patches studied with the dehydration/rehydration method (DHRH) vs. the cloud method. *The tables give the number of patches with either no channels ("empty patches"), or with channels displaying "square-top" events only (illustrated in Figure 5.2), or "spiky" events only (illustrated in Figure 5.3), or a mixture of both behaviors ("Mixed", as illustrated in Figure 5.4). A total of 544 patches were obtained with reconstituted NSP4 VPD in the course of this study. The reconstitution efficiency was calculated by dividing the number of patches with activity by the total number of patches.*

calcium, and barium ions. However, we were unable to show that the channel was any more selective for calcium than potassium ions. The permeability of NSP4 VPD for divalent ions, however, sets it apart from many other viroporins, which, although more selective for cations than anions, are not reported to pass divalent cations (Hyser, 2015). The lack of calcium selectivity may not be an impediment *in vivo*, because the magnitude of the calcium gradient across the ER membrane where NSP4 resides is such that large calcium currents can be sustained, even through a non-selective channel. In addition, we established that the kinetics of NSP4 VPD is predominantly fast, with frequent transient openings. This kinetic behavior is similar to that reported for other viroporins such as HCV p7 (Premkumar et al., 2004) and Influenza A's PB1-F2 (Henkel et al., 2010). However, this may also be due to the fact that only the VPD was used in these experiments, and the channel may not have formed stable oligomers due to the lack of the

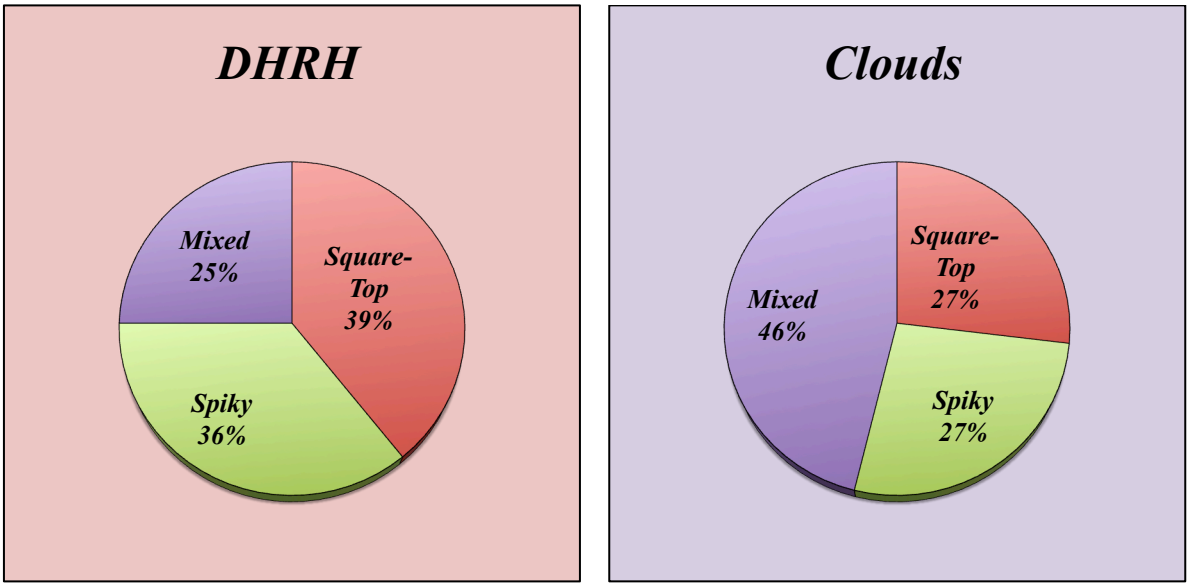

Figure 5.10 Distribution of NSP4 VPD kinetics observed with the two reconstitution methods. *The percentages were calculated from the data in Table 5.2, using the total number of active patches as 100 % (28 for the DHRH method, and 26 for the cloud method).*

CCD domain, known to control oligomerization.

It was our hope to also investigate other NSP4 constructs in this study, in particular peptides containing the VPD and the CCD. Due to time constraints and technical difficulties, fewer experiments were done with these other constructs. Table 5.4 summarizes our attempts not only with NSP4 VPD, but also the long peptide (47-139) which includes the CCD domain, the full-length peptide (1-175), the NSP4 VPD mutant ASDASA which has been shown to be devoid of channel activity *in vivo* (Hyser, personal communication), and microsome fractions from insect cells expressing GFP-tagged NSP4. We have documented our attempts in the hope that future studies could possibly improve upon our techniques to make electrophysiological characterization of viroporins a great deal less challenging technically.

	Planar Lipid Bilayer	***Patch Clamp***
VPD (47-90)	*Symmetric buffer A, asymmetric buffer A/C, A/CA – rare well-defined kinetics but more commonly spiky – attempted cloud liposome fusion using urea and salt gradient (Woodbury and Hall. 1988), detergent did not improve insertion rate*	*Symmetric A, A/C, A/CA, and symmetric barium – Cloud method not any more efficient than DHRH – 1:4000 to 1:20 P:L ratios – (-80C, 4C, RT storage) – Detergent attempted in both methods – Sonication in attempt to break up NSP4 precipitates – kinetics often a mixture of well-defined and spiky transitions*
Long Peptide (47-139)	*Buffer T - Very little to no activity detected, difficult to insert in planar lipid bilayer, when activity was detected saturation often occurred resulting in membrane rupture*	*Does not reconstitute well in liposomes in either method (1 experiment in water dilution and clouds, numerous empty patches captured indicating even lower reconstitution rates)*
Full Length (1-175)	*Buffer T and A - Never achieved insertions in planar lipid bilayer even after overnight incubation in chamber*	*Does not reconstitute well in liposomes in DHRH (clouds not tried)*
Mutant Short Peptide (ASDASA)	*Buffer T – Appears less active and more infrequent comparative to WT*	
Microsome	*Attempted to fuse microsome vesicles to planar lipid bilayer membranes using various gradients (salt gradient, urea, glycerol) - failed*	*Channels of very large conductance with very long dwell times – most likely endogenous channel contamination and thus disregarded as NSP4 activity*

Table 5.4 Summary of findings on various NSP4 constructs using electrophysiological techniques.

CHAPTER 6

Concluding Remarks

The first antibiotic to be discovered was penicillin in 1928 (Rudramurthy et al., 2016). Many other classes of antibiotics have been discovered since then, such as the cephalosporins and tetracyclines. However, only one antibiotic, teixobactin, has been found in the past 30 years, and it is distinctly difficult to produce in laboratory conditions (Ling et al., 2015). Recently, the improper usage of antibiotics has cultivated a rise in antibiotic resistance (Karam et al., 2016; Rudramurthy et al., 2016). For example, one of the most prominent cases of antibiotic resistance is seen widely in hospitals, methicillin-resistance *Staphylcoccus aureus* or MRSA, with over 25% of reporting countries in Europe maintaining a greater than 25% presence of MRSA in the population (Karam et al., 2016). Even broad-spectrum antibiotics such as the fluoroquinolones have been well guarded against by bacterial pathogens and boast greater than 50% resistance in some countries (Karam et al., 2016). This trend in antibiotic resistance poses a major cause for concern globally. Consequently, there has been a growing interest in the field seeking to establish more viable therapeutic alternatives to antibiotics.

Urinary tract infections (UTIs) are a particularly common ailment (Chin et al., 2016) and affect nearly 150 million people each year globally (Steadman et al., 2014). Their prevalence in the United States triggers a large quantity of prescriptions for antibiotics, and the improper usage of the drugs is a major cause of increasing bacterial resistance (Chin et al., 2016). In uropathogenic *E. coli* (UPEC), the causative agent for UTIs, P pili are critical determinants to establishing the infectious process. These pili mediate bacterial adhesion to host uroepithelial cells in the urinary tract. The very function of these pili is to confer resistance to shear stress from primary filtrate flow and pili are paramount in the bacterium pathogenicity (Subashchandrabose and Mobley,

2015). Consequently, P pili serve as major virulence factors for UPEC and thus present a prime target for drug design and therapeutics. These pili require the PapC usher and the chaperone PapD for biogenesis and translocation to the bacterial cell surface, and in order for biogenesis to occur, the plug domain which gates the usher closed must displace towards the periplasm to provide incoming subunits with access to the barrel lumen. The exact molecular mechanism underlying this event was still largely unknown until now.

In this work, we examined four key communities of highly conserved and co-evolved residues within the PapC usher. These residues were postulated to form a pathway from one community to the next creating a means by which an allosteric signal could be propagated upon the binding of the complex of the first subunit and chaperone, PapDG. This signal would consequently trigger plug displacement and allow pilus biogenesis to initiate. More specifically, this signal is believed to be the culmination of a series of small conformational changes, such as residue side-chain fluctuations, that results in a large global conformational change to promote the displacement of the plug domain. By utilizing electrophysiological techniques, we established the importance of these residues in usher function, as suggested by the altered cellular phenotypes of mutants at those residues (Chapter 3). Moreover, we confirmed the existence of an evolutionarily conserved network of residues that function to modulate plug displacement. We also examined three networks composed of electrostatic interactions between residues of the PapC usher (Chapter 4). One network in particular is comprised of arginine pairs forming repulsive electrostatic interactions that appear to function in maintaining the plug domain in a close configuration in the native PapC usher. We proposed that the weakening of interactions between the arginines of this pair provides

the necessary step in the gating mechanism of the usher required for pilus biogenesis. Interestingly, although there is no overlap of residues found in either the allosteric or electrostatic networks discovered, a majority of key residues were found localized to the same region at the interface of the plug domain with either the plug linkers or barrel wall. Together, we believe both the allosteric network of conserved residues and a pair of arginines located on the plug linkers near the periplasmic side serve to modulate usher pore gating in concert. Specifically, it is possible that the binding of the first chaperone-subunit complex triggers the propagation of an allosteric signal along the four conserved communities. This would subsequently result in the weakening of the electrostatic network between the plug linkers at the base of the barrel (periplasmic side) to induce plug displacement. Prior to our work, it was unclear exactly which residues were key mediators in allowing the usher to open, assemble, and translocate a growing pilus. Here, we have provided mechanistic insight into PapC usher gating by identifying, on a larger scale, conserved regions acting in concert to gate the usher pore. We have also specifically identified the key residues within these proposed communities and networks that are essential to initiating pilus biogenesis.

Because of the problem of antibiotic resistance, the scientific community is considering alternative targets to, at least, diminish the virulence of pathogens. As such, secretion systems, which are often involved in the release or biogenesis of virulence factors, appear to be good candidates. This would be particularly true for the chaperone-usher system of UPEC, since the natural ability of the body to clear the bladder of bacteria through urination would be effective, as long as the bacteria were prevented to attach to the epithelium by the pili. Thus, a current potential therapeutic alternative to

antibiotic treatment of UPEC related UTIs involves targeting and inhibiting the action of the chaperones in the chaperone-usher pathway (Steadman et al., 2014). Although the drug, termed "pilicide", was designed to bind at and disrupt the interface between the chaperone and its subunit (Steadman et al., 2014), it was instead found to bind the region of the chaperone shown previously to interact with the N-terminal domain of the PapC usher (Pinkner et al., 2006). This disruption is believed to have a significant impact on pilus biogenesis; however, the effectiveness of pilicides is still being tested in animal models (Steadman et al., 2014). Alternatively, as we have demonstrated here in our work, a large cluster of key residues is located at the periplasmic base of the β-barrel, and is particularly critical at the plug linker junction. By stabilizing this region against the plug displacement-triggering effect of chaperone-subunit binding, one could then negatively impact the ability of the usher to open, thereby preventing pilus biogenesis and reducing pathogenicity. Thus, we have provided a basis for the design of potential drug specifically targeted at this region.

In terms of continuing work more specifically along the lines of this dissertation, it would be interesting to determine the average threshold voltages for each of the allosteric network mutants via the patch-clamp technique, in a similar fashion to what was done for the electrostatic network mutants. For example, the mutations of the S444 and K427 residues resulted in particularly closed electrophysiological signatures in planar lipid bilayer, indicating a possible role of these residues in modulating the displacement of the plug. Interestingly, these mutants were defective for pilus assembly but had a completely WT phenotype for SDS and antibiotic sensitivities, similarly to the R-Pairs electrostatic network mutant. Therefore, it would be worth exploring whether S444 and

K427 also play a key role in plug displacement. Also, since the core "Hot Spot" residues were implicated to establish a physical pathway upon which an allosteric signal could be transmitted, a mutant usher with multiple alanine substitutions along this path may possibly abolish plug displacement entirely. We can envisage investigating mutant ushers where each of the four communities harbors multiple mutations, or even one with alanine substitutions at the five residues with the strongest electrophysiological and cellular phenotypes disclosed here (V327, T331, K427, F438, S444). In a similar fashion because the β12-13 patch is highly conserved in the *fim* system, alanine scanning mutagenesis of residues along this patch and subsequent cellular assay and patch-clamp analysis may reveal other key residues implicated in plug displacement. Likewise, it would also be interesting to explore in depth the exact role of the β12-13 latch located at the base of the barrel interfaced with the plug domain. Because the β12-13 latch was found in different conformations in the closed and open states of the *fim* usher, perhaps this latch also serves to govern plug displacement in the PapC usher. In order to determine whether this is possibly the case, it would be interesting to engineer a physical link via disulfide bond between the latch and either the plug domain or barrel wall to disable movement of the latch. Likewise, introducing a disulfide bond to tether the plug linkers to each other would permit to test the hypothesis that the plug linkers must move relative to each other to allow plug displacement. The expectation from these tethering experiments would be that the threshold voltage for plug displacement is drastically increased relative to that of WT, if indeed motion of these regions is required for plug displacement to occur.

Similarly, we have also established here that voltage-induced plug displacement can be used to study the effects of chaperone-subunit on usher function. For example, we

saw that in the presence of PapDG, the channel conductance during plug displacement was nearly halved, indicating engagement of the subunit in one of the barrel monomers. To verify this hypothesis, similar experiments could be conducted on purified monomers of PapC in the presence of PapDG. If the interpretation of subunit engagement is correct, one would expect to see full block of the monomeric channel in the presence of PapDG. Finally, domain PapC mutants could be investigated with respect to PapDG activation. It is hypothesized that PapDG first binds to the N-terminal globular domain, before being handed over to the C-terminal domain for insertion into the barrel. A mutant lacking both N-terminal and C-terminal domains does not reconstitute well, but we could investigate single deletion mutants lacking either the N-terminal or C-terminal domains. It is anticipated that the PapDG effect of decreasing the threshold voltage would be abrogated in the N-terminal domain deletion mutant. On the other hand, the C-terminal domain deletion mutant might show a WT threshold voltage for plug displacement, but be unable to engage the subunit into the channel, which would be seen as a lack of effect on conductance.

Similarly to UPEC P pili, the rotavirus NSP4 also serves as a major virulence factor in the infectious process. Hyser et al. (2013) showed that NSP4 expression alone was capable of causing an increase in intracellular calcium concentration required by rotavirus for viral replication and the assembly of new virions. Because of this disruption in calcium homeostasis, he subsequently postulated that NSP4 was a virally encoded channel, or viroporin, located in the ER membrane where it could disrupt calcium homeostasis by leaking ER calcium stores out into the cytoplasm. Electrophysiological techniques have often been used to characterize viroporins, however, no previous studies,

to the best of our knowledge, have shown viroporin selectivity of divalent cations such as calcium over monovalent cations (Zhou et al., 2009). In our work, we showed that the viroporin domain (VPD) alone could form a channel in artificial bilayers, capable of conducting ions with well-defined levels of conductance, and thereby is a *bona fide* ion channel (Chapter 5). We have also demonstrated that, unlike most viroporins, the NSP4 VPD could also conduct calcium and barium ions. We showed that canonical calcium channel inhibitors, such as cadmium and nickel ions, have an inhibitory effect on the NSP4 VPD in patch-clamp studies, but more work is needed in order to confirm this. We have shown the effect of various solvents on NSP4 synthetic peptide reconstitution and kinetics. Although we were unable to increase the reconstitution efficiency of the VPD into artificial bilayers and liposomes, we have provided here a basis for the optimization of future viroporin studies utilizing electrophysiological techniques.

Although not explored in this dissertation, future studies could investigate the effect of different lipid compositions used for reconstitution. For example, NSP4 is believed to localize to lipid rafts comprised of cholesterol, sphingomyelin, and glycolipids (Storey et al., 2007). The presence of cholesterol may stiffen liposome patches and confer more stability during buffer perfusions in patch-clamp as well. In addition, these lipids may allow the channel to insert in the membrane in a more reproducible fashion.

Although rotavirus vaccines are widely used in the West, the World Health Organization estimates coverage at only 14% globally. Re-infection by rotavirus has been shown to impair cognitive abilities in children and in some cases also physical development (Lorntz et al., 2006). This establishes a growing need for the development

of antiviral drug therapies as an alternative. Our collaborator, Joseph Hyser, has shown that NSP4 viroporin has a key role in rotavirus infection, and its deletion or knockdown reduces the virulence of the virus. Therefore, NSP4 could serve as a potential drug target. Our initial results suggest that calcium channel blockers could be a therapeutic alternative, but this would need to be shown conclusively by electrophysiology. In order to establish this further, future studies on NSP4 utilizing electrophysiological techniques could test the effect of various calcium channel blockers on NSP4 function. In particular, since the "square-top" opening events of NSP4 can display a conductance in the range of ~40-60 pS, similar to the conductance of L-type calcium channels, it is possible that NSP4 be affected by L-type calcium channel blockers such as the benzothiazepine, dihydropyridine, or phenylalkylamine classes of blockers. Such drugs could be tested in electrophysiological experiments. If L-type calcium channel blockers fail to elicit any effect on the NSP4 VPD alone, similar experiments could be conducted on the full-length protein.

Indeed, it would be useful to gain more insight into the molecular properties of the channel, in particular the full-length protein. The coiled-coil domain (CCD) of the NSP4 viroporin contains a putative calcium-binding site, but the constructs primarily used in our work are lacking this domain. The calcium-binding properties of this domain have already been shown to depend on oligomerization (Chacko et al., 2011). Future experiments could be designed to determine how the oligomerization state of the CCD influences channel properties. It has been shown that the tetrameric CCD binds Ca^{2+} with high affinity and is favored at neutral pH, while the pentamer is formed at low pH and does not bind Ca^{2+} (Sastri et al., 2014). Reconstitution and electrophysiology of full-

length proteins could be undertaken at pH 7 or 5.6, to explore whether the channel properties (conductance and calcium permeability) are influenced by the oligomerization state. As a control, experiments would also be performed with the VPD domain only, to test the effect of pH strictly on the pore-forming domain, independently of the oligomerization state. Additionally, the calcium binding property of the CCD should be investigated with respect to the ability of the channel to pass calcium, and to the potential calcium modulation of channel activity, as seen in natural channels residing in the ER. For this, one can use NSP4 mutant proteins where the CCD residues involved in coordinating the calcium ion (E120 and Q123) have been mutated to alanine. Comparing the channel properties and modulation of this mutant with those of the wildtype channel would shed some light on the role of the Ca^{2+}-coordinating site of the CCD. Finally, resolving the crystal structure of the NSP4 viroporin would provide a firm base for structure-function studies since the membrane topology of the channel is still unclear. The discovery of the exact architecture of the channel could show how calcium ions are conducted through this viroporin.

ANDERSEN, C., HUGHES, C. & KORONAKIS, V. 2002a. Electrophysiological behavior of the TolC channel-tunnel in planar lipid bilayers. *J Membr Biol,* 185**,** 83-92.

ANDERSEN, C., KORONAKIS, E., BOKMA, E., ESWARAN, J., HUMPHREYS, D., HUGHES, C. & KORONAKIS, V. 2002b. Transition to the open state of the TolC periplasmic tunnel entrance. *Proc Natl Acad Sci U S A,* 99**,** 11103-8.

ASSALKHOU, R., BALASINGHAM, S., COLLINS, R. F., FRYE, S. A., DAVIDSEN, T., BENAM, A. V., BJORAS, M., DERRICK, J. P. & TONJUM, T. 2007. The outer membrane secretin PilQ from Neisseria meningitidis binds DNA. *Microbiology,* 153**,** 1593-603.

BALASINGHAM, S. V., COLLINS, R. F., ASSALKHOU, R., HOMBERSET, H., FRYE, S. A., DERRICK, J. P. & TONJUM, T. 2007. Interactions between the lipoprotein PilP and the secretin PilQ in Neisseria meningitidis. *J Bacteriol,* 189**,** 5716-27.

BATTLE, A. R., PETROV, E., PAL, P. & MARTINAC, B. 2009. Rapid and improved reconstitution of bacterial mechanosensitive ion channel proteins MscS and MscL into liposomes using a modified sucrose method. *FEBS Lett,* 583**,** 407-12.

BAUD, C., GUERIN, J., PETIT, E., LESNE, E., DUPRE, E., LOCHT, C. & JACOB-DUBUISSON, F. 2014. Translocation path of a substrate protein through its Omp85 transporter. *Nat Commun,* 5**,** 5271.

BERKOVA, Z., CRAWFORD, S. E., TRUGNAN, G., YOSHIMORI, T., MORRIS, A. P. & ESTES, M. K. 2006. Rotavirus NSP4 induces a novel vesicular compartment regulated by calcium and associated with viroplasms. *J Virol,* 80**,** 6061-71.

BERKOVA, Z., MORRIS, A. P. & ESTES, M. K. 2003. Cytoplasmic calcium measurement in rotavirus enterotoxin-enhanced green fluorescent protein (NSP4-EGFP) expressing cells loaded with Fura-2. *Cell Calcium,* 34**,** 55-68.

BITTER, W., KOSTER, M., LATIJNHOUWERS, M., DE COCK, H. & TOMMASSEN, J. 1998. Formation of oligomeric rings by XcpQ and PilQ, which are involved in protein transport across the outer membrane of Pseudomonas aeruginosa. *Mol Microbiol,* 27**,** 209-19.

BLOMFIELD, I. C., MCCLAIN, M. S. & EISENSTEIN, B. I. 1991. Type 1 fimbriae mutants of Escherichia coli K12: characterization of recognized afimbriate strains and construction of new fim deletion mutants. *Mol Microbiol,* 5**,** 1439-45.

BONARDI, F., HALZA, E., WALKO, M., DU PLESSIS, F., NOUWEN, N., FERINGA, B. L. & DRIESSEN, A. J. 2011. Probing the SecYEG translocation pore size with

preproteins conjugated with sizable rigid spherical molecules. *Proc Natl Acad Sci U S A,* 108**,** 7775-80.

BOWMAN, G. D., NODELMAN, I. M., LEVY, O., LIN, S. L., TIAN, P., ZAMB, T. J., UDEM, S. A., VENKATARAGHAVAN, B. & SCHUTT, C. E. 2000. Crystal structure of the oligomerization domain of NSP4 from rotavirus reveals a core metal-binding site. *J Mol Biol,* 304**,** 861-71.

BRAUN, V. & WOLFF, H. 1975. Attachment of lipoprotein to murein (peptidoglycan) of Escherichia coli in the presence and absence of penicillin FL 1060. *J Bacteriol,* 123**,** 888-97.

BREDEMEIER, R., SCHLEGEL, T., ERTEL, F., VOJTA, A., BORISSENKO, L., BOHNSACK, M. T., GROLL, M., VON HAESELER, A. & SCHLEIFF, E. 2007. Functional and phylogenetic properties of the pore-forming beta-barrel transporters of the Omp85 family. *J Biol Chem,* 282**,** 1882-90.

BREYTON, C., HAASE, W., RAPOPORT, T. A., KUHLBRANDT, W. & COLLINSON, I. 2002. Three-dimensional structure of the bacterial protein-translocation complex SecYEG. *Nature,* 418**,** 662-5.

BROK, R., VAN GELDER, P., WINTERHALTER, M., ZIESE, U., KOSTER, A. J., DE COCK, H., KOSTER, M., TOMMASSEN, J. & BITTER, W. 1999. The C-terminal domain of the Pseudomonas secretin XcpQ forms oligomeric rings with pore activity. *J Mol Biol,* 294**,** 1169-79.

BURGHOUT, P., VAN BOXTEL, R., VAN GELDER, P., RINGLER, P., MULLER, S. A., TOMMASSEN, J. & KOSTER, M. 2004. Structure and electrophysiological properties of the YscC secretin from the type III secretion system of Yersinia enterocolitica. *J Bacteriol,* 186**,** 4645-54.

BURKINSHAW, B. J. & STRYNADKA, N. C. 2014. Assembly and structure of the T3SS. *Biochim Biophys Acta,* 1843**,** 1649-63.

BUSCH, A. & WAKSMAN, G. 2012. Chaperone-usher pathways: diversity and pilus assembly mechanism. *Philos Trans R Soc Lond B Biol Sci,* 367**,** 1112-22.

CARRASCO, L. 1978. Membrane leakiness after viral infection and a new approach to the development of antiviral agents. *Nature,* 272**,** 694-9.

CASCALES, E., BUCHANAN, S. K., DUCHE, D., KLEANTHOUS, C., LLOUBES, R., POSTLE, K., RILEY, M., SLATIN, S. & CAVARD, D. 2007. Colicin biology. *Microbiol Mol Biol Rev,* 71**,** 158-229.

CASTILLO, K., CONTRERAS, G. F., PUPO, A., TORRES, Y. P., NEELY, A., GONZALEZ, C. & LATORRE, R. 2015a. Molecular mechanism underlying

beta1 regulation in voltage- and calcium-activated potassium (BK) channels. *Proc Natl Acad Sci U S A,* 112**,** 4809-14.

CASTILLO, K., PUPO, A., BAEZ-NIETO, D., CONTRERAS, G. F., MORERA, F. J., NEELY, A., LATORRE, R. & GONZALEZ, C. 2015b. Voltage-gated proton (H(v)1) channels, a singular voltage sensing domain. *FEBS Lett,* 589**,** 3471-8.

CHACKO, A. R., ARIFULLAH, M., SASTRI, N. P., JEYAKANTHAN, J., UENO, G., SEKAR, K., READ, R. J., DODSON, E. J., RAO, D. C. & SUGUNA, K. 2011. Novel pentameric structure of the diarrhea-inducing region of the rotavirus enterotoxigenic protein NSP4. *J Virol,* 85**,** 12721-32.

CHAMBERLIN, A., QIU, F., REBOLLEDO, S., WANG, Y., NOSKOV, S. Y. & LARSSON, H. P. 2014. Hydrophobic plug functions as a gate in voltage-gated proton channels. *Proc Natl Acad Sci U S A,* 111**,** E273-82.

CHAMBERLIN, A., QIU, F., WANG, Y., NOSKOV, S. Y. & LARSSON, H. P. 2015. Mapping the gating and permeation pathways in the voltage-gated proton channel Hv1. *J Mol Biol,* 427**,** 131-45.

CHATZI, K. E., SARDIS, M. F., ECONOMOU, A. & KARAMANOU, S. 2014. SecA-mediated targeting and translocation of secretory proteins. *Biochim Biophys Acta,* 1843**,** 1466-74.

CHEW, C. F., VIJAYAN, R., CHANG, J., ZITZMANN, N. & BIGGIN, P. C. 2009. Determination of pore-lining residues in the hepatitis C virus p7 protein. *Biophys J,* 96**,** L10-2.

CHIN, T. L., MCNULTY, C., BECK, C. & MACGOWAN, A. 2016. Antimicrobial resistance surveillance in urinary tract infections in primary care. *J Antimicrob Chemother*.

CIAMPOR, F., BAYLEY, P. M., NERMUT, M. V., HIRST, E. M., SUGRUE, R. J. & HAY, A. J. 1992. Evidence that the amantadine-induced, M2-mediated conversion of influenza A virus hemagglutinin to the low pH conformation occurs in an acidic trans Golgi compartment. *Virology,* 188**,** 14-24.

CLANTIN, B., DELATTRE, A. S., RUCKTOOA, P., SAINT, N., MELI, A. C., LOCHT, C., JACOB-DUBUISSON, F. & VILLERET, V. 2007. Structure of the membrane protein FhaC: a member of the Omp85-TpsB transporter superfamily. *Science,* 317**,** 957-61.

CLARKE, D., GRIFFIN, S., BEALES, L., GELAIS, C. S., BURGESS, S., HARRIS, M. & ROWLANDS, D. 2006. Evidence for the formation of a heptameric ion channel complex by the hepatitis C virus p7 protein in vitro. *J Biol Chem,* 281**,** 37057-68.

COLLINS, R. F., FORD, R. C., KITMITTO, A., OLSEN, R. O., TONJUM, T. & DERRICK, J. P. 2003. Three-dimensional structure of the Neisseria meningitidis secretin PilQ determined from negative-stain transmission electron microscopy. *J Bacteriol,* 185**,** 2611-7.

CORDES, F. S., KOMORIYA, K., LARQUET, E., YANG, S., EGELMAN, E. H., BLOCKER, A. & LEA, S. M. 2003. Helical structure of the needle of the type III secretion system of Shigella flexneri. *J Biol Chem,* 278**,** 17103-7.

CORNELIS, G. R. 2002. The Yersinia Ysc-Yop 'type III' weaponry. *Nat Rev Mol Cell Biol,* 3**,** 742-52.

CORNELIS, G. R. 2010. The type III secretion injectisome, a complex nanomachine for intracellular 'toxin' delivery. *Biol Chem,* 391**,** 745-51.

CORNELIS, G. R. & WOLF-WATZ, H. 1997. The Yersinia Yop virulon: a bacterial system for subverting eukaryotic cells. *Mol Microbiol,* 23**,** 861-7.

COUTTE, L., ANTOINE, R., DROBECQ, H., LOCHT, C. & JACOB-DUBUISSON, F. 2001. Subtilisin-like autotransporter serves as maturation protease in a bacterial secretion pathway. *EMBO J,* 20**,** 5040-8.

COWAN, S. W., SCHIRMER, T., RUMMEL, G., STEIERT, M., GHOSH, R., PAUPTIT, R. A., JANSONIUS, J. N. & ROSENBUSCH, J. P. 1992. Crystal structures explain functional properties of two E. coli porins. *Nature,* 358**,** 727-33.

CRAGO, A. M. & KORONAKIS, V. 1998. Salmonella InvG forms a ring-like multimer that requires the InvH lipoprotein for outer membrane localization. *Mol Microbiol,* 30**,** 47-56.

CREPIN, S., HOULE, S., CHARBONNEAU, M. E., MOUREZ, M., HAREL, J. & DOZOIS, C. M. 2012. Decreased expression of type 1 fimbriae by a pst mutant of uropathogenic Escherichia coli reduces urinary tract infection. *Infect Immun,* 80**,** 2802-15.

D'ENFERT, C., REYSS, I., WANDERSMAN, C. & PUGSLEY, A. P. 1989. Protein secretion by gram-negative bacteria. Characterization of two membrane proteins required for pullulanase secretion by Escherichia coli K-12. *J Biol Chem,* 264**,** 17462-8.

D'ENFERT, C., RYTER, A. & PUGSLEY, A. P. 1987. Cloning and expression in Escherichia coli of the Klebsiella pneumoniae genes for production, surface localization and secretion of the lipoprotein pullulanase. *EMBO J,* 6**,** 3531-8.

DALBEY, R. E. & KUHN, A. 2012. Protein traffic in Gram-negative bacteria--how exported and secreted proteins find their way. *FEMS Microbiol Rev,* 36**,** 1023-45.

DEEPA, R., DURGA RAO, C. & SUGUNA, K. 2007. Structure of the extended diarrhea-inducing domain of rotavirus enterotoxigenic protein NSP4. *Arch Virol,* 152**,** 847-59.

DELCOUR, A. H. 2003. Solute uptake through general porins. *Front Biosci,* 8**,** d1055-71.

DELCOUR, A. H. 2015. *Electrophysiology of Unconventional Channels and Pores,* Cham, Springer International Publishing : Imprint: Springer.

DELCOUR, A. H., MARTINAC, B., ADLER, J. & KUNG, C. 1989. Modified reconstitution method used in patch-clamp studies of Escherichia coli ion channels. *Biophys J,* 56**,** 631-6.

DIAZ, Y., CHEMELLO, M. E., PENA, F., ARISTIMUNO, O. C., ZAMBRANO, J. L., ROJAS, H., BARTOLI, F., SALAZAR, L., CHWETZOFF, S., SAPIN, C., TRUGNAN, G., MICHELANGELI, F. & RUIZ, M. C. 2008. Expression of nonstructural rotavirus protein NSP4 mimics Ca2+ homeostasis changes induced by rotavirus infection in cultured cells. *J Virol,* 82**,** 11331-43.

DISCONZI, E., GUILVOUT, I., CHAMI, M., MASI, M., HUYSMANS, G. H., PUGSLEY, A. P. & BAYAN, N. 2014. Bacterial secretins form constitutively open pores akin to general porins. *J Bacteriol,* 196**,** 121-8.

DOEDENS, J. R. & KIRKEGAARD, K. 1995. Inhibition of cellular protein secretion by poliovirus proteins 2B and 3A. *EMBO J,* 14**,** 894-907.

DOHLICH, K., ZUMSTEG, A. B., GOOSMANN, C. & KOLBE, M. 2014. A substrate-fusion protein is trapped inside the Type III Secretion System channel in Shigella flexneri. *PLoS Pathog,* 10**,** e1003881.

DRIESSEN, A. J. & NOUWEN, N. 2008. Protein translocation across the bacterial cytoplasmic membrane. *Annu Rev Biochem,* 77**,** 643-67.

DU, D., VAN VEEN, H. W. & LUISI, B. F. 2015. Assembly and operation of bacterial tripartite multidrug efflux pumps. *Trends Microbiol,* 23**,** 311-9.

DU, D., WANG, Z., JAMES, N. R., VOSS, J. E., KLIMONT, E., OHENE-AGYEI, T., VENTER, H., CHIU, W. & LUISI, B. F. 2014. Structure of the AcrAB-TolC multidrug efflux pump. *Nature,* 509**,** 512-5.

DUNN, J. P., KENEDY, M. R., IQBAL, H. & AKINS, D. R. 2015. Characterization of the beta-barrel assembly machine accessory lipoproteins from Borrelia burgdorferi. *BMC Microbiol,* 15**,** 70.

DURET, G. & DELCOUR, A. H. 2006. Deoxycholic acid blocks vibrio cholerae OmpT but not OmpU porin. *J Biol Chem,* 281**,** 19899-905.

DURET, G., SZYMANSKI, M., CHOI, K. J., YEO, H. J. & DELCOUR, A. H. 2008. The TpsB translocator HMW1B of haemophilus influenzae forms a large conductance channel. *J Biol Chem,* 283**,** 15771-8.

ESTRADA MALLARINO, L., FAN, E., ODERMATT, M., MULLER, M., LIN, M., LIANG, J., HEINZELMANN, M., FRITSCHE, F., APELL, H. J. & WELTE, W. 2015. TtOmp85, a beta-barrel assembly protein, functions by barrel augmentation. *Biochemistry,* 54**,** 844-52.

FARABELLA, I., PHAM, T., HENDERSON, N. S., GEIBEL, S., PHAN, G., THANASSI, D. G., DELCOUR, A. H., WAKSMAN, G. & TOPF, M. 2014. Allosteric signalling in the outer membrane translocation domain of PapC usher. *Elife,* 3.

FAUDRY, E., JOB, V., DESSEN, A., ATTREE, I. & FORGE, V. 2007. Type III secretion system translocator has a molten globule conformation both in its free and chaperone-bound forms. *FEBS J,* 274**,** 3601-10.

FAUDRY, E., VERNIER, G., NEUMANN, E., FORGE, V. & ATTREE, I. 2006. Synergistic pore formation by type III toxin translocators of Pseudomonas aeruginosa. *Biochemistry,* 45**,** 8117-23.

FERREIRA, G., YI, J., RIOS, E. & SHIROKOV, R. 1997. Ion-dependent inactivation of barium current through L-type calcium channels. *J Gen Physiol,* 109**,** 449-61.

FORD, B., REGO, A. T., RAGAN, T. J., PINKNER, J., DODSON, K., DRISCOLL, P. C., HULTGREN, S. & WAKSMAN, G. 2010. Structural homology between the C-terminal domain of the PapC usher and its plug. *J Bacteriol,* 192**,** 1824-31.

GAN, S. W., TAN, E., LIN, X., YU, D., WANG, J., TAN, G. M., VARARATTANAVECH, A., YEO, C. Y., SOON, C. H., SOONG, T. W., PERVUSHIN, K. & TORRES, J. 2012. The small hydrophobic protein of the human respiratory syncytial virus forms pentameric ion channels. *J Biol Chem,* 287**,** 24671-89.

GEIBEL, S. & WAKSMAN, G. 2014. The molecular dissection of the chaperone-usher pathway. *Biochim Biophys Acta,* 1843**,** 1559-67.

GENTLE, I. E., BURRI, L. & LITHGOW, T. 2005. Molecular architecture and function of the Omp85 family of proteins. *Mol Microbiol,* 58**,** 1216-25.

GIORDA, K. M. & HEBERT, D. N. 2013. Viroporins customize host cells for efficient viral propagation. *DNA Cell Biol,* 32**,** 557-64.

GONZALEZ, M. E. 2015. Vpu Protein: The Viroporin Encoded by HIV-1. *Viruses,* 7**,** 4352-68.

GONZALEZ, M. E. & CARRASCO, L. 2003. Viroporins. *FEBS Lett,* 552**,** 28-34.

GOURE, J., PASTOR, A., FAUDRY, E., CHABERT, J., DESSEN, A. & ATTREE, I. 2004. The V antigen of Pseudomonas aeruginosa is required for assembly of the functional PopB/PopD translocation pore in host cell membranes. *Infect Immun,* 72**,** 4741-50.

GRANT, S. G., JESSEE, J., BLOOM, F. R. & HANAHAN, D. 1990. Differential plasmid rescue from transgenic mouse DNAs into Escherichia coli methylation-restriction mutants. *Proc Natl Acad Sci U S A,* 87**,** 4645-9.

GRIFFIN, S. D., BEALES, L. P., CLARKE, D. S., WORSFOLD, O., EVANS, S. D., JAEGER, J., HARRIS, M. P. & ROWLANDS, D. J. 2003. The p7 protein of hepatitis C virus forms an ion channel that is blocked by the antiviral drug, Amantadine. *FEBS Lett,* 535**,** 34-8.

GUERIN, J., BAUD, C., TOUATI, N., SAINT, N., WILLERY, E., LOCHT, C., VEZIN, H. & JACOB-DUBUISSON, F. 2014. Conformational dynamics of protein transporter FhaC: large-scale motions of plug helix. *Mol Microbiol,* 92**,** 1164-76.

HATKOFF, M., RUNCO, L. M., PUJOL, C., JAYATILAKA, I., FURIE, M. B., BLISKA, J. B. & THANASSI, D. G. 2012. Roles of chaperone/usher pathways of Yersinia pestis in a murine model of plague and adhesion to host cells. *Infect Immun,* 80**,** 3490-500.

HENDERSON, N. S., NG, T. W., TALUKDER, I. & THANASSI, D. G. 2011. Function of the usher N-terminus in catalysing pilus assembly. *Mol Microbiol,* 79**,** 954-67.

HENDERSON, N. S. & THANASSI, D. G. 2013. Purification of the outer membrane usher protein and periplasmic chaperone-subunit complexes from the P and type 1 pilus systems. *Methods Mol Biol,* 966**,** 37-52.

HENKEL, M., MITZNER, D., HENKLEIN, P., MEYER-ALMES, F. J., MORONI, A., DIFRANCESCO, M. L., HENKES, L. M., KREIM, M., KAST, S. M., SCHUBERT, U. & THIEL, G. 2010. The proapoptotic influenza A virus protein PB1-F2 forms a nonselective ion channel. *PLoS One,* 5**,** e11112.

HOGAN, P. G. & RAO, A. 2015. Store-operated calcium entry: Mechanisms and modulation. *Biochem Biophys Res Commun,* 460**,** 40-9.

HOLLAND, I. B. 2010. The extraordinary diversity of bacterial protein secretion mechanisms. *Methods Mol Biol,* 619**,** 1-20.

HONG, H., SZABO, G. & TAMM, L. K. 2006. Electrostatic couplings in OmpA ion-channel gating suggest a mechanism for pore opening. *Nat Chem Biol,* 2**,** 627-35.

HYSER, J. M. 2015. Viroporins. *In:* DELCOUR, A. H. (ed.) *Electrophysiology of Unconventional Channels and Pores.* Heidelberg: Springer.

HYSER, J. M., COLLINSON-PAUTZ, M. R., UTAMA, B. & ESTES, M. K. 2010. Rotavirus disrupts calcium homeostasis by NSP4 viroporin activity. *MBio,* 1.

HYSER, J. M. & ESTES, M. K. 2015. Pathophysiological Consequences of Calcium-Conducting Viroporins. *Annu Rev Virol,* 2**,** 473-96.

ISHERWOOD, B. J. & PATEL, A. H. 2005. Analysis of the processing and transmembrane topology of the E2p7 protein of hepatitis C virus. *J Gen Virol,* 86**,** 667-76.

JACOB-DUBUISSON, F., EL-HAMEL, C., SAINT, N., GUEDIN, S., WILLERY, E., MOLLE, G. & LOCHT, C. 1999. Channel formation by FhaC, the outer membrane protein involved in the secretion of the Bordetella pertussis filamentous hemagglutinin. *J Biol Chem,* 274**,** 37731-5.

JACOB-DUBUISSON, F., VILLERET, V., CLANTIN, B., DELATTRE, A. S. & SAINT, N. 2009. First structural insights into the TpsB/Omp85 superfamily. *Biol Chem,* 390**,** 675-84.

JAKES, K. S. & CRAMER, W. A. 2012. Border crossings: colicins and transporters. *Annu Rev Genet,* 46**,** 209-31.

KAMIO, Y. & NIKAIDO, H. 1976. Outer membrane of Salmonella typhimurium: accessibility of phospholipid head groups to phospholipase c and cyanogen bromide activated dextran in the external medium. *Biochemistry,* 15**,** 2561-70.

KARAM, G., CHASTRE, J., WILCOX, M. H. & VINCENT, J. L. 2016. Antibiotic strategies in the era of multidrug resistance. *Crit Care,* 20**,** 136.

KELLY, M. L., COOK, J. A., BROWN-AUGSBURGER, P., HEINZ, B. A., SMITH, M. C. & PINTO, L. H. 2003. Demonstrating the intrinsic ion channel activity of virally encoded proteins. *FEBS Lett,* 552**,** 61-7.

KLINE, K. A., DODSON, K. W., CAPARON, M. G. & HULTGREN, S. J. 2010. A tale of two pili: assembly and function of pili in bacteria. *Trends Microbiol,* 18**,** 224-32.

KNYAZEV, D. G., WINTER, L., BAUER, B. W., SILIGAN, C. & POHL, P. 2014. Ion conductivity of the bacterial translocation channel SecYEG engaged in translocation. *J Biol Chem,* 289**,** 24611-6.

KOEBNIK, R., LOCHER, K. P. & VAN GELDER, P. 2000. Structure and function of bacterial outer membrane proteins: barrels in a nutshell. *Mol Microbiol,* 37**,** 239-53.

KONNINGER, U. W., HOBBIE, S., BENZ, R. & BRAUN, V. 1999. The haemolysin-secreting ShlB protein of the outer membrane of Serratia marcescens: determination of surface-exposed residues and formation of ion-permeable pores by ShlB mutants in artificial lipid bilayer membranes. *Mol Microbiol,* 32**,** 1212-25.

KORONAKIS, V., SHARFF, A., KORONAKIS, E., LUISI, B. & HUGHES, C. 2000. Crystal structure of the bacterial membrane protein TolC central to multidrug efflux and protein export. *Nature,* 405**,** 914-9.

KOROTKOV, K. V., GONEN, T. & HOL, W. G. 2011. Secretins: dynamic channels for protein transport across membranes. *Trends Biochem Sci,* 36**,** 433-43.

KOSAREWICZ, A., KONIGSMAIER, L. & MARLOVITS, T. C. 2012. The blueprint of the type-3 injectisome. *Philos Trans R Soc Lond B Biol Sci,* 367**,** 1140-54.

KOSTER, M., BITTER, W., DE COCK, H., ALLAOUI, A., CORNELIS, G. R. & TOMMASSEN, J. 1997. The outer membrane component, YscC, of the Yop secretion machinery of Yersinia enterocolitica forms a ring-shaped multimeric complex. *Mol Microbiol,* 26**,** 789-97.

KOVACS-SIMON, A., TITBALL, R. W. & MICHELL, S. L. 2011. Lipoproteins of bacterial pathogens. *Infect Immun,* 79**,** 548-61.

KOWAL, J., CHAMI, M., RINGLER, P., MULLER, S. A., KUDRYASHEV, M., CASTANO-DIEZ, D., AMSTUTZ, M., CORNELIS, G. R., STAHLBERG, H. & ENGEL, A. 2013. Structure of the dodecameric Yersinia enterocolitica secretin YscC and its trypsin-resistant core. *Structure,* 21**,** 2152-61.

KOZAKOV, D., CHUANG, G. Y., BEGLOV, D. & VAJDA, S. 2010. Where does amantadine bind to the influenza virus M2 proton channel? *Trends Biochem Sci,* 35**,** 471-5.

LEE, D., LEE, J. & SEOK, C. 2013. What stabilizes close arginine pairing in proteins? *Phys Chem Chem Phys,* 15**,** 5844-53.

LEO, J. C., GRIN, I. & LINKE, D. 2012. Type V secretion: mechanism(s) of autotransport through the bacterial outer membrane. *Philos Trans R Soc Lond B Biol Sci,* 367**,** 1088-101.

LI, H., QIAN, L., CHEN, Z., THIBAULT, D., LIU, G., LIU, T. & THANASSI, D. G. 2004. The outer membrane usher forms a twin-pore secretion complex. *J Mol Biol,* 344**,** 1397-407.

LI, Q., NG, T. W., DODSON, K. W., SO, S. S., BAYLE, K. M., PINKNER, J. S., SCARLATA, S., HULTGREN, S. J. & THANASSI, D. G. 2010. The differential

affinity of the usher for chaperone-subunit complexes is required for assembly of complete pili. *Mol Microbiol,* 76**,** 159-72.

LING, L. L., SCHNEIDER, T., PEOPLES, A. J., SPOERING, A. L., ENGELS, I., CONLON, B. P., MUELLER, A., SCHABERLE, T. F., HUGHES, D. E., EPSTEIN, S., JONES, M., LAZARIDES, L., STEADMAN, V. A., COHEN, D. R., FELIX, C. R., FETTERMAN, K. A., MILLETT, W. P., NITTI, A. G., ZULLO, A. M., CHEN, C. & LEWIS, K. 2015. A new antibiotic kills pathogens without detectable resistance. *Nature,* 517**,** 455-9.

LIU, Y. & BAHAR, I. 2012. Sequence evolution correlates with structural dynamics. *Mol Biol Evol,* 29**,** 2253-63.

LOCHT, C., BERTIN, P., MENOZZI, F. D. & RENAULD, G. 1993. The filamentous haemagglutinin, a multifaceted adhesion produced by virulent Bordetella spp. *Mol Microbiol,* 9**,** 653-60.

LORNTZ, B., SOARES, A. M., MOORE, S. R., PINKERTON, R., GANSNEDER, B., BOVBJERG, V. E., GUYATT, H., LIMA, A. M. & GUERRANT, R. L. 2006. Early childhood diarrhea predicts impaired school performance. *Pediatr Infect Dis J,* 25**,** 513-20.

LYU, Z. X. & ZHAO, X. S. 2015. Periplasmic quality control in biogenesis of outer membrane proteins. *Biochem Soc Trans,* 43**,** 133-8.

MAASS, D. R. & ATKINSON, P. H. 1990. Rotavirus proteins VP7, NS28, and VP4 form oligomeric structures. *J Virol,* 64**,** 2632-41.

MADAN, V. & BARTENSCHLAGER, R. 2015. Structural and Functional Properties of the Hepatitis C Virus p7 Viroporin. *Viruses,* 7**,** 4461-81.

MAPINGIRE, O. S., HENDERSON, N. S., DURET, G., THANASSI, D. G. & DELCOUR, A. H. 2009. Modulating effects of the plug, helix, and N- and C-terminal domains on channel properties of the PapC usher. *J Biol Chem,* 284**,** 36324-33.

MARTINEZ, J. J., MULVEY, M. A., SCHILLING, J. D., PINKNER, J. S. & HULTGREN, S. J. 2000. Type 1 pilus-mediated bacterial invasion of bladder epithelial cells. *EMBO J,* 19**,** 2803-12.

MARTINEZ-GIL, L., BANO-POLO, M., REDONDO, N., SANCHEZ-MARTINEZ, S., NIEVA, J. L., CARRASCO, L. & MINGARRO, I. 2011a. Membrane integration of poliovirus 2B viroporin. *J Virol,* 85**,** 11315-24.

MARTINEZ-GIL, L. & MINGARRO, I. 2015. Viroporins, Examples of the Two-Stage Membrane Protein Folding Model. *Viruses,* 7**,** 3462-82.

MARTINEZ-GIL, L., SAURI, A., MARTI-RENOM, M. A. & MINGARRO, I. 2011b. Membrane protein integration into the endoplasmic reticulum. *FEBS J,* 278**,** 3846-58.

MATTEI, P. J., FAUDRY, E., JOB, V., IZORE, T., ATTREE, I. & DESSEN, A. 2011. Membrane targeting and pore formation by the type III secretion system translocon. *FEBS J,* 278**,** 414-26.

MATTOO, S., FOREMAN-WYKERT, A. K., COTTER, P. A. & MILLER, J. F. 2001. Mechanisms of Bordetella pathogenesis. *Front Biosci,* 6**,** E168-86.

MELI, A. C., HODAK, H., CLANTIN, B., LOCHT, C., MOLLE, G., JACOB-DUBUISSON, F. & SAINT, N. 2006. Channel properties of TpsB transporter FhaC point to two functional domains with a C-terminal protein-conducting pore. *J Biol Chem,* 281**,** 158-66.

MELI, A. C., KONDRATOVA, M., MOLLE, V., COQUET, L., KAJAVA, A. V. & SAINT, N. 2009. EtpB is a pore-forming outer membrane protein showing TpsB protein features involved in the two-partner secretion system. *J Membr Biol,* 230**,** 143-54.

MERDANOVIC, M., CLAUSEN, T., KAISER, M., HUBER, R. & EHRMANN, M. 2011. Protein quality control in the bacterial periplasm. *Annu Rev Microbiol,* 65**,** 149-68.

MICHELANGELI, F., RUIZ, M. C., DEL CASTILLO, J. R., LUDERT, J. E. & LIPRANDI, F. 1991. Effect of rotavirus infection on intracellular calcium homeostasis in cultured cells. *Virology,* 181**,** 520-7.

MIYADAI, H., TANAKA-MASUDA, K., MATSUYAMA, S. & TOKUDA, H. 2004. Effects of lipoprotein overproduction on the induction of DegP (HtrA) involved in quality control in the Escherichia coli periplasm. *J Biol Chem,* 279**,** 39807-13.

MONTAGNER, C., ARQUINT, C. & CORNELIS, G. R. 2011. Translocators YopB and YopD from Yersinia enterocolitica form a multimeric integral membrane complex in eukaryotic cell membranes. *J Bacteriol,* 193**,** 6923-8.

MORADPOUR, D. & PENIN, F. 2013. Hepatitis C virus proteins: from structure to function. *Curr Top Microbiol Immunol,* 369**,** 113-42.

MUELLER, C. A., BROZ, P. & CORNELIS, G. R. 2008. The type III secretion system tip complex and translocon. *Mol Microbiol,* 68**,** 1085-95.

MULLINEAUX, C. W., NENNINGER, A., RAY, N. & ROBINSON, C. 2006. Diffusion of green fluorescent protein in three cell environments in Escherichia coli. *J Bacteriol,* 188**,** 3442-8.

NIETO-TORRES, J. L., VERDIA-BAGUENA, C., CASTANO-RODRIGUEZ, C., AGUILELLA, V. M. & ENJUANES, L. 2015. Relevance of Viroporin Ion Channel Activity on Viral Replication and Pathogenesis. *Viruses,* 7**,** 3552-73.

NIEVA, J. L., AGIRRE, A., NIR, S. & CARRASCO, L. 2003. Mechanisms of membrane permeabilization by picornavirus 2B viroporin. *FEBS Lett,* 552**,** 68-73.

NIEVA, J. L., MADAN, V. & CARRASCO, L. 2012. Viroporins: structure and biological functions. *Nat Rev Microbiol,* 10**,** 563-74.

NIKAIDO, H. 2003. Molecular basis of bacterial outer membrane permeability revisited. *Microbiol Mol Biol Rev,* 67**,** 593-656.

NIKAIDO, H. 2009. Multidrug resistance in bacteria. *Annu Rev Biochem,* 78**,** 119-46.

NOINAJ, N., KUSZAK, A. J., GUMBART, J. C., LUKACIK, P., CHANG, H., EASLEY, N. C., LITHGOW, T. & BUCHANAN, S. K. 2013. Structural insight into the biogenesis of beta-barrel membrane proteins. *Nature,* 501**,** 385-90.

NOUWEN, N., RANSON, N., SAIBIL, H., WOLPENSINGER, B., ENGEL, A., GHAZI, A. & PUGSLEY, A. P. 1999. Secretin PulD: association with pilot PulS, structure, and ion-conducting channel formation. *Proc Natl Acad Sci U S A,* 96**,** 8173-7.

OOMEN, C. J., VAN ULSEN, P., VAN GELDER, P., FEIJEN, M., TOMMASSEN, J. & GROS, P. 2004. Structure of the translocator domain of a bacterial autotransporter. *EMBO J,* 23**,** 1257-66.

OUYANG, B. & CHOU, J. J. 2014. The minimalist architectures of viroporins and their therapeutic implications. *Biochim Biophys Acta,* 1838**,** 1058-67.

PARASHAR, U. D., GIBSON, C. J., BRESEE, J. S. & GLASS, R. I. 2006. Rotavirus and severe childhood diarrhea. *Emerg Infect Dis,* 12**,** 304-6.

PARK, E., MENETRET, J. F., GUMBART, J. C., LUDTKE, S. J., LI, W., WHYNOT, A., RAPOPORT, T. A. & AKEY, C. W. 2014. Structure of the SecY channel during initiation of protein translocation. *Nature,* 506**,** 102-6.

PARK, E. & RAPOPORT, T. A. 2011. Preserving the membrane barrier for small molecules during bacterial protein translocation. *Nature,* 473**,** 239-42.

PAVLOVIC, D., NEVILLE, D. C., ARGAUD, O., BLUMBERG, B., DWEK, R. A., FISCHER, W. B. & ZITZMANN, N. 2003. The hepatitis C virus p7 protein forms an ion channel that is inhibited by long-alkyl-chain iminosugar derivatives. *Proc Natl Acad Sci U S A,* 100**,** 6104-8.

PEREZ, J. F., CHEMELLO, M. E., LIPRANDI, F., RUIZ, M. C. & MICHELANGELI, F. 1998. Oncosis in MA104 cells is induced by rotavirus infection through an increase in intracellular Ca2+ concentration. *Virology,* 252**,** 17-27.

PERUTZ, M. F. 1978. Electrostatic effects in proteins. *Science,* 201**,** 1187-91.

PERVUSHIN, K., TAN, E., PARTHASARATHY, K., LIN, X., JIANG, F. L., YU, D., VARARATTANAVECH, A., SOONG, T. W., LIU, D. X. & TORRES, J. 2009. Structure and inhibition of the SARS coronavirus envelope protein ion channel. *PLoS Pathog,* 5**,** e1000511.

PHAN, G., REMAUT, H., WANG, T., ALLEN, W. J., PIRKER, K. F., LEBEDEV, A., HENDERSON, N. S., GEIBEL, S., VOLKAN, E., YAN, J., KUNZE, M. B., PINKNER, J. S., FORD, B., KAY, C. W., LI, H., HULTGREN, S. J., THANASSI, D. G. & WAKSMAN, G. 2011. Crystal structure of the FimD usher bound to its cognate FimC-FimH substrate. *Nature,* 474**,** 49-53.

PINKNER, J. S., REMAUT, H., BUELENS, F., MILLER, E., ABERG, V., PEMBERTON, N., HEDENSTROM, M., LARSSON, A., SEED, P., WAKSMAN, G., HULTGREN, S. J. & ALMQVIST, F. 2006. Rationally designed small compounds inhibit pilus biogenesis in uropathogenic bacteria. *Proc Natl Acad Sci U S A,* 103**,** 17897-902.

PINTO, L. H., HOLSINGER, L. J. & LAMB, R. A. 1992. Influenza virus M2 protein has ion channel activity. *Cell,* 69**,** 517-28.

PREMKUMAR, A., WILSON, L., EWART, G. D. & GAGE, P. W. 2004. Cation-selective ion channels formed by p7 of hepatitis C virus are blocked by hexamethylene amiloride. *FEBS Lett,* 557**,** 99-103.

PRILIPOV, A., PHALE, P. S., VAN GELDER, P., ROSENBUSCH, J. P. & KOEBNIK, R. 1998. Coupling site-directed mutagenesis with high-level expression: large scale production of mutant porins from E. coli. *FEMS Microbiol Lett,* 163**,** 65-72.

RADICS, J., KONIGSMAIER, L. & MARLOVITS, T. C. 2014. Structure of a pathogenic type 3 secretion system in action. *Nat Struct Mol Biol,* 21**,** 82-7.

REMAUT, H., TANG, C., HENDERSON, N. S., PINKNER, J. S., WANG, T., HULTGREN, S. J., THANASSI, D. G., WAKSMAN, G. & LI, H. 2008. Fiber formation across the bacterial outer membrane by the chaperone/usher pathway. *Cell,* 133**,** 640-52.

RILEY, M. A. & WERTZ, J. E. 2002a. Bacteriocin diversity: ecological and evolutionary perspectives. *Biochimie,* 84**,** 357-64.

RILEY, M. A. & WERTZ, J. E. 2002b. Bacteriocins: evolution, ecology, and application. *Annu Rev Microbiol,* 56**,** 117-37.

ROBERT, V., VOLOKHINA, E. B., SENF, F., BOS, M. P., VAN GELDER, P. & TOMMASSEN, J. 2006. Assembly factor Omp85 recognizes its outer membrane protein substrates by a species-specific C-terminal motif. *PLoS Biol,* 4**,** e377.

ROUSSEL-JAZEDE, V., VAN GELDER, P., SIJBRANDI, R., RUTTEN, L., OTTO, B. R., LUIRINK, J., GROS, P., TOMMASSEN, J. & VAN ULSEN, P. 2011. Channel properties of the translocator domain of the autotransporter Hbp of Escherichia coli. *Mol Membr Biol,* 28**,** 158-70.

ROYLE, J., DOBSON, S. J., MULLER, M. & MACDONALD, A. 2015. Emerging Roles of Viroporins Encoded by DNA Viruses: Novel Targets for Antivirals? *Viruses,* 7**,** 5375-87.

RUDRAMURTHY, G. R., SWAMY, M. K., SINNIAH, U. R. & GHASEMZADEH, A. 2016. Nanoparticles: Alternatives Against Drug-Resistant Pathogenic Microbes. *Molecules,* 21.

SAKAGUCHI, T. 1997a. [Structure and function of the influenza virus M2 ion channel protein]. *Nihon Rinsho,* 55**,** 2587-92.

SAKAGUCHI, T. 1997b. [Viral ion channel: structure and function of influenza virus M2 protein]. *Uirusu,* 47**,** 177-86.

SAKAGUCHI, T., TU, Q., PINTO, L. H. & LAMB, R. A. 1997. The active oligomeric state of the minimalistic influenza virus M2 ion channel is a tetramer. *Proc Natl Acad Sci U S A,* 94**,** 5000-5.

SAPAROV, S. M., ERLANDSON, K., CANNON, K., SCHALETZKY, J., SCHULMAN, S., RAPOPORT, T. A. & POHL, P. 2007. Determining the conductance of the SecY protein translocation channel for small molecules. *Mol Cell,* 26**,** 501-9.

SASTRI, N. P., VISKOVSKA, M., HYSER, J. M., TANNER, M. R., HORTON, L. B., SANKARAN, B., PRASAD, B. V. & ESTES, M. K. 2014. Structural plasticity of the coiled-coil domain of rotavirus NSP4. *J Virol,* 88**,** 13602-12.

SAULINO, E. T., THANASSI, D. G., PINKNER, J. S. & HULTGREN, S. J. 1998. Ramifications of kinetic partitioning on usher-mediated pilus biogenesis. *EMBO J,* 17**,** 2177-85.

SCHUBERT, U., FERRER-MONTIEL, A. V., OBLATT-MONTAL, M., HENKLEIN, P., STREBEL, K. & MONTAL, M. 1996. Identification of an ion channel activity of the Vpu transmembrane domain and its involvement in the regulation of virus release from HIV-1-infected cells. *FEBS Lett,* 398**,** 12-8.

SCOTT, C. & GRIFFIN, S. 2015. Viroporins: structure, function and potential as antiviral targets. *J Gen Virol,* 96**,** 2000-27.

SELKRIG, J., LEYTON, D. L., WEBB, C. T. & LITHGOW, T. 2014. Assembly of beta-barrel proteins into bacterial outer membranes. *Biochim Biophys Acta,* 1843**,** 1542-50.

SERRA, D. O., CONOVER, M. S., ARNAL, L., SLOAN, G. P., RODRIGUEZ, M. E., YANTORNO, O. M. & DEORA, R. 2011. FHA-mediated cell-substrate and cell-cell adhesions are critical for Bordetella pertussis biofilm formation on abiotic surfaces and in the mouse nose and the trachea. *PLoS One,* 6**,** e28811.

SILHAVY, T. J., KAHNE, D. & WALKER, S. 2010. The bacterial cell envelope. *Cold Spring Harb Perspect Biol,* 2**,** a000414.

SIMON, S. M. & BLOBEL, G. 1992. Signal peptides open protein-conducting channels in E. coli. *Cell,* 69**,** 677-84.

STEADMAN, D., LO, A., WAKSMAN, G. & REMAUT, H. 2014. Bacterial surface appendages as targets for novel antibacterial therapeutics. *Future Microbiol,* 9**,** 887-900.

STEGMEIER, J. F. & ANDERSEN, C. 2006. Characterization of pores formed by YaeT (Omp85) from Escherichia coli. *J Biochem,* 140**,** 275-83.

STOREY, S. M., GIBBONS, T. F., WILLIAMS, C. V., PARR, R. D., SCHROEDER, F. & BALL, J. M. 2007. Full-length, glycosylated NSP4 is localized to plasma membrane caveolae by a novel raft isolation technique. *J Virol,* 81**,** 5472-83.

SUBASHCHANDRABOSE, S. & MOBLEY, H. L. 2015. Virulence and Fitness Determinants of Uropathogenic Escherichia coli. *Microbiol Spectr,* 3.

SUEL, G. M., LOCKLESS, S. W., WALL, M. A. & RANGANATHAN, R. 2003. Evolutionarily conserved networks of residues mediate allosteric communication in proteins. *Nat Struct Biol,* 10**,** 59-69.

SUGAWARA, E. & NIKAIDO, H. 1992. Pore-forming activity of OmpA protein of Escherichia coli. *J Biol Chem,* 267**,** 2507-11.

SUGAWARA, E. & NIKAIDO, H. 1994. OmpA protein of Escherichia coli outer membrane occurs in open and closed channel forms. *J Biol Chem,* 269**,** 17981-7.

SZE, C. W. & TAN, Y. J. 2015. Viral Membrane Channels: Role and Function in the Virus Life Cycle. *Viruses,* 7**,** 3261-84.

TAJIMA, N., KAWAI, F., PARK, S. Y. & TAME, J. R. 2010. A novel intein-like autoproteolytic mechanism in autotransporter proteins. *J Mol Biol,* 402**,** 645-56.

TANG, S., LIAO, J. C., DUNN, A. R., ALTMAN, R. B., SPUDICH, J. A. & SCHMIDT, J. P. 2007. Predicting allosteric communication in myosin via a pathway of conserved residues. *J Mol Biol,* 373**,** 1361-73.

TANG, Y., PAN, X., CHEN, Y., TAI, P. C. & SUI, S. F. 2011. Dimeric SecA couples the preprotein translocation in an asymmetric manner. *PLoS One,* 6**,** e16498.

TARDY, F., HOMBLE, F., NEYT, C., WATTIEZ, R., CORNELIS, G. R., RUYSSCHAERT, J. M. & CABIAUX, V. 1999. Yersinia enterocolitica type III secretion-translocation system: channel formation by secreted Yops. *EMBO J,* 18**,** 6793-9.

THANASSI, D. G., BLISKA, J. B. & CHRISTIE, P. J. 2012. Surface organelles assembled by secretion systems of Gram-negative bacteria: diversity in structure and function. *FEMS Microbiol Rev,* 36**,** 1046-82.

TIAN, P., ESTES, M. K., HU, Y., BALL, J. M., ZENG, C. Q. & SCHILLING, W. P. 1995. The rotavirus nonstructural glycoprotein NSP4 mobilizes Ca2+ from the endoplasmic reticulum. *J Virol,* 69**,** 5763-72.

TOSI, T., ESTROZI, L. F., JOB, V., GUILVOUT, I., PUGSLEY, A. P., SCHOEHN, G. & DESSEN, A. 2014. Structural similarity of secretins from type II and type III secretion systems. *Structure,* 22**,** 1348-55.

TRASK, S. D., MCDONALD, S. M. & PATTON, J. T. 2012. Structural insights into the coupling of virion assembly and rotavirus replication. *Nat Rev Microbiol,* 10**,** 165-77.

TSIEN, R. W. & TSIEN, R. Y. 1990. Calcium channels, stores, and oscillations. *Annu Rev Cell Biol,* 6**,** 715-60.

VAN DEN BERG, B., CLEMONS, W. M., JR., COLLINSON, I., MODIS, Y., HARTMANN, E., HARRISON, S. C. & RAPOPORT, T. A. 2004. X-ray structure of a protein-conducting channel. *Nature,* 427**,** 36-44.

VAN KUPPEVELD, F. J., HOENDEROP, J. G., SMEETS, R. L., WILLEMS, P. H., DIJKMAN, H. B., GALAMA, J. M. & MELCHERS, W. J. 1997. Coxsackievirus protein 2B modifies endoplasmic reticulum membrane and plasma membrane permeability and facilitates virus release. *EMBO J,* 16**,** 3519-32.

VAN ULSEN, P., RAHMAN, S., JONG, W. S., DALEKE-SCHERMERHORN, M. H. & LUIRINK, J. 2014. Type V secretion: from biogenesis to biotechnology. *Biochim Biophys Acta,* 1843**,** 1592-611.

VISKOVSKA, M., ANISH, R., HU, L., CHOW, D. C., HURWITZ, A. M., BROWN, N. G., PALZKILL, T., ESTES, M. K. & PRASAD, B. V. 2014. Probing the sites of interactions of rotaviral proteins involved in replication. *J Virol,* 88**,** 12866-81.

VOLKAN, E., KALAS, V., PINKNER, J. S., DODSON, K. W., HENDERSON, N. S., PHAM, T., WAKSMAN, G., DELCOUR, A. H., THANASSI, D. G. & HULTGREN, S. J. 2013. Molecular basis of usher pore gating in Escherichia coli pilus biogenesis. *Proc Natl Acad Sci U S A,* 110**,** 20741-6.

VOLLMER, W., BLANOT, D. & DE PEDRO, M. A. 2008a. Peptidoglycan structure and architecture. *FEMS Microbiol Rev,* 32**,** 149-67.

VOLLMER, W., JORIS, B., CHARLIER, P. & FOSTER, S. 2008b. Bacterial peptidoglycan (murein) hydrolases. *FEMS Microbiol Rev,* 32**,** 259-86.

VONDRASEK, J., MASON, P. E., HEYDA, J., COLLINS, K. D. & JUNGWIRTH, P. 2009. The molecular origin of like-charge arginine-arginine pairing in water. *J Phys Chem B,* 113**,** 9041-5.

WAGER, B., FAUDRY, E., WILLS, T., ATTREE, I. & DELCOUR, A. H. 2013. Current fluctuation analysis of the PopB and PopD translocon components of the Pseudomonas aeruginosa type III secretion system. *Biophys J,* 104**,** 1445-55.

WAKSMAN, G. & HULTGREN, S. J. 2009. Structural biology of the chaperone-usher pathway of pilus biogenesis. *Nat Rev Microbiol,* 7**,** 765-74.

WALDBURGER, C. D., SCHILDBACH, J. F. & SAUER, R. T. 1995. Are buried salt bridges important for protein stability and conformational specificity? *Nat Struct Biol,* 2**,** 122-8.

WALTON, T. A., SANDOVAL, C. M., FOWLER, C. A., PARDI, A. & SOUSA, M. C. 2009. The cavity-chaperone Skp protects its substrate from aggregation but allows independent folding of substrate domains. *Proc Natl Acad Sci U S A,* 106**,** 1772-7.

WATANABE, S., WATANABE, T. & KAWAOKA, Y. 2009. Influenza A virus lacking M2 protein as a live attenuated vaccine. *J Virol,* 83**,** 5947-50.

WEIDEL, W. & PELZER, H. 1964. Bagshaped Macromolecules--a New Outlook on Bacterial Cell Walls. *Adv Enzymol Relat Areas Mol Biol,* 26**,** 193-232.

WERNEBURG, G. T., HENDERSON, N. S., PORTNOY, E. B., SAROWAR, S., HULTGREN, S. J., LI, H. & THANASSI, D. G. 2015. The pilus usher controls protein interactions via domain masking and is functional as an oligomer. *Nat Struct Mol Biol,* 22**,** 540-6.

WETHERILL, L. F., HOLMES, K. K., VEROW, M., MULLER, M., HOWELL, G., HARRIS, M., FISHWICK, C., STONEHOUSE, N., FOSTER, R., BLAIR, G. E., GRIFFIN, S. & MACDONALD, A. 2012. High-risk human papillomavirus E5 oncoprotein displays channel-forming activity sensitive to small-molecule inhibitors. *J Virol,* 86**,** 5341-51.

WHITFIELD, T., MILES, A. J., SCHEINOST, J. C., OFFER, J., WENTWORTH, P., JR., DWEK, R. A., WALLACE, B. A., BIGGIN, P. C. & ZITZMANN, N. 2011. The influence of different lipid environments on the structure and function of the hepatitis C virus p7 ion channel protein. *Mol Membr Biol,* 28**,** 254-64.

WRIGHT, K. J., SEED, P. C. & HULTGREN, S. J. 2007. Development of intracellular bacterial communities of uropathogenic Escherichia coli depends on type 1 pili. *Cell Microbiol,* 9**,** 2230-41.

WU, T., MALINVERNI, J., RUIZ, N., KIM, S., SILHAVY, T. J. & KAHNE, D. 2005. Identification of a multicomponent complex required for outer membrane biogenesis in Escherichia coli. *Cell,* 121**,** 235-45.

XIE, K. & DALBEY, R. E. 2008. Inserting proteins into the bacterial cytoplasmic membrane using the Sec and YidC translocases. *Nat Rev Microbiol,* 6**,** 234-44.

YANG, A. S., SHARP, K. A. & HONIG, B. 1992. Analysis of the heat capacity dependence of protein folding. *J Mol Biol,* 227**,** 889-900.

YANG, J., YANG, H., SUN, X., DELALOYE, K., YANG, X., MOLLER, A., SHI, J. & CUI, J. 2013. Interaction between residues in the Mg2+-binding site regulates BK channel activation. *J Gen Physiol,* 141**,** 217-28.

YANG, L., HARROUN, T. A., WEISS, T. M., DING, L. & HUANG, H. W. 2001. Barrel-stave model or toroidal model? A case study on melittin pores. *Biophys J,* 81**,** 1475-85.

ZAKHAROV, S. D., EROUKOVA, V. Y., ROKITSKAYA, T. I., ZHALNINA, M. V., SHARMA, O., LOLL, P. J., ZGURSKAYA, H. I., ANTONENKO, Y. N. & CRAMER, W. A. 2004. Colicin occlusion of OmpF and TolC channels: outer membrane translocons for colicin import. *Biophys J,* 87**,** 3901-11.

ZAKHAROV, S. D., SHARMA, O., ZHALNINA, M., YAMASHITA, E. & CRAMER, W. A. 2012. Pathways of colicin import: utilization of BtuB, OmpF porin and the TolC drug-export protein. *Biochem Soc Trans,* 40**,** 1463-8.

ZAMBRANO, J. L., DIAZ, Y., PENA, F., VIZZI, E., RUIZ, M. C., MICHELANGELI, F., LIPRANDI, F. & LUDERT, J. E. 2008. Silencing of rotavirus NSP4 or VP7 expression reduces alterations in Ca2+ homeostasis induced by infection of cultured cells. *J Virol,* 82**,** 5815-24.

ZGURSKAYA, H. I., KRISHNAMOORTHY, G., NTREH, A. & LU, S. 2011. Mechanism and Function of the Outer Membrane Channel TolC in Multidrug Resistance and Physiology of Enterobacteria. *Front Microbiol,* 2**,** 189.

ZGURSKAYA, H. I., WEEKS, J. W., NTREH, A. T., NICKELS, L. M. & WOLLOSCHECK, D. 2015. Mechanism of coupling drug transport reactions located in two different membranes. *Front Microbiol,* 6**,** 100.

ZHANG, G., YANG, H., LIANG, H., YANG, J., SHI, J., MCFARLAND, K., CHEN, Y. & CUI, J. 2014. A charged residue in S4 regulates coupling among the activation gate, voltage, and Ca2+ sensors in BK channels. *J Neurosci,* 34**,** 12280-8.

ZHOU, Y., FREY, T. K. & YANG, J. J. 2009. Viral calciomics: interplays between Ca2+ and virus. *Cell Calcium,* 46**,** 1-17.

ZHU, Q. & CASEY, J. R. 2007. Topology of transmembrane proteins by scanning cysteine accessibility mutagenesis methodology. *Methods,* 41**,** 439-50.

ZIMMER, J., NAM, Y. & RAPOPORT, T. A. 2008. Structure of a complex of the ATPase SecA and the protein-translocation channel. *Nature,* 455**,** 936-43.